Katholieke
Universiteit
Leuven

FACULTEIT WETENSCHAPPEN
Departement Scheikunde
Afdeling Coördinatiechemie

Structure and Thermal Behaviour of Lanthanide(III) Soaps

Proefschrift ingediend voor het behalen van de
graad van Doctor in de Wetenschappen

Promotoren
Prof. Dr. K. Binnemans
Prof. Dr. C. Görller-Walrand

Liesbet Jongen

2002

Een top bereik je
met geduld,
met inspanning
met verwachting.

Een top bereik je
uit jezelf,
met krachten die
je zelf ontdekken kunt,
met denkwerk,
of met het werk
van je handen.

En toch is het best
dat je niet te snel
die top bereikt.
het streven naar
vult soms een ganse
leven, geeft er zin aan,
draagt sterkte bij
om menige beproeving
te weerstaan en
voldaan de top
te bereiken

Freek Dumarais

Dankjewel, iedereen die me het begin van mijn reis toonde.
Dankjewel, iedereen die met me meegegaan is.
Dankjewel, iedereen die me vertrouwde dat ik de weg vond.
Dankjewel, iedereen die me als een wegwijzer de weg wees.
Dankjewel, iedereen die me onderweg een plekje gaf om even te rusten en daarna weer op weg zette.
Dankjewel, iedereen die me even van mijn weg afhaalde om me ook een andere top te laten beklimmen.

Dankjewel, iedereen, voor alles.

Dankjewel: mama & papa; prof. Görller-Walrand, Koen, prof. Meyer, Rita, prof. D'Olieslager; Sandy, Ward, Steven en de rest van het labo; Walter, Edith; Dirk, Claudia B, Monika und alle Kölner; Majke & Karel & Herman, Bieke & Luc & Lise & Thijs, Greetje & Jacky & Anne & Jan, Mathieu;
en tot slot iedereen die een bijdrage geleverd heeft maar hier niet bij staat.

Leden van de examencommissie

Prof. Dr. K. Binnemans (promotor)
Prof. Dr. C. Görller-Walrand (promotor)

Prof. Dr. W. Dehaen
Prof. Dr. W. D'Olieslaeger
Prof. Dr. G. Meyer (extern jurylid, Universität zu Köln)
Prof. Dr. H. Reynaers
Prof. Dr. J. Thoen
Prof. Dr. L. Vanquickenborne

Abbrevations

A	absorbance
C	concentration
C	cubic mesophase
Cr	crystalline phase
Cx	total number of carbon atoms in an alkyl chain
d	optical path length
d	layer spacing in smectic phases
D	dipole strength
DSC	differential scanning calorimetry
DTA	differential thermal analysis
EW	ethylene glycol/water
ε	molar absorptivity
H	hexagonal mesophase
I	isotropic phase
I	intensity
L	lamellar mesophase
λ	wave length
M	mesophase M
n	refractive index
n	director
N	nematic mesophase
ν	wave number
SmA	smectic A mesophase
SmC	smectic C mesophase
T_c	clearing temperature
TG	thermogravimetry
T_m	melting temperature
θ	scattering angle in XRD measurements
s	1/*d* in synchrotron measurements
x	mole fraction
XRD	X-ray diffraction

Introduction

Lanthanide(III) soaps are an often overlooked class of complexes. These compounds have several interesting applications. They can be used as stabilisers of PVC, catalysts for e.g. the synthesis of *cis*-polybutadiene or as optical amplifiers.

In spite of this broad area of use it is surprising how little fundamental research has been done on the physicochemical properties of these lanthanide(III) soaps. During the last few years these compounds were the topic of some investigations, although the complexes were mainly studied in solution where the viscosity and the critical micelle concentration were measured.

At the start of this project, it was very frustrating to find out that the data on the physicochemical properties (and in particular the thermal properties) were not reliable. Only two papers existed describing the mesomorphic behaviour of lanthanide(III) soaps.

During this project the structure and thermal behaviour of lanthanide(III) soaps were studied. We tried to find out the determining factors for the existence of mesophases in lanthanide(III) alkanoates. When this is known, (small) changes can be introduced to find stable lanthanide containing mesophases.

We started with the synthesis and characterisation of lanthanide(III) alkanoates, followed by mesophase induction experiments (mixing of a mesogenic and a non-mesogenic compound, and introduction of a neutral ligand) and by adaption of the ligand (4-alkoxybenzoic acids and alkylsulphates as ligands). Finally, some general remarks on the structure and thermal behaviour of all these compounds are given.

Inleiding

Lanthanidezepen zijn een groep verbindingen die vaak over het hoofd gezien worden, ondanks hun groot aantal interessante toepassingen. Deze verbindingen kunnen namelijk gebruikt worden voor de stabilisatie van PVC, als katalysators bij bijvoorbeeld de synthese van *cis*-polybutadieen of als optische versterkers.

Ondanks het brede toepassingsgebied van lanthanidezepen, is het verwonderlijk dat slechts weinig fundamenteel onderzoek gedaan is naar de fysicochemische eigenschappen van deze verbindingen. De laatste jaren is het onderzoek hiernaar wel toegenomen, maar deze complexen werden vaak in oplossing bestudeerd. Hierbij werd de viscositeit en de kritische micelconcentratie bepaald.

Bij het begin van dit project was het erg frustrerend dat de data over de fysicochemische eigenschappen, en in het bijzonder over de thermische eigenschappen, niet betrouwbaar waren. Er waren slechts twee artikels beschikbaar over het mesomorfe gedrag van lanthanidezepen.

Tijdens dit project hebben we de structuur en de thermische eigenschappen van lanthanidezepen onderzocht. We hebben gezocht naar de factoren die bepalen of een mesofase gevormd wordt. Wanneer deze gekend zijn, kunnen (kleine) veranderingen aangebracht worden zodat een stabiele mesofase bekomen wordt.
De synthese en karakterisatie van lanthanidealkanoaten waren het eerste onderwerp tijdens dit project. Dit werd gevolgd door mesofase-inductie-experimenten (mengen van een mesogene en een niet-mesogene verbinding, en introductie van een neutraal ligand) en door aanpassing van de liganden (4-alkoxybenzoëzuren en alkylsulfaten als ligand). Tot slot worden er nog een aantal algemene opmerkingen gegeven over de structuur en thermische eigenschappen van al deze verbindingen.

Chapter 1 Introduction to Liquid Crystals

1.1 What are Liquid Crystals

Most organic and coordination compounds show a simple thermal behaviour. At heating, the solid phase melts at a given temperature (= melting point). At further heating thermal decomposition occurs. The transition between the solid state and different crystal structures can often be observed by thermal analysis, like e.g. differential scanning calorimetry.

Liquid crystals (or mesogens) show a more complex, but also more interesting thermal behaviour. They have two melting points. When heating such compounds, the solid will first change to a turbid liquid (i.e. the mesophase) at the melting point. This liquid will be transformed in a clear liquid at further heating (i.e. second melting point or clearing point).

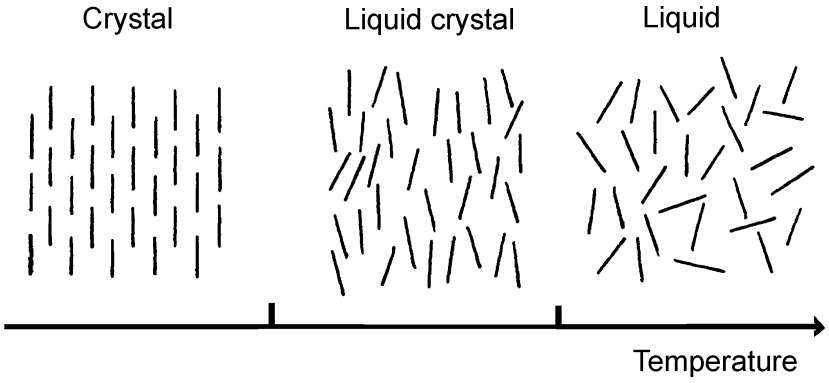

Figure 1-1 Schematic thermal behaviour of a liquid crystal

In the mesophase the molecular order is in between that of an ordered crystalline phase and a disordered liquid. When a mesophase is formed under influence of temperature,

we call these mesogens thermotropic liquid crystals. This is in contrast to lyotropic liquid crystals that form a mesophase in the presence of a solvent.
A mesophase is an anisotropic liquid, which means that the physical properties depend on the direction along which they are measured. The clear liquid formed above the clearing point is isotropic because of total molecular disorder (Figure 1-1).

Thermotropic liquid crystals can be divided in two classes based on their molecular structure. Calamitic liquid crystals are rod like molecules existing of a rigid core of two or more aromatic rings and flexible aliphatic chains.
Discotic mesogens have a flat, disc like structure. The flexible terminal chains are arranged in such a way that a two-dimensional structure is formed. Both calamitic and discotic mesogens can form several types of mesophases.
Mesogens can be pure organic compounds. However, metal-containing liquid crystals also exist. They are called 'metallomesogens'. In this kind of compounds, properties of the ligands and of the metal ions are combined to optimise the mesogenic properties.
[1 - 4]

1.2 Thermotropic Liquid Crystals

1.2.1 Mesophases Formed by Calamitic Mesogens

The nematic phase N is the most simple of all the thermotropic mesophases and also the least ordered. In the nematic phase the long molecular axis is on average parallel to a preferential direction, although there is no positional order. This preferential direction is called 'director' (*n*). This means that there is orientational order in one dimension, but no positional order is present.

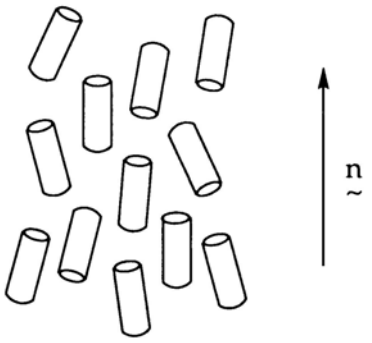

Figure 1-2 Molecular order in a nematic mesophase

The smectic mesophases differ from the nematic phase, in the sense that there is some kind of positional order besides the orientational order that is present in all the liquid crystalline phases. In a smectic phase the molecules are situated in layers. Because of the higher degree of order in comparison with the nematic phase, smectic phases are normally found at lower temperatures than the nematic phase.

Contrary to the nematic phase, several types of smectic phases can be observed. The least ordered smectic phase is the smectic A phase (SmA). Just like the nematic phase the SmA phase possesses some orientational order. Additionally there is some weak short-range translational order, which results in a layered structure. In de SmA phase the director *n* is perpendicular to the layer plane.

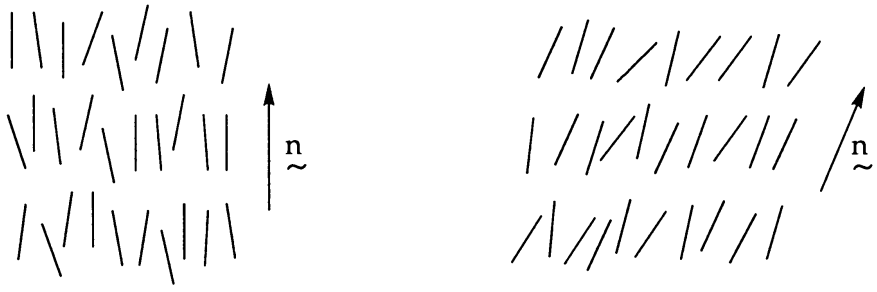

Figure 1-3 Two types of smectic mesophases: SmA (left) and SmC

The smectic C phase differs from the SmA phase because the director is tilted by an angle θ with regard to the normal of the layer plane. Besides the smectic A and C phase several other types of smectic phases exist. The molecular order is much higher

in these phases. For example in the SmF and the SmI phases the molecules show a hexagonal order in the layers.

1.2.2 Mesophases Formed by Discotic Mesogens

The least ordered mesophase formed by discotic molecules and which is very rare, is the nematic phase N_D, and is totally analogous with the calamitic nematic mesophase. The molecules show orientational order, but no translational.

More often the molecules are placed in columns, forming columnar mesophases. Moreover the columns are often ordered in a two-dimensional structure. These columnar mesophases resemble in some points the smectic phases of calamitic molecules. Whereas the smectic phases can be seen as two-dimensional liquids (they possess positional order in one dimension and disorder in the other two), columnar mesophases can be seen as one-dimensional liquids (positional order in two dimensions, disorder in one dimension). The disorder can be found in the columns. When classifying columnar mesophases three points must be considered: symmetry of the two-dimensional lattice, orientation of the core with respect to the column axis, and the degree of order in the columns. There exist discotic mesophases with a hexagonal symmetry, tetragonal or orthorhombic symmetry.

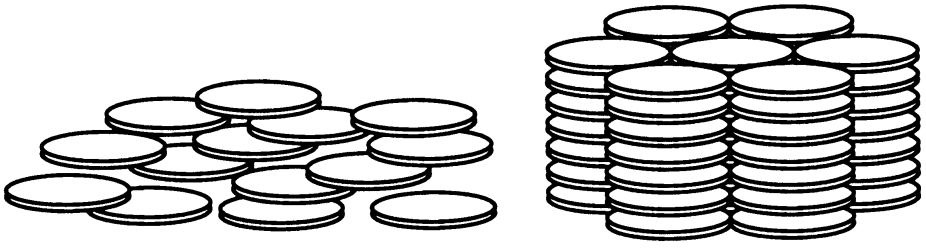

Figure 1-4 Molecular order in discotic mesophases: nematic (left) and hexagonal columnar mesophase

1.3 Lyotropic Liquid Crystals

In the case of lyotropic liquid crystals, mixtures of two components are used (a solid compound and a solvent). These mixtures can exhibit different phases not only as the temperature is changed, but also as the concentration of one component of the mixture is varied.

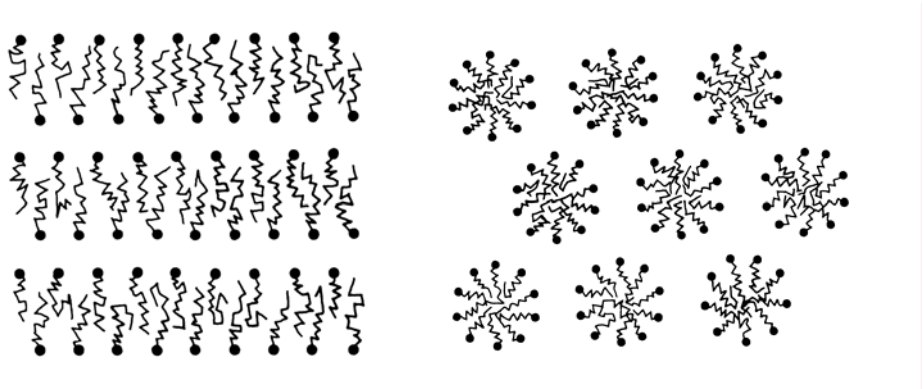

Figure 1-5 Structure of the lamellar lyotropic liquid crystal phase (left) and of the hexagonal lyotropic liquid crystal phase

Most lyotropic mesogens are molecules with end groups with different properties. In the case of amphiphilic compounds one end of the molecule is placed in the solvent while the other end tends to exclude water by arranging themselves together. This results in structures of various shapes (spheres and cylinders are common) whereby the molecules can still move through the structure. Because there is some rotational and positional order these compounds are real liquid crystals.

However, molecular organisation of amphiphilic molecules in solvents only occurs above a certain concentration called the critical micelle concentration. Above this point, the molecules form micelles. Increasing the concentration of the compound gives rise to the formation of lyotropic mesophases.

The most common kind of a lyotropic liquid crystal are soap molecules. The possibility of the soap to dissolve oil and dirt is directly related to the ordered structures the soap molecules form in water. A second example are the biologically important molecules called phospholipids.

1.4 Characterisation of the Mesophases

There are three major experimental techniques that can be used for the characterisation of liquid crystals: thermo-optical microscopy, differential scanning calorimetry and X-ray diffraction at high temperatures. These three techniques are complementary.

1.4.1 Thermo-optical Microscopy

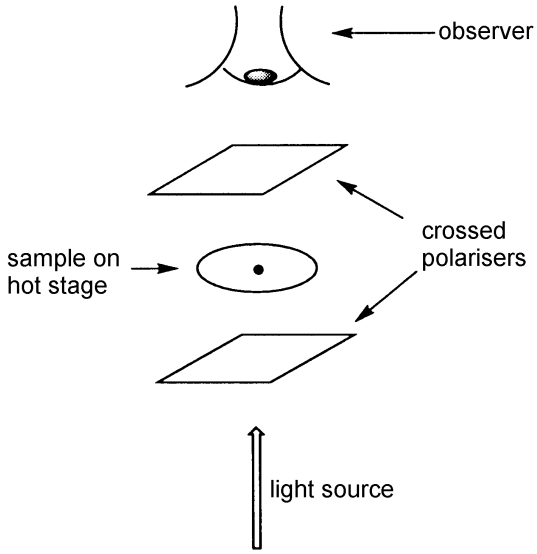

Figure 1-6 Experimental set-up of a thermo-optical microscope

Thermo-optical microscopy is most often used for the study of liquid crystals. The technique makes use of the birefringence of mesophases.

Typically, the sample is sandwiched between two microscope cover slips and then placed on a suitably controlled hot-stage through which there is an optical path. The hot-stage is mounted on the working stage of the microscope. The light incident on the sample is first plane polarised, and a second polariser is placed at 90° to the first (see Figure 1-6). In the mesophase two refracted rays result and these interfere with one

another to give characteristic patterns. This contrasts with the situation where the material is in the isotropic state when the sample appears black between the crossed polaroids.

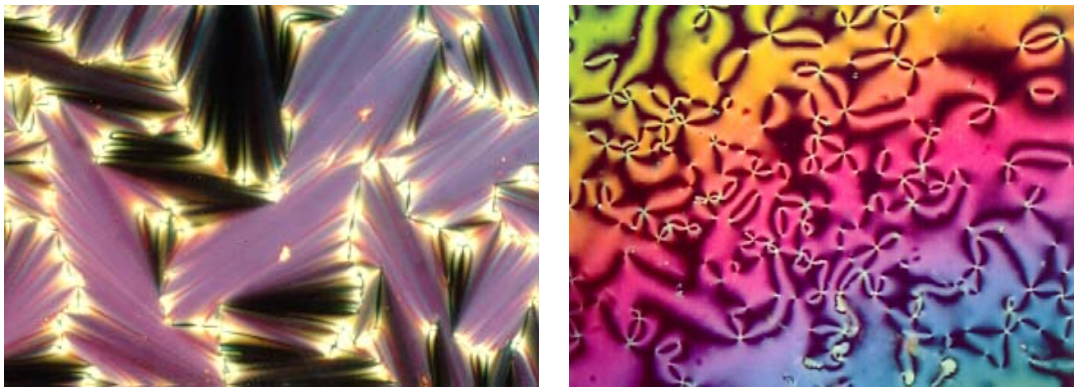

Figure 1-7 Fanlike texture of a Smectic A phase (left) and Schlieren texture of a nematic phase

The texture obtained in thermo-optical microscopy is typical for each mesophase although different mesophases can show similar textures. In Figure 1-7 typical textures of a smectic A and of a nematic phase are given.

Identification of a lyotropic mesophase via thermo-optical microscopy is often easier than in the case of thermotropic liquid crystals, because of the small number of different lyotropic mesophases and thus different textures. In Figure 1-8 typical textures of some lyotropic mesophases are given.

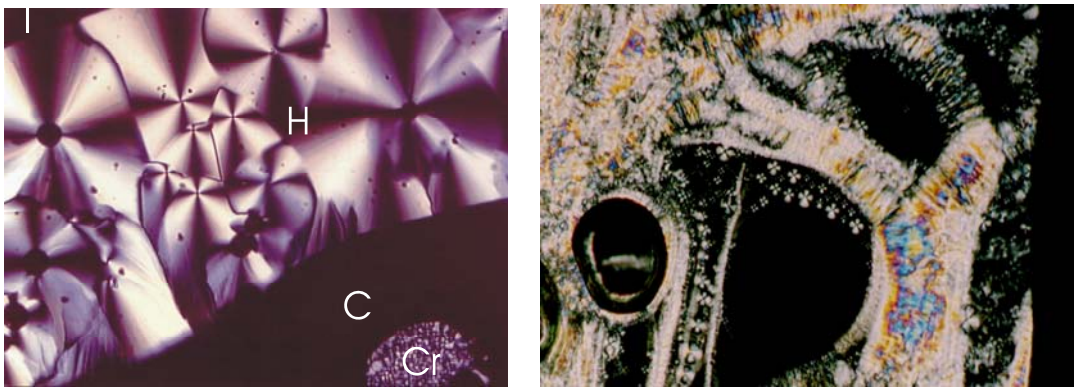

Figure 1-8 Textures of different lyotropic mesophases (left) and Malteser Crosses and oily strikes in the lamellar phase

1.4.2 Differential Scanning Calorimetry

The transitions between the solid crystalline phase and a mesophase, or between a mesophase and the isotropic liquid give rise to an enthalpy change. A DSC instrument measures the difference in heat flux necessary to keep the temperature of the sample and a reference equal. Plotting the heat flux as a function of the temperature allows determining the enthalpy change for a given transition and the exact transition temperatures.

The enthalpy change of a given transition is an indication for the transition type. For example, the enthalpy change for a crystal to mesophase transition is about 30 - 50 kJ mol^{-1}, for a mesophase to mesophase transition this value is less than 1 kJ mol^{-1} and for a mesophase to isotropic liquid transition 1 - 5 kJ mol^{-1} [5].

Although sometimes a mesophase - to - mesophase transition can be seen in thermo-optical microscopy (but this is not always the case), this kind of transitions can clearly be seen in DSC measurements. However, the contrary is also true.

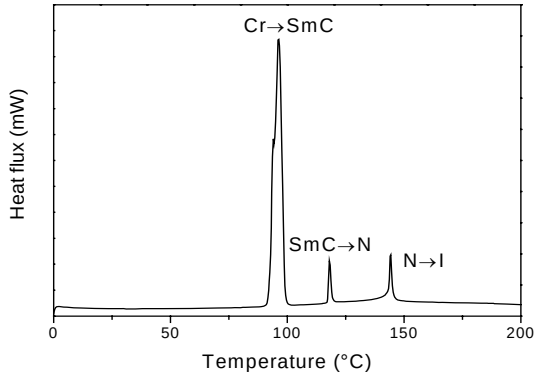

Figure 1-9 DSC thermogram of 4-nonyloxybenzoic acid.

1.4.3 X-ray Diffraction and Synchrotron Measurements

Small angle X-ray diffraction (SAXS) is a very powerful technique to characterise a mesophase.
It is often not possible to determine the single crystal structure of the compounds, but the determination of molecular order and of the phase behaviour can be done by combined small-angle and wide-angle X-ray diffraction (WAXD).
In the most simple approach one is interested in the position of the diffracted rays which is related to the fundamental spacing in the structure by Braggs' law:

Equation 1-1

$$2d \sin\theta = \lambda$$

with $2\theta < 5$ à 6 degrees.
Following the SAXS and WAXD diffraction patterns as a function of the temperature allows us to assign a mesophase on a given transition. For example in the case of a smectic A phase the *d* spacing of the layers decreases at increasing temperatures whereas for a smectic C phase the *d* spacing increases.

Although small angle X-ray diffraction (done in collaboration with the Institut für anorganische Chemie, Universität Köln, Germany) is a very powerful technique, it was sometimes necessary to get more diffraction information, especially time-resolved measurements. Therefore synchrotron measurements were executed at the European Synchrotron Radiation Facility in Grenoble (ESRF, France). Here it is possible to obtain complete diffraction information, both SAXS and WAXD simultaneously, while heating the samples at different heating rates. In the present study this was done using a heating rate of 10°C min^{-1}, allowing a detailed time-resolved study of the phase behaviour of the lanthanide(III) 4-alkoxybenzoates.

References

[1] *Handbook of Liquid Crystals* (ed. D. Demus, F. Goodby, G. W. Gray, H.-W. Spiess, V. Vill) vol.1 VCH-Wiley Weinheim **1998.**

[2] *Metallomesogens* (ed. J. L. Serrano) VCH-Wiley Weinheim **1996**.

[3] P. J. Collings *Liquid Crystals, a Delicate Phase of Matter* Adam Hilger Bristol **1990**.

[4] P. J. Collings, M. Hird *Introduction to Liquid Crystals* Taylor and Francis London **1997**.

[5] G. W. H. Höhne, W. Hemminger, H. J. Flammersheim in *Differential Scanning Calorimetry* Springer-Verlag Berlin **1996**.

Chapter 2 Introduction to Metal Soaps

2.1 Metal Soaps

The term ‘soap’ is used for sodium and potassium salts of alkanoic acids with long aliphatic chains (fatty acids), like potassium stearate (potassium octadecanoate). Soaps are water-soluble and have been used for centuries for cleaning of textile and for body care. The so called ‘metal soaps’ are the salts of fatty acids different from the alkali soaps. These are compounds with earth alkaline and transition metals or elements from group IIIa. Metal soaps are water insoluble, but can be dissolved in organic solvents. Moreover these compounds possess some properties that can be useful for certain applications.

From historical point of view, metal soaps are a result of the search for better lubricants. Findings are that a gel formed by the dissolution of a metal soap in a liquid organic solvent shows good greasing properties [1]. Because of their insolubility in water and their difficult moistness metal soaps are used in water repulsive materials and in flotation solvents [2]. The presence of a transition metal makes these compounds useful for catalytic applications, as paint dryers or as stabilisers for polymers. The fact that metal soaps have been used for several decennia is evident from the papers of Braun and Elliot [3 - 4].
In 1956 Figgis and Martin discovered the existence of very weak covalent copper - copper bonds in anhydrous and hydrated copper acetates and n-alkanoates by magnetic susceptibility measurements [5 - 6]. They proposed a dimer structure where two copper atoms are hold together by four bidentate bridging carboxylate groups.
This dimer structure was confirmed by the crystal structure of anhydrous copper butyrate and decanoate [7 - 8].

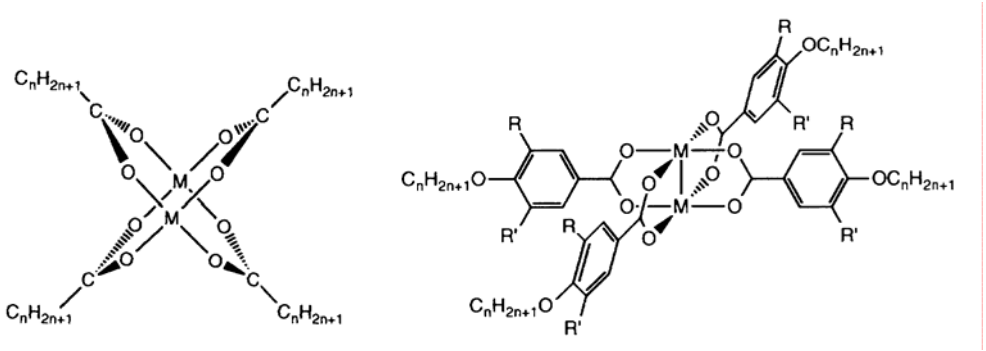

Figure 2-1 Dimeric structure of metal(II) alkanoates (left) and of metal(II) alkoxybenzoates [9]

In 1964 Grant observed the mesomorphic behaviour of copper(II) alkanoates, but their mesophases were not characterised [10]. In the eighties the group of Giroud thoroughly investigated the thermal properties of copper soaps [11].

These compounds show mesomorphism for $x \geq 3$. The mesophase was characterised as a hexagonal columnar mesophase with disorder in the columns. However, copper butyrate forms a columnar mesophase with rectangular symmetry. The difference between this short homologue with the longer ones might be due to the short length of the alkyl chains, which are unable to fill the intercolumnar space as effectively as in the case of the long-chain compounds.

Subsequently, Giroud and coworkers studied the mesomorphic behaviour of analogous rhodium(II) and ruthenium(II) carboxylates. These compounds have the same phase behaviour as copper alkanoates [12 - 17].

The investigation of linear-chain alkanoates was extended to metal carboxylates containing branched and unsaturated chains [14, 17 - 20]. Branching or incorporation of double bonds into the chains depresses the melting temperatures compared with those of saturated straight chain complexes. Most of this kind of d-block element complexes are mesomorphic and show a hexagonal columnar mesophase.

Serrano synthesised rhodium(II) 4-alkoxybenzoates [21]. These molecules contain four aromatic rings attached to the dinuclear carboxylate unit, leading to a larger central core. These compounds show rectangular columnar mesophases, because the small number of chains is not enough to fill the space around the larger core efficiently, and

therefore the chains tend to align in a preferred direction, leading to a rectangular mesophase.

Some metal carboxylates show lamellar structures. Mercury carboxylates are not mesogenic, while thallium carboxylates give rise to stable lamellar phases with branched alkyl chains and SmC phases have been reported for lead(II) alkanoates [17, 22 - 24].

2.2 Lanthanide Soaps

In the early sixties the first papers on lanthanide(III) soaps were published [25 - 26]. The reason for this late date was that lanthanide(III) salts with a sufficient high purity were scarce, but also because the synthesis of metal soaps with trivalent ions was difficult due to hydrolysis.

However, industrial laboratories have been interested in these lanthanide(III) soaps because of, for example, their catalytic properties.
Cerium(III) stearate gives rise to a high thermal stability of PVC. Metal carboxylates inhibit the dehydrochlorination reaction when PVC is subjected to heat and light [27 - 29]. An extra advantage of the addition of cerium(III) stearate in contrary to for example calcium- and barium soaps, is that the PVC gets a better rheological behaviour during the extrusion process.
On the other hand, cerium soaps are added to polyethene, polystyrene or polypropylene plastics to obtain a faster photodegradibility [30 - 31]. Sunlight induces a fast crispness in the polymer. This causes crumbling of the polymer so a faster biodegradation is possible.

From industrial point of view, the catalytic applications are very important. Because of their amphiphilic behaviour metal soaps can show catalytic activity in the interphase

between an aqueous and an organic phase. Neodymium(III) soaps are used in the polymerisation of 1,4-butadiene. In the presence of the catalyst a large excess of the *cis*-polymer is formed [32 - 33]. Cerium soaps are added to diesel and fuel for a better combustion, which reduces emission of soot particles [28, 34].

A great advantage of lanthanide soaps in comparison to lanthanide salts is their solubility in molten polymers. This means that transparent polymer plates, films or fibres doped by trivalent lanthanide ions can be made [35]. Optical polymer fibres have advantages in comparison with glass fibres: low price, easy to handle, low weight. It is interesting to dope a polymer matrix with spectroscopically active lanthanide ions, e.g. optical fibres doped with Nd^{3+} can be used as optical amplifiers [36 - 37].

In spite of this broad area of uses it is surprising how little fundamental investigation has been carried out on the physicochemical properties of these lanthanide soaps. During the last few years lanthanide soaps were the topic of some research, although mostly the complexes were studied in solution, measuring the viscosity and the critical micelle concentration [38 - 44]. When comparing melting points many inconsistencies are found. Often even the melting points are not given although this is an important indication for the purity of the compounds.

Less is known about the structure of lanthanide(III) alkanoates. In the past X-ray powder diffraction measurements were done and they pointed out that lanthanide(III) alkanoates have a bilayered structure with the alkyl chains in *all trans* conformation [45 -50].
Deacon and Phillips reviewed the relationship between the carbon-oxygen infrared stretching frequencies of carboxylate complexes and the type of carboxylate coordination [51]. Marques studied in detail the infrared spectra of cerium(III) alkanoates [52]. The difference between the asymmetric and symmetric carboxylate stretching ($\Delta\nu = \nu_{as} - \nu_s$) for a bidentate chelating coordination ($\Delta\nu$ = 100 cm^{-1}) is much lower than in the case of a bidentate bridging coordination ($\Delta\nu$ = 150-170 cm^{-1}).

$\Delta\nu$ is 138 cm^{-1} for an ionic coordination. Because $\Delta\nu$ is 130 cm^{-1} for cerium(III) alkanoates Marques stipulated that the coordination of lanthanide ions by carboxylate groups must be bidentate chelating.

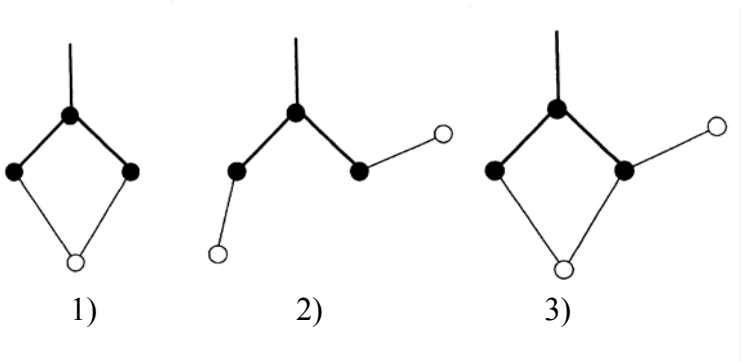

Figure 2-2 Schematic representation of coordination modes of carboxylate groups in metal soaps: 1) chelating bidentate; 2) *Z,E* bridging bidentate; 3) bridging tridentate; open circles represent the metal ion, the black circles represent the carboxylate group COO^- [53]

Crystal structure data are available for the short chain lanthanide(III) alkanoates like acetates and propionates. The structure of hydrated rare earth acetates $Ln(CH_3CO_2)_3 \cdot xH_2O$ (x = 1, 1.5, 3, 4) is well known [54 - 57]. In all these crystals, the acetate groups bridge two rare earth ions, forming dimers (x = 3, 4), chains (x = 1) or a mixture of both (x = 1.5). Besides these structural features, coordinating water molecules are incorporated in the crystal structure. The coordination numbers of the rare earth ions are 9 or 10.

Hardly any crystal structure of the higher homologues of the lanthanide(III) alkanoates is available. Nabar and Barve determined the structural parameters of lanthanide(III) butyrate dihydrate $Ln(C_3H_7CO_2)_3 \cdot 2H_2O$ (Ln = Nd, Tb, Er, Tm, Yb and Y) by X-ray powder diffraction. They proposed the monoclinic space group $P2_1/m$ [58]. The group of Meyer described the crystal structure of praseodymium(III) propionate trihydrate, $Pr(C_2H_5CO_2)_3 \cdot 3H_2O$ [59]. To our knowledge, this is the only crystal structure of the higher homologues of lanthanide(III) alkanoates. The crystal structure consists of chains parallel to [100]. Four bidentate bridging propionate groups coordinate two crystallographically different praseodymium ions. Additionally, Pr1 is coordinated by three water molecules and Pr2 by two bidentate propionate groups. It can be expected

that by increasing the chain length of the lanthanide(III) alkanoates, other structural types can be obtained.

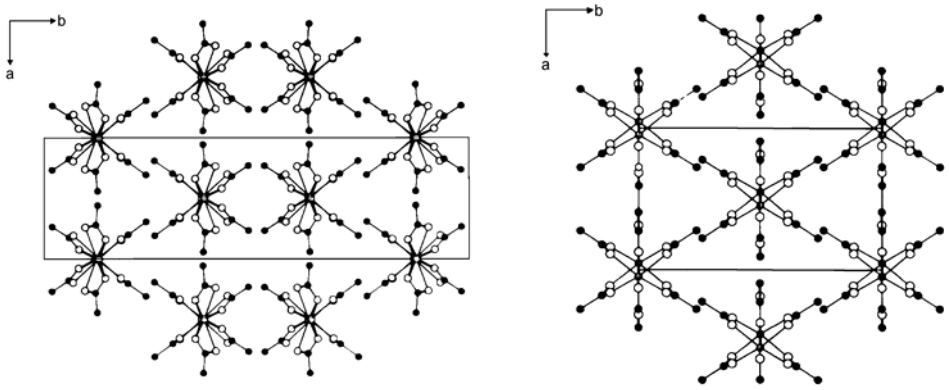

Figure 2-3 Crystal structure of $Lu(CH_3CO_2)_3$ (left) and of $Ho(CH_3CO_2)_3$ [55]

Corkery and Martin investigated europium(III) dodecanoate and mixtures of europium(III) and lanthanum(III) dodecanoate by high-resolution luminescence spectroscopy [60]. They found that at least two symmetrically distinct europium(III) sites are present in samples obtained by slow cooling of melts.

It was not before 1998 that the mesomorphic behaviour of lanthanide(III) alkanoates was investigated. Marques found liquid crystallinity in cerium(III) soaps and, based on the textures observed by thermo-optical microscopy, the authors suggested that cerium tetradecanoate and its higher homologues formed disordered smectic mesophases, whereas more complex mesophase behaviour was observed for cerium soaps with shorter chain lengths [52]. Binnemans identified the mesophase formed by lanthanum(III) tetradecanoate and its higher homologues as a smectic A phase. These compounds were found to adopt a lamellar bilayer structure. The layer spacing in the crystalline lamellar phase at moderate temperature was close to the calculated thickness of a bilayer with the *all trans* alkyl tails normal to the ionic sublayer [61].
Since Binnemans observed a very pronounced effect of the contraction of the lanthanide ion radius on the transition temperatures of lanthanide containing metallo-

mesogens with Schiff's base ligands, we were interested in ascertaining whether a similar effect could be found for the lanthanide(III) alkanoates [62].

A very interesting point are the adducts of lanthanide(III) alkanoates with 1,10-phenanthroline Lebedev synthesised in 1995 [$Eu(C_5H_{11}CO_2)_3$·1,10-phenanthroline] [63]. This compound crystallises in the space group $P2_1/n$ ($Z = 4$). The crystals are built of centrosymmetric dimeric molecules, whereby three different carboxylate groups are present. The coordination of the europium atom is supplemented by the bidentate phenanthroline molecule, resulting in the coordination number nine. The structure of [$Ce(CH_3CO_2)_3$·1,10-phenanthroline] and of [$Gd(CH_3CO_2)_3$·1,10-phenanthroline] are also known [64]. These compounds are well studied because of their optical properties (in particular because of the strong luminescence of the europium adducts) [65 - 68].

Another topic is the complexation of lanthanides with 4-alkoxybenzoic acids. It is well known that these ligands are mesomorphic [69 - 70]. Most of the compounds from the series $C_xH_{2x+1}OC_6H_4CO_2H$ show several mesophases like a smectic C and a nematic phase. It is not so surprising that these compounds are that much studied because of their rigid core built by hydrogen bonds [71 - 76]. However, 4-alkoxybenzoic acids are often used as starting products for the synthesis of ligands [77 - 78].
Until now, no information is available on the complexes of lanthanide ions with 4-alkoxybenzoic acids as ligands, although some papers have been published on the synthesis and structure of benzoates and derivatives hereof [79 - 82].

A last point of interest are the lanthanide(III) alkylsulphates. These compounds are well known for there catalytic behaviour in aldol reactions [83 - 86]. In the past the lyotropic mesomorphism of sodium dodecylsulphate was investigated thoroughly [87 - 91]. The existence of a lyotropic mesophase in lanthanide(III) alkylsulphates was used for the synthesis of nanostructural polymers, although these groups did not use pure lanthanide(III) alkylsulphates [92 - 94].

Lanthanide(III) alkylsulphates were used in the last few years as counter ions in for example lanthanide Schiff's base complexes [95 - 96]. Moreover our group found that lanthanide(III) dodecylsulphates show lyotropic mesomorphism in the presence of water and ethylene glycol [97]. However less information is available on the structure and thermal behaviour of these complexes [98 - 99]. So a detailed study of the structure and the lyotropic mesomorphism is very interesting.

References

[1] E. R. Braithwaite *Solid Lubricants and Surfaces* Pergamon Press, Oxford **1964.**

[2] R. H. Perry, D. W. Green, J. O. Maloney, *Perry's Chemical Engineers' Handbook, sixth edition* McGrow-Hill Book Co, Singapore **1984.**

[3] H. J. Braun *Die Metalseifen* Otto Spamer Verlag, Leipzig **1932**.

[4] S. B. Elliot *The Alkali-Earth and Heavy-Metal Soaps* Reinhold, New York **1946**.

[5] B. N. Figgis, R. L. Martin *J. Chem. Soc.* (1956) 3837.

[6] R. L. Martin, H. Watermans *J. Chem.Soc.* (1957) 2147.

[7] M. J. Bird, T. R. Lomer *Acta Cryst.* **B28** (1972) 242.

[8] T. R. Lomer, K. Perera *Acta Cryst.* **B30** (1974) 2912.

[9] J. Barbéra in *Metallomesogens* (ed. J. L. Serrano) VCH-Wiley, Weinheim **1996**.

[10] R. F. Grant *Can. J. Chem.* **42** (1964) 951.

[11] A. M. Giroud-Godquin in *Handbook of Liquid Crystals, vol. 2B* VCH-Wiley Weinheim **1998**.

[12] A.M. Giroud-Godquin, J.C. Marchon, D. Guillon, A. Skoulios *J. Phys. Chem.* **90** (1986) 5502.

[13] P. Maldivi, A. M. Giroud-Godquin, J. C. Marchon, D. Guillon, A. Skoulios *Chem. Phys. Lett.* **157** (1989) 552.

[14] L. Bonnet, F. D. Cubiernik, P. Maldivi, A. M. Giroud-Godquin, J. C. Marchon, M. Ibn-Elhaj, D. Guillon, A. Skoulios *Chem. Mater.* **6** (1994) 31.

[15] H. Abied, D. Guillon, A. Skoulis, P. Weber, A. M. Giroud-Godquin, J. C. Marchon *Liq. Cryst.* **2** (1987) 269.

[16] A. M. Giroud-Godquin, J. C. Marchon, D. Guillon, A. Skoulios, *J. Physique. Lett.* **45** (1984) 682.

[17] M. Ibn-Elhaj, D. Guillon, A. Skoulios, A. M. Giroud-Godquin, P. Maldivi *Liq. Cryst.* **11** (1992) 731.

[18] G. S. Attard, P. R. Cullum *Liq. Cryst.* **8** (1990) 299.

[19] G. S. Attard, R. H. Templer *J. Mater. Chem.* **3** (1993) 207.

[20] P. Maldivi, L. Bonnet, A. M. Giroud-Godquin, M. Ibn-Elhaj, D. Guillon, A. Skoulios *Adv. Mater.* **5** (1993) 909.

[21] J. Barbéra, M. A. Esteruelas, A. M. Levelut, L. A. Oro, J. L. Serrano, E. Sola *Inorg. Chem.* **31** (1992) 732.

[22] A. Skoulios, V. Luzatti *Nature (London)* **183** (1959) 1310.

[23] A. Skoulios, V. Luzatti *Acta Cryst.* **14** (1961) 278.

[24] P. A. Spegt, A. Skoulios *Acta Cryst.* **16** (1963) 301.

[25] S. N. Misra, T. N. Misra, R. C. Mehrotra *J. Inorg. Nucl. Chem.* **25** (1963) 195.

[26] S. N. Misra, T. N. Misra, R. C. Mehrotra *J. Inorg. Nucl. Chem.* **25** (1963) 201.

[27] L. Carette, M. Gay *Patentno. FR2,534,263* (1984) [CA 101:131860g]

[28] P. Ducros *J. Less-Common Met.* **111** (1985) 37.

[29] R. Hussain, F. Mahmood *J. Chem. Soc. Pakistan* **16** (1994) 225.

[30] I. Hakozaki, Y. Ishikawa *Plastic Age* **36** (1990) 173.

[31] Y. Lin *J. Rare Earths* **14** (1996) 98.

[32] M. C. Throckmorton *Kaut. Gummi Kunstst.* **22** (1969) 293.

[33] G. N. Sauvion, P. Ducros *J. Les-Common Met.* **111** (1985) 23.

[34] A. M. Mourao, C. H. Faist *Patentno. US4,522,631* (1985) [CA 103:56613q].

[35] K. Ida *Patentno. JP 60,161,458* (1985) [CA 104:6692q].

[36] A. Zhang, H. Ming, Y. Zhai *Polymer International* **41** (1996) 413.

[37] A. Zhang, H. Ming, Y. Zhai *J. Appl. Polym. Sci.* **62** (1996) 887.

[38] R. P. Varma, R. Jindal *Tenside Detergents* **20** ((1982) 193.

[39] K. N. Mehrotra, R. K. Shukl, M. Chauhan *J. Appl. Polymer Sci.* **39** (1990) 1745.

[40] K. N. Mehrotra, S. Gupta *J. Indian Chem. Soc.* **70** (1993) 577.

[41] A. Kumar, *Phys. Chem. Liq.* **28** (1994) 57.

[42] S. K. Upadhyaya *Phys. Chem. Liq.* **27** (1994) 11.

[43] K. N. Mehrotra, N. Sharma *Monatsh. Chem.* **127** (1996) 257.

[44] K. N. Mehrotra, R. K. Shukla, M. Chauhan *Colloids and Surfaces A: Physicochem. Eng. Aspects* **119** (1996) 67.

[45] K. N. Mehrotra, M. Chauhan, R. K. Shukla *Monatsh. Chem.* **120** (1989) 1063.

[46] K. N. Mehrotra, A. S. Gahlaut, M. Sharma *J. Indian Chem. Soc.* **64** (1987) 309.

[47] K. N. Mehrotra, S. K. Upadhyaya *Polish J. Chem.* **65** (1991) 1035.

[48] K. N. Mehrotra, V. Kumari, A. Kumar *Polish. J. Chem.* **67** (1993) 2065.

[49] S. K. Upadhyaya, P. S. Sharma *J. Indian Chem. Soc.* **70** (1993) 735.

[50] K. N. Mehrotra, N. Sharma *Polish J. Chem.* **70** (1996) 1236.

[51] G. B. Deacon, R. J. Philips *Coord. Chem. Rev.* **33** (1980) 227.

[52] E. F. Marques, H. D. Burrows, M. da Graça Miguel *J. Chem. Soc. Faraday Trans.* **94** (1998) 1729.

[53] A. Ouchi, Y. Suzuki, Y. Ohki, Y. Koizumi *Coord. Chem. Rev.* **92** (1988) 29.

[54] Gmelin Handbook on Inorganic Chemistry, Sc, Y, La-Lu, Carboxylates, Vol D5, 1984.

[55] G. Meyer, D. Gieseke-Vollmer *Z. anorg. Allg. Chem.* **619** (1993) 1603.

[56] A. Lossin, G. Meyer *Z. anorg. Allg. Chem.* **619** (1993) 1609.

[57] A. Lossin, G. Meyer *Z. anorg. Allg. Chem.* **620** (1994) 438.

[58] M. A. Nabar, S. D. Barve *J. Appl. Crystallogr.* **17** (1984) 39.

[59] D. Deiters, G. Meyer *Z. anorg. allg. Chem.* **622** (1996) 325.

[60] R. W. Corkery, J. P. D. Martin *J. Lumin.* **82** (1999) 1.

[61] K. Binnemans, B. Heinrich, D. Guillon, D. W. Bruce *Liq. Cryst.* **26** (1999) 1717.

[62] K. Binnemans, R. Van Deun, D. W. Bruce, Y. G. Galyametdinov *Chem. Phys.Lett.* **300** (1999) 509.

[63] M. A. Poraikoshits, A. S. Antsyshkina, G. G. Sadikov, E. N. Lebedeva, S. S. Korovin, R. N. Shchelokov, V. G. Lebedev *Russian J. Inorg. Chem.* **40** (1995) 748.

[64] A. Panagiotopoulos, T. F. Zafiropoulos, S. P. Perlepes, E. Bakalbassis, E. Masson-Ramade, O. Kahn, A. Terzis, C. Raptopolou *Inorg. Chem.* **34** (1995) 4918.

[65] B. Yan, H. J. Zhang, S. B. Wang, J. Z. Ni *Spectr. Lett.* **31** (1998) 603.

[66] R. F. Wang, L. S. Li, S. Z. Lu *J. Rare Earths* **16** (1998) 149.

[67] V. Tsaryuk, V. Zolin, J. Legendziewicz *Spectr. Acta. A Molec. Biomolec. Spectr.* **54** (1998) 2247.

[68] Z. M. Wang, L. J. van de Burgt, G. R. Choppin *Inorg. Chim. Acta* **293** (199) 167.

[69] A. J. Herbert *Trans. Faraday Soc.* **63** (1967) 555.

[70] A. Blumstein, L. Platel *Mol. Cryst. Liq. Cryst.* **48** (1978) 151.

[71] R. F. Bryan, P. Hartley, R. W. Miller, M. S. Shen *Mol. Cryst. Liq. Cryst.* **62** (1980) 281.

[72] R. F. Bryan, P. Hartley *Mol. Cryst. Liq. Cryst.* **62** (1980) 259.

[73] L. M. Babkov, O. V. Gorshkov, N. A. Golovina, G. A. Puchkovskay, I. N. Khakimov *J. Struct. Chem.* **36** (1995) 302.

[74] T. Kato, Y. Kubota, M. Nakano, T. Uryu *Chem. Lett.* **1995** 1127.

[75] M. Plass *Z. Phys. Chem. Int. Ed.* **194** (1996) 223.

[76] P. Painter, C. Cleveland, M. Coleman *Mol. Cryst. Liq. Cryst.* **348** (2000) 269.

[77] K. Binnemans, D. W. Bruce, S. R. Collinson, R. Van Deun, Y. G. Galyametdinov, F. Martin *Phil. Trans. R. Soc. Lond A.* **357** (1999) 3063.

[78] K. Binnemans, Y. G. Galyametdinov, R. Van Deun, D. W. Bruce, S. R. Collinson, A. P. Polishchuk, I. Bikchantaev, W. Haase, A. V. Prosvirin, L. Tinchurina, I. Litvinov, A. Gubajdullin, A. Takhmatullin, K. Uytterhoeven, L. Van Meervelt *J. Am. Chem. Soc.* **122** (2000) 4335.

[79] A. Kula, W. Brzyska *Polish J. Chem.* **74** (2000) 45.

[80] Z. Keli, Y. Jibing, Y. Liangjie, S. Jutang *J. Rare Earths* **17** (1999) 255.

[81] M. D. Taylor, C. P. Carter, C. I. Wynter *J. inorg. nucl. Chem.* **30** (1968) 1503.

[82] W. Ferenc, B. Bocian, D. Mazur *Croatica Chimica Acta* **72** (1999) 779.

[83] S. Kobayashi, T. Wakabayashi *Tetrahedron Lett.* **39** (1998) 5389.

[84] K. Manabe, S. Kobayashi *Chem.Comm.* **2000** 669.

[85] K. Manabe, S. Kobayashi *Tetrahedron Lett.* **40** (1999) 3773.

[86] K. Manabe, Y. Mori, S. Kobayashi *Tetrahedron* **55** (1999) 11203.

[87] S. Yano, K. Tadano, K.Aoki *Mol. Cryst. Liq. Cryst.* **92** (1983) 99.

[88] X. Auvray, C. Pepitas, I. Rico, A. Lattes *Liq.Cryst.* **17** (1994) 109.

[89] R. Itri, L. Q. Amaral, P. Mariani *Phys. Rev. E* **54** (1996) 5211.

[90] P. Kekicheff, B. Cabane *Acta Cryst. B* **44** (1988) 395.

[91] M. P. McDonnald, W. E. Peel *J. Chem. Soc. Faraday Trans.* **72** (1976) 2274.

[92] H. Deng, L. Gin, R. C. Smith *J. Am. Chem. Soc.* **120** (1998) 3522.

[93] M. Yada, H. Kitamura, M. Machida, T. Kijima *Inorg. Chem.* **37** (1998) 6470.

[94] M. Yada, M. Ohya, M. Machida, T. Kijima *Chem. Comm.* **1998** 1941.

[95] Y. G. Galyametdinov, G. I. Ivanova, I. V. Ovchinnikov, K. Binnemans, D. W. Bruce *Russ. Chem. Bull.* **48** (1999) 385.

[96] R. Van Deun, K. Binnemans *Liq.Cryst.* **28** (2001) 621.

[97] Y. Galyametdinov, H. B. Jervis, C. W. Bruce, K. Binnemans *Liq. Cryst.* **28** (2001) 1877.

[98] G. Schaack, J. A. Koningstein *Can. J. Chem.* **51** (1973) 1023.

[99] Y. Kato, T. Krimoto, T. Takenaka *Spectrochimica. Acta* **33A** (1977) 1033.

Chapter 3 Lanthanide(III) Complexes of n-Alkanoic Acids

3.1 Synthesis and Characterisation

Here the synthesis and characterisation of the series $Nd(C_xH_{2x+1}CO_2)_3$ is described. The synthesis and characterisation of all the compounds of the series $Ln(C_{11}H_{23}CO_2)_3$, $La(C_xH_{2x+1}CO_2)_3$, $Ce(C_xH_{2x+1}CO_2)_3$, $Pr(C_xH_{2x+1}CO_2)_3$, $Sm(C_xH_{2x+1}CO_2)_3$ and $Eu(C_xH_{2x+1}CO_2)_3$ is analogous to this first series. In Table 1.1-1 - Table 1.1-8, Appendix 1 the elemental analysis results of all these series can be found.

3.1.1 Synthesis

3.1.1.1 Synthesis

The series of homologous neodymium(III) alkanoates from neodymium(III) butyrate, $Nd(C_3H_7CO_2)_3$, to neodymium(III) eicosanoate, $Nd(C_{19}H_{39}CO_2)_3$, was synthesized by a metathesis reaction between the sodium salt of the corresponding fatty acid and neodymium(III) nitrate hexahydrate in an aqueous ethanol solution (ethanol:water 1:1). For the neodymium(III) alkanoates with short chain lengths (neodymium(III) octanoate and shorter homologues), water was the reaction medium, because the neodymium(III) soaps are too soluble in an ethanol:water mixture. For the compounds with the longest chain lengths (neodymium(III) tetradecanoate and the higher

homologues), it was necessary to carry out the reaction in ethanol due to solubility problems with the corresponding sodium salts.

The neodymium(III) alkanoates are waxy, blue-violet powders (i.e. with the colour of the corresponding trivalent lanthanide ion [1]).

The reactions are pH dependent, in the sense that for the reactions the pH of the sodium alkanoate solution has to be adapted between 7 and 12. When pH < 6, no complexes are formed because the alkanoate anion is transformed into the corresponding fatty acid. At pH > 12 mixed hydroxy complexes of the type $Nd(OH)_y(C_xH_{2x+1}CO_2)_{3-y}$ ($0 < y \leq 3$) are formed.

3.1.1.2 Synthesis of Neodymium(III) Butyrate

Nd(III) butyrate was prepared by a reaction between Nd(III) hydroxide and butyric acid. Pure $Nd(OH)_3$ was obtained through hydrothermal synthesis. Neodymium nitrate hexahydrate, $Nd(NO_3)_3 \cdot 6H_2O$, (1.00 g, 2.28 mmol) and NaOH (3.00g, 25 mmol) were dissolved in water (15 mL), and the resulting solution was heated in a teflon bomb for 4 days at 220°C. Afterward, the solution was left to slowly cool down to room temperature, at a cooling rate of 4°C/hour. Crystalline $Nd(OH)_3$ was obtained and its purity was checked by X-ray powder diffraction. The pure hydroxide was dissolved in diluted butyric acid (butyric acid:water 1:1). Single crystals suitable for X-ray analysis were obtained by slow evaporation of the solution in air. The transparent crystals were lath-like and had the typical purple colour of the trivalent neodymium ion.

Exptl. for $Nd(C_3H_7CO_2)_3 \cdot H_2O$: Experimental for C: 33.84%, for H: 5.27%; Calculated for C: 34.03%, for H: 5.47%

3.1.1.3 Synthesis of Neodymium(III) Pentanoate

Pentanoic acid (1.024g, 10.04 mmol) and triethylamine (1.016 g, 10.04 mmol) were dissolved in toluene (50 mL), and $NdCl_3 \cdot 6H_2O$ (0.599 g, 1.67 mmol) was added. The solution was heated at reflux for 48 hours. After leaving the solution to cool to room temperature, water was added to the toluene solution to dissolve triethylammonium chloride. The precipitate was filtered and washed with water and ethanol to remove traces of the neodymium salt, the fatty acid or triethylammonium chloride. Neodymium(III) pentanoate was dried for 24 hours in vacuum at 50 °C. Yield: 0.14 g (19 %).

Exptl. for $Nd(C_4H_9CO_2)_3 \cdot H_2O$: Experimental for C: 38.80%, for H: 6.26%; Calculated for C: 38.69%, for H: 6.28%

3.1.1.4 Synthesis of Neodymium(III) Dodecanoate

Dodecanoic acid (2.75 g, 13.8 mmol) was dissolved in 100 mL of an ethanol:water mixture (1:1), and transformed into sodium dodecanoate by adding an equivalent amount of a 0.5 M NaOH standard solution (addition via a burette). Neodymium nitrate hexahydrate (2.00 g, 4.56 mmol) was dissolved in 100 mL of an ethanol:water mixture (1:1). The neodymium(III) nitrate solution was added dropwise to a stirred solution of sodium dodecanoate (at ambient temperature). A light blue-purple precipitate immediately formed. After addition was complete, the mixture was stirred for one hour at ambient temperature. Subsequently, the precipitate was filtered on a Büchner funnel, washed with water, ethanol and acetone, in order to remove traces of the neodymium(III) salt or of the dodecanoic acid. The crude neodymium(III) dodecanoate was dried for 24 hours in vacuum at 50 °C, and recrystallised from a 1-pentanol:ethanol (5:1) mixture. Placing the solution in a refrigerator completed crystallisation. The purified soap was filtered on a funnel, washed with ethanol to

remove most of the 1-pentanol, and dried in vacuum (10^{-3} mbar) at 50 °C for at least 24 hours. Neodymium(III) dodecanoate was obtained as a light violet powder. Yield: 2.85 g (84 %).
All the other neodymium(III) alkanoates were prepared by a similar method.

Exptl. for $Nd(C_{11}H_{23}CO_2)_3 \cdot ½H_2O$: Experimental for C: 57.61%, for H: 9.40%; Calculated for C: 57.69%, for H: 9.42%

3.1.2 Characterisation

All the compounds were characterised by CH elemental analysis, infrared spectroscopy and X-ray diffraction at room temperature. The lanthanide(III) content of the series $Ln(C_{11}H_{23}CO_2)_3$ and $Nd(C_xH_{2x+1}CO_2)_3$ was determined titrimetically.

3.1.2.1 Elemental Analysis

The carbon and hydrogen content of the lanthanide(III) soaps were determined by CH elemental microanalysis (combustion analysis).
The analysis results are consistent with an alkanoic acid to lanthanide(III) ratio of 3:1, but also indicate that under the given reaction conditions the compounds cannot be obtained in a total anhydrous form. In nearly all lanthanide(III) alkanoates water molecules were present. The compounds were hemihydrates, $Ln(C_xH_{2x+1}CO_2)_3 \cdot ½H_2O$, or monohydrates, $Ln(C_xH_{2x+1}CO_2)_3 \cdot H_2O$. Only the long chain homologues are anhydrous.

3.1.2.2 Determination of the Lanthanide(III) Content

200 mg of the compound was dissolved in 15 mL of a hot 0.1 M H_2SO_4 solution. After cooling, the solution was extracted with diethyl ether to remove dodecanoic acid. The lanthanide solution was transferred to a volumetric flask and water was added till 20 mL.

5 mL hereof was put in a beaker with a volumetric pipette, and the pH was adjusted by a hexamethylenetetramine buffer to pH = 6. Xylenol orange was added as an indicator, and the solution was titrated with a 0.01 M EDTA standard solution, until the indicator changed colour from purple to yellow. The solution was heated to 60 °C to make the colour change better visible.

3.1.2.3 Infrared Spectroscopy

Infrared spectra in the spectral region from 400 – 4000 cm^{-1} were recorded for all the lanthanide(III) alkanoates. In Figure 3-1 the infrared spectra of some neodymium(III) alkanoates and some lanthanide(III) dodecanoates are given.

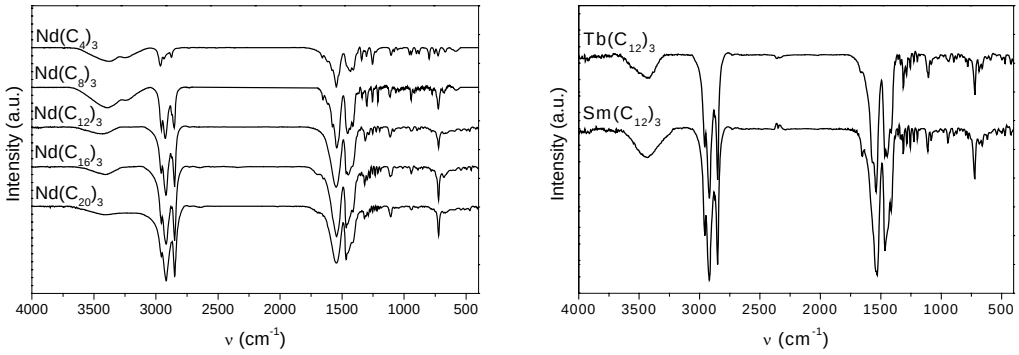

Figure 3-1 Infrared spectra of selected neodymium(III) alkanoates (left) and lanthanide(III) dodecanoates

The most remarkable difference between the infrared spectra of different complexes is the number of CH_2 wagging progression bands, observable in the 1350-1150 cm^{-1}

spectral region as a set of regularly spaced peaks. These bands are an indication that the chains are in *all trans* conformation [2]. For an even number of carbon atoms in the alkyl chain, the number of IR bands is n/2 (n being the total number of carbon atoms in the alkyl chain). For an odd number of carbon atoms, the number of IR bands is equal to (n+1)/2.

The C=O stretching vibration observed in the alkanoic acid at ca. 1700 cm^{-1} disappears after complexation of the carboxylic acid with a lanthanide ion and is replaced by two new absorption bands. These bands correspond to the symmetric stretching vibration of the carboxylate anion (1410 – 1420 cm^{-1}) and the asymmetric stretching vibration (1520 – 1550 cm^{-1}). The interaction between the lanthanide(III) ion and the carboxylate group might be evaluated by considering the splitting of the two carboxylate bands, being 120 – 130 cm^{-1} in our complexes. This splitting remains constant for complexes with different lanthanide(III) ions and different chain lengths. In comparison to the carboxylate stretching vibrations in sodium alkanoates (ν_s at 1427 cm^{-1} and ν_{as} at 1565 cm^{-1}, $\Delta\nu$ = 138 cm^{-1}) [3] , both infrared bands are shifted to lower wave numbers and the splitting is reduced. Although $\Delta\nu$ is often used to probe the carboxylate coordination [4], we do not think that this approach is very suitable for lanthanide(III) alkanoates, because the single-crystal structure of some lanthanide(III) butyrates monohydrates indicates that more than one type of carboxylate coordination is present in each compound. *(see further)*

The other transitions in the infrared spectra correspond to vibrations due to the alkyl chains except for a broad band at ca. 3450 cm^{-1} (OH-stretching of water molecules) [3].

The fact that $\Delta\nu$ is independent of the alkyl chain length is an indication that no major structural changes occur when extending the alkyl chain length toward higher homologues. Moreover $\Delta\nu$ is also independent of the lanthanide ion. This means that the overall structure proposed for a given lanthanide(III) alkanoate is also valuable for alkanoates with other chain lengths or lanthanide ions.

Table 3.1-1 IR assignment for $Nd(C_7H_{15}CO_2)_3$, $Nd(C_{11}H_{23}CO_2)_3$ and $Sm(C_{11}H_{23}CO_2)_3$

Assignment[a]	Intensity[b]	$Nd(C_7H_{15}CO_2)_3$ / cm^{-1}	$Nd(C_{11}H_{23}CO_2)_3$ / cm^{-1}	$Sm(C_{11}H_{23}CO_2)_3$ / cm^{-1}
ν_{as} (CH_2)	m	2956	2956	2956
ν_{as} (CH_3)	s	2926	2918	2921
ν_s (CH_3)	m	2872	2873	2879
ν_s (CH_2)	s	2852	2851	2850
ν_{as} (COO)	s	1543	1544	1540
δ_{as} (CH_2)	s	1456	1466	1465
δ_{as} (CH_3)	s	1435	1449	1452
ν_s (COO)	s	1414	1415	1413
long chain rocking	w	723	721	721

[a] ν_{as} denotes asymmetric stretching, ν_s symmetric stretching, δ_{as} asymmetric bending
[b] s = strong, m = medium, w = weak

3.1.2.4 X-ray Diffraction at Room Temperature

Room temperature X-ray powder diffractograms were recorded for the entire series $Ln(C_{11}H_{23}CO_2)_3$, $La(C_xH_{2x+1}CO_2)_3$ and $Nd(C_xH_{2x+1}CO_2)_3$. Up to eight peaks were observed in the small-angle region of the X-ray powder diffractograms of the solid lanthanide(III) alkanoates, with the peak at the smallest angles being by far the highest intensity. The X-ray diffractograms of $La(C_5H_{11}CO_2)_3$ and $Nd(C_{13}H_{27}CO_2)_3$ are given in Figure 3-2.

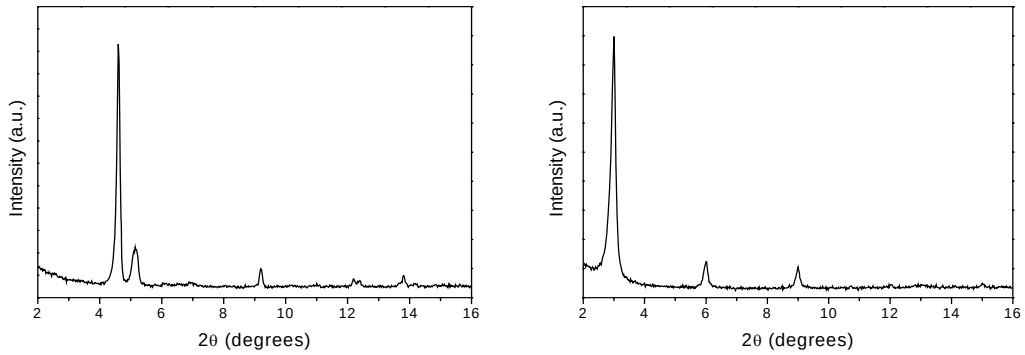

Figure 3-2 X-ray diffractograms of $La(C_5H_{11}CO_2)_3$ (left) and $Nd(C_{13}H_{27}CO_2)_3$, room temperature

The *d* spacing values in the low angle region are in the ratio 1:1/2:1/3…1/n. These diffraction peaks correspond to the successive (00*l*) reflections and indicate the presence of a lamellar structure. The polar groups of the lanthanide(III) alkanoates are localized in infinite, parallel, and equidistant planes. These planes are separated from each other by a bilayer of alkyl chains in the *all trans* conformation. The interplanar layer spacing *d* corresponds to the distance between two successive layers of lanthanide(III) ions.

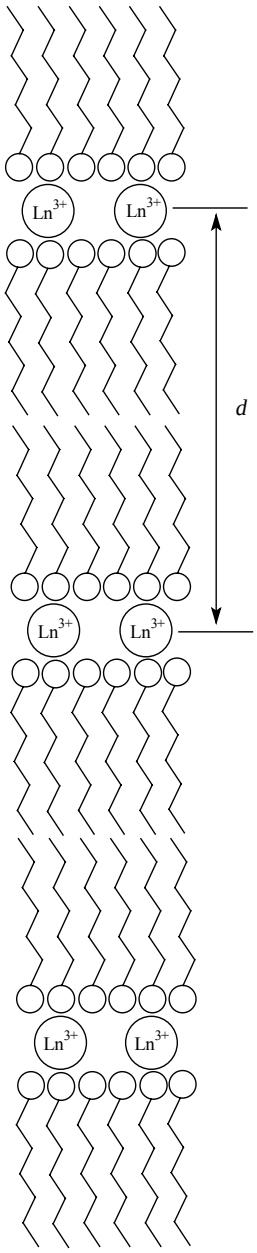

Figure 3-3 Schematic representation of the layered structure of lanthanide(III) alkanoates

The fact that the alkyl chains are in *all trans* conformation is supported by the good agreement between experimental and calculated maximal average *d* spacing values (d_{max}) (see Table 1.2-1 - Table 1.2-3, Appendix 1). The maximal average *d* spacing of the bilayer structure was calculated for an *all trans* conformation of the alkyl chain perpendicular to the metal ion base plane using the formula [5] :

Equation 3-1

$$d_{\max} = 2d_{C-H} + 2(n-1)d_{C-C}\sin 55° + 2d_{C-O} + 2r_{Nd^{3+}}$$

where *n* = total number of carbon atoms, $d_{C\text{-}H}$ = 1.09Å, $d_{C\text{-}C}$ = 1.54Å, and $d_{C\text{-}O}$ = 1.36Å. The ionic radius of the lanthanide(III) ions (coordination number 9) are taken from Shannon [6]. The calculated *d* value for $Sm(C_{11}H_{23}CO_2)_3$ is 34.57 Å, the experimental *d* value hereof is 34.44 Å.

The increment in *d* spacing due to addition of a CH_2-group is 2.52 Å with the alkyl chain in *all trans* conformation. Experimentally, we find an average increment of 2.41 Å. This constant increment is also an indication that the crystal structure of the compounds does not change drastically when varying the alkyl chain length.

For some of the short chain homologues of the series $La(C_xH_{2x+1}CO_2)_3$ and $Nd(C_xH_{2x+1}CO_2)_3$ (x = 4 – 8) the (00*l*) reflection is split in two peaks, and the second peak has a *d* spacing which is 1 to 4 Å shorter than the *d* spacing corresponding to the (00*l*) peak with the highest intensity (see Figure 3-2). The appearance of this second peak is an indication that more than one crystal modification is present in our samples. Because of the purity (+99%) of the fatty acids used for synthesis of the lanthanide(III) alkanoates, the possibility that the satellite peaks are due to impurities of compounds with shorter chain lengths can be neglected.
In the wide-angle region ($2\theta \sim 22°$) a broad weak band is observed for the compounds with long alkyl chains. This indicates absence of long range order of the alkyl chains in the bilayers.

It should be noted that although these compounds are not anhydrous, the presence of water does not influence the lamellar structure. This is because the water molecules are situated in the ionic layer of these compounds.

The bilayer structure described herein is not restricted to lanthanide soaps. In fact, Skoulios and Luzatti first described this mesophase structure for alkali metal soaps in the ‘neat soap’ lamellar mesophase [7].

3.2 Crystal Structure of $La(C_3H_7CO_2)_3 \cdot H_2O$ and of $Nd(C_3H_7CO_2)_3 \cdot H_2O$

Lanthanum(III) butyrate monohydrate and neodymium(III) butyrate monohydrate crystallise in the triclinic space group $P\bar{1}$ (no. 2). In the crystal structure, two crystallographically different lanthanide ions are present, both having coordination number 9. The coordination polyhedra can be described as monocapped square antiprisms (Figure 3-4) and is the same for both lanthanide(III) butyrates.

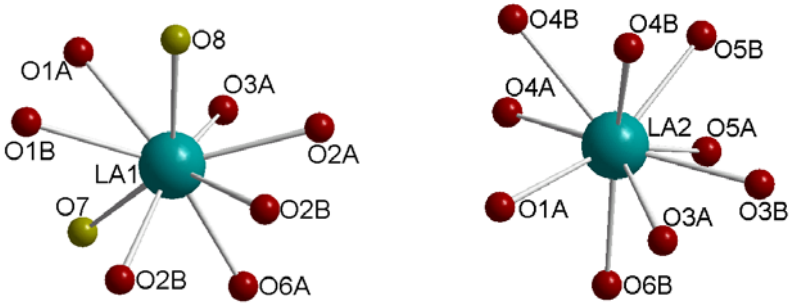

Figure 3-4 First coordination sphere of La1 and La2 in lanthanum(III) butyrate monohydrate

La1 is surrounded by two oxygens of water molecules and by seven oxygens of five carboxylate groups. Four of these carboxylate groups are bridging tridentate and one is *Z,E* type bridging bidentate. La2 is coordinated by nine oxygens originating from four bridging tridentate carboxylates, one *Z,E* type bridging bidentate carboxylate group and one chelating type bidentate (for the several types of coordination, see Figure 2-2). The coordination polyhedra are connected via common edges to zigzag chains (see Figure 3-6). These common edges consist of two oxygen atoms, each belonging to a bridging tridentate carboxylate group. Such a bridging tridentate coordination of carboxylate groups is discussed by Ouchi [8].

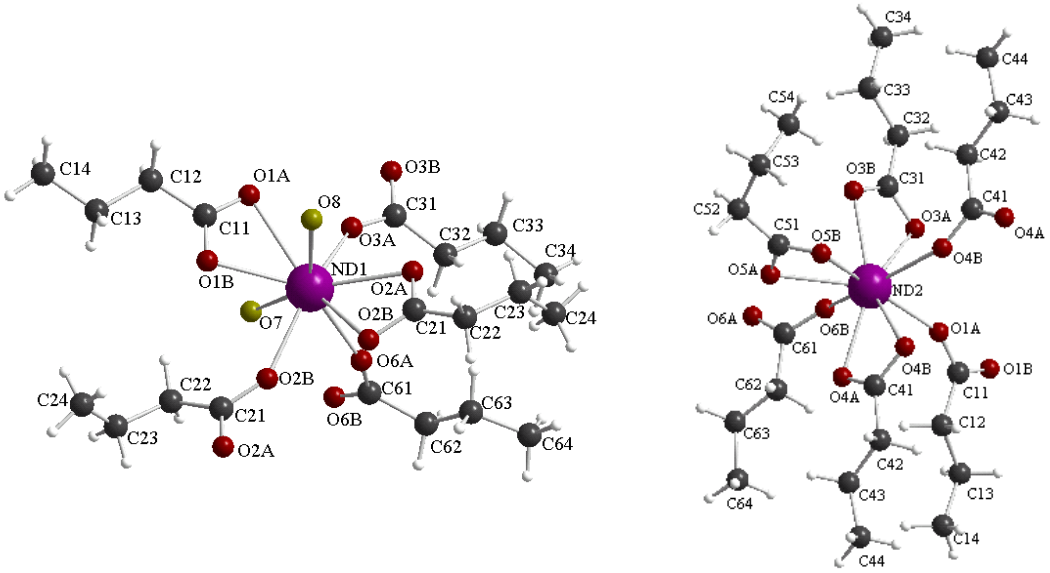

Figure 3-5 Coordination of the two different entities in the crystal structure of neodymium(III) butyrate monohydrate

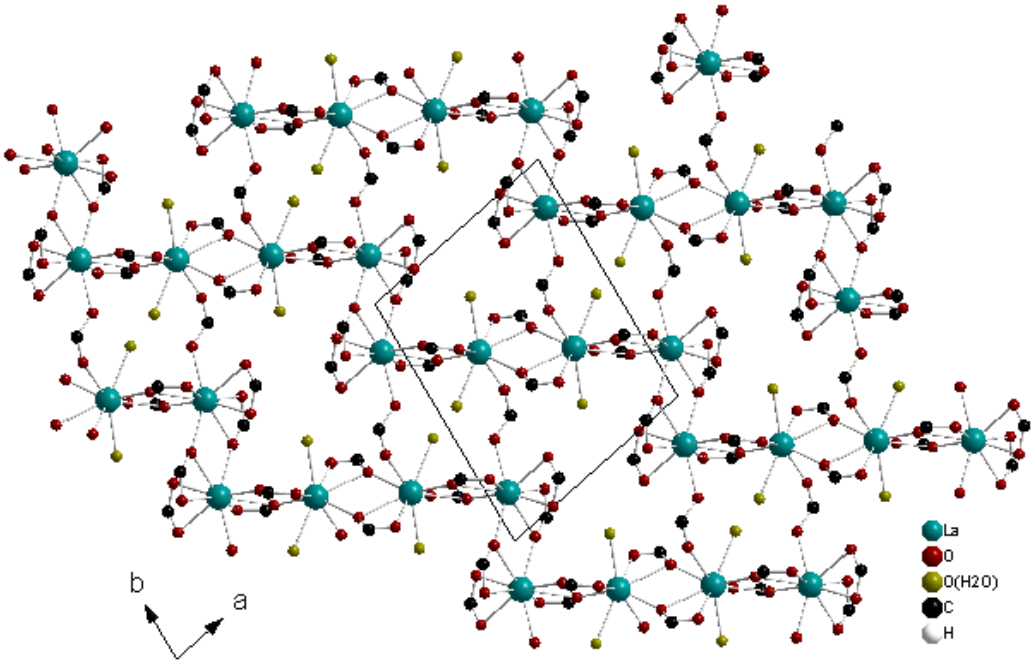

Figure 3-6 Zigzag chains of lanthanum(III) ions in lanthanum(III) butyrate monohydrate

The chains of lanthanide ions are connected to one another by bridging bidentate carboxylate groups. The alkyl chains of the butyrate groups are in the *all trans* conformation and are placed perpendicular to the lanthanide layers. In fact, these compounds form a polymeric structure, which has large consequences for the thermal behaviour.

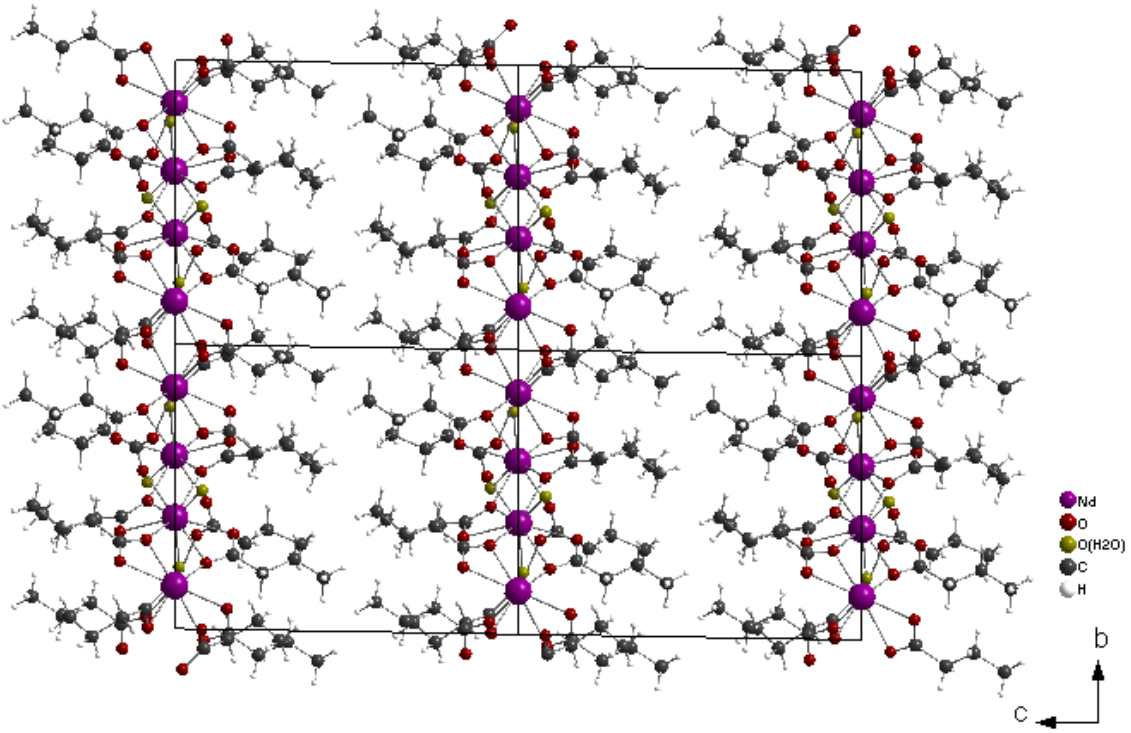

Figure 3-7 Crystal structure of neodymium(III) butyrate monohydrate viewed down the *a*-axis

The temperature factors of the terminal methyl groups are relatively large, which is due to a strong disorder of these groups. The large R-values of both structures can be explained by the fact that it is very difficult to obtain good crystals of layered structures for structure analysis.

Crystallographic information and data collection parameters for lanthanum(III) butyrate monohydrate and neodymium(III) butyrate monohydrate can be found in Table 3.2-1 and Table 3.2-2. Selected bond lengths and angles are listed in Table 1.3-1 and Table 1.3-2, Appendix 1.

Because the infrared spectroscopy and X-ray powder diffraction at room temperature results are analogous for the entire series $Ln(C_xH_{2x+1}CO_2)_3$ (Ln = La, Ce – Lu except Pm, x = 3 – 19), it is acceptable that there is no major structural difference between the lanthanide(III) butyrates and the higher lanthanide(III) alkanoates.

We propose that the bilayered polymeric structure as pointed out in the crystal structure determination of lanthanum(III) and neodymium(III) butyrate can be used for the investigation of the thermal behaviour of the entire series of lanthanide(III) alkanoates. Lanthanide(III) alkanoates form thus bilayered structures. The lanthanide ions are held together by carboxylate groups and form infinite polymeric layers. The alkyl chains are placed perpendicular to these ionic layers and are in the *all trans* conformation.

Moreover, the fact that lanthanum(III) and neodymium(III) butyrate are monohydrates does not influence this extrapolation, because in the case of hemihydrates or water free compounds, the carboxylate groups can rearrange to a structure with more tridentate carboxylate groups.

The layer like structure of these complexes contrasts to the infinite chains of $Pr(C_2H_5CO_2)_3 \cdot H_2O$ [9]. The alkyl chains of the propionate groups are not long enough to force themselves to a parallel alignment in layers. The butyrate compounds are thus the smallest members in the series of lanthanide(III) alkanoates with the typical bilayer structure of metal soaps [10 - 13].

Table 3.2-1 Summary of crystallographic data for lanthanum(III) butyrate monohydrate

Emperical formula	$C_{24}H_{42}La_2O_{14}$
Fw	832.06
Space group	$P\bar{1}$ (No. 2)
Unit cell dimensions (Å, °)	a = 9.940(2)
	b = 12.182(2)
	c = 14.652(4)
	α = 85.98(3)
	β = 75.62(3)
	γ = 78.17(2)
V (Å^3)	1681.7(7)
Z	2
D_{calc} (g cm^{-1})	1.643
T (K)	293(2)
λ (Å)	0.7107 (Mo-Kα graphite)
θ limits (deg)	2.48 - 26.00
μ (mm^{-1})	2.391
No. of parameters	356
F(000)	824
Reflections collected / unique	13367 / 6178 [R(int) = 0.1938]
Goodness-of-fit on F^2	0.745
Final R indices [$I_0>2\sigma(I_0)$]	R1 = 0.0736, wR2 = 0.1687
R indices (all data)	R1 = 0.1997, wR2 = 0.2089

Table 3.2-2 Summary of crystallographic data for neodymium(III) butyrate monohydrate

Empirical formula	$C_{24}H_{42}Nd_2O_{14}$
Fw	842.72
Space group	$P\bar{1}$ (No. 2)
Unit cell dimensions (Å, °)	a = 9.824(2)
	b = 11.974(2)
	c = 14.633(2)
	α = 86.21(2)
	β = 75.95(2)
	γ = 77.97(2)
V, Å^3	1633.0(5)
Z	2
D_{calc}, g cm^{-3}	1.714
T, K	293
λ, Å	0.7107 (Mo-Kα graphite)
θ limits, deg	2.50-28.13
μ, mm^{-1}	3.018
No. of parameters	362
F(000)	836
Reflections collected / unique	15616 / 7255 [R_{int} = 0.0667]
Goodness-of-fit on F^2	1.046
Final R indices [$I_o > 2\sigma(I)$]	R1 = 0.0879, wR2 = 0.2494
R indices (all data)	R1 = 0.1063, wR2 = 0.2626

3.3 Thermal Behaviour of $Ln(C_xH_{2x+1}CO_2)_3$

3.3.1 Influence of the Lanthanide(III) Ion on the Thermal Behaviour of the Series $Ln(C_{11}H_{23}CO_2)_3$

Whereas in the DSC thermograms of $Ln(C_{11}H_{23}CO_2)_3$ with Ln = Sm – Lu only a single peak is observed (corresponding to the melting point), the DSC thermograms of the dodecanoates of La^{3+}, Ce^{3+}, Pr^{3+} and Nd^{3+} show an additional weaker peak above the melting point, indicating that these compounds form a mesophase on heating.

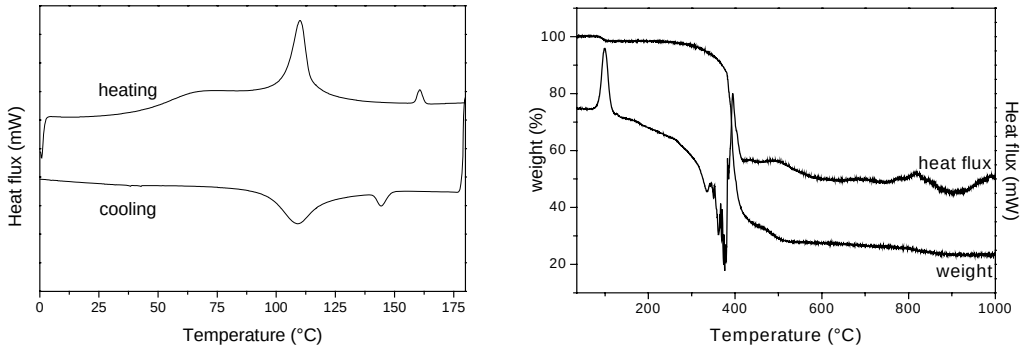

Figure 3-8 DSC thermogram of $La(C_{11}H_{23}CO_2)_3$ (left) and TG/DTA thermogram of $Pr(C_{11}H_{23}CO_2)_3$; endothermic peaks are pointing upwards

The melting peak is rather broad and shows a much higher enthalpy change than the clearing peak. In the cooling run of the DSC measurement a slight supercooling is observed for the clearing transition.

The formation of a mesophase was also evident from the melting point determinations by thermo-optical microscopy. Whereas the compounds showing only one peak in their DSC thermograms melted directly to the isotropic liquid, the La^{3+}, Ce^{3+}, Pr^{3+} and Nd^{3+} dodecanoates first melted to a viscous birefringent liquid. However, it proved to be very difficult to obtain a good defect texture, even by cooling the isotropic liquid, as the compounds showed a very strong tendency to align homeotropically. By

pressing a needle on the cover glass it was possible to observe birefringence, but the molecules quickly reoriented to the homeotropic alignment. The texture was suggestive for a smectic mesophase, most probably a smectic A phase (considering the presence of regions with a homeotropic alignment, see Figure 3-9). It was not easy to visually observe the melting points of the mesomorphic lanthanide(III) alkanoates owing to the high viscosities of the mesophases. The melting temperatures are thus quoted as the temperatures at which the compounds show some fluidity. These temperatures are corroborated by the DSC thermograms and correspond to the maxima of the endothermic melting peaks. The clearing points were detected by thermo-optical microscopy. The transition temperatures and the corresponding enthalpy changes are listed in Table 1.4-1 - Table 1.4-8, Appendix 1. The mesophases have very high viscosities as, unlike in most neutral mesogenic organic molecules or metallomesogens, the lanthanide soaps are built by polymeric sheets of lanthanide ions and carboxylate groups.

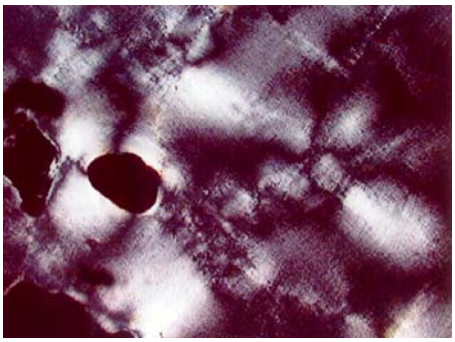

Figure 3-9 Texture of $La(C_{11}H_{23}CO_2)_3$ in the mesophase at 120°C

Large differences in the melting enthalpy were observed between the first and the second heating runs in the DSC measurements. However, the enthalpy values of the clearing peak are consistent for the various compounds. The fact that the melting enthalpy of the first heating run is much higher than that of the second run, can be attributed to the loss of water. This only occurs at the first heating run. Moreover, the compounds do not crystallise completely when cooling from the isotropic liquid, so the compounds are partially amorphous when the second heating run starts. Therefore only the transition temperatures and melting enthalpies of the first heating run were

used. The loss of water in the first heating cycle is confirmed by thermogravimetry (Figure 3-8).

The thermal behaviour of the mesomorphic lanthanide(III) dodecanoates has been investigated by high temperature X-ray diffraction analysis. Although the general features of the X-ray diffractograms in the mesophase remained the same in comparison to those of the solid compounds (except for the disappearance of the higher order peaks), decreases in the *d* spacings were observed at the melting points. The X-ray diffractogram of each mesophase was consistent with a disordered smectic mesophase, indicating that the layered structure present in the solid phase is retained in the mesophase whereas the in plane ordering is largely lost. The latter is reflected by the disappearance of the peak at large angles (at $2\theta \sim 22°$, equivalent to $d \sim 4.2$ Å) and the appearance of a much broader one, which is typical for disordered alkyl chains. Thus, the bilayer structure seen in the solid phase still represents an energetically favourable packing of the carboxylate groups in the mesophase, although the alkyl chains are not longer in the *all trans* conformation. Additionally, the ratio of the peak positions in the low angle region is 1:1/2, indicating a one-dimensional stacking of the layers.

The mesophase can be identified as a smectic A mesophase in that the layer spacings decrease with increasing temperature. For a smectic C phase, an increase in layer spacing would be expected with increasing temperature [14].

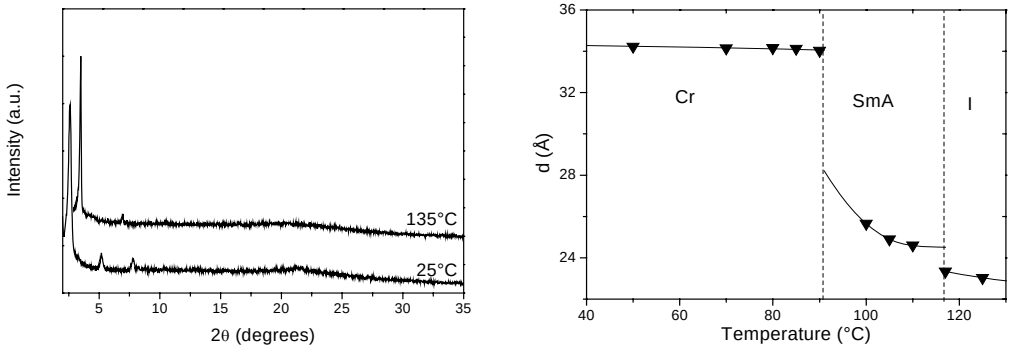

Figure 3-10 X-ray diffractogram of $La(C_{11}H_{23}CO_2)_3$ at room temperature and in the mesophase (left) and the evolution of the *d* spacing of $Nd(C_{11}H_{23}CO_2)_3$ in function of the temperature

The formation of random domains in the bulk of the isotropic phase is expressed in the existence of a broad less intense peak in XRD measurements. When an isotropic liquid would be formed, no diffraction peak would be seen with this technique.

The size of the lanthanide ion does have a significant effect on the thermal behaviour of the lanthanide(III) dodecanoates. As the ionic radius of the lanthanide cation decreases, the distance between the carboxylate groups mutually opposite with respect to the plane containing the lanthanide ions also decreases. The thermal vibrations increase in amplitude at increasing temperature and thereby induce unfavourable electrostatic interactions (repulsion) between the carboxylate groups, not only of the two opposing layers, but also between adjacent carboxylate groups within the same layer. When the repulsive forces between the negative charges are stronger than the attractive forces between the negative (carboxylate groups) and positive charges (lanthanide ions), the bilayer structure of the solid metal soap is not longer stable and breaks down. In this case, a rearrangement of the carboxylate groups and lanthanide ions to obtain a more stable solid-state structure (i.e. a crystal - crystal transition) might be expected. However, melting of the compounds is observed. The alkyl chains have sufficient thermal energy such that when the layer structure breaks down, their *all trans* conformation is lost and they adopt a less extended conformation (which is more or less random). A mesophase is formed when, at the melting point of the alkyl chains, the electrostatic interactions between the lanthanide ions and the carboxylate groups are still sufficiently favourable to maintain a layer structure. This is the case for La^{3+}, Ce^{3+}, Pr^{3+} and Nd^{3+} dodecanoates. At further heating a second phase transition occurs for the mesomorphic lanthanide(III) dodecanoates and the metal soaps are transformed into a less-ordered isotropic structure. This is also the structure of the non-mesogenic lanthanide(III) dodecanoates after melting. The bulk of this isotropic phase is formed by random domains (see also Chapter 6).

The melting point of the lanthanide(III) dodecanoates decreases over the lanthanide series. This can be explained by the size of the lanthanide ion. The smaller the

lanthanide ion, the more unstable the layer structure becomes, and hence less thermal energy is required to break down the solid state structure.
Also the clearing point decreases through the lanthanide series. Heating affects the thermal vibrations of the carboxylate groups not only in the crystalline phase, but also in the mesophase. The smaller the lanthanide ion, the lower the temperature whereby the ionic layer is not longer stable and hence the mesophase will be transformed into a less-ordered structure at lower temperatures. In Figure 3-11 the phase diagram of lanthanide(III) dodecanoates is given.

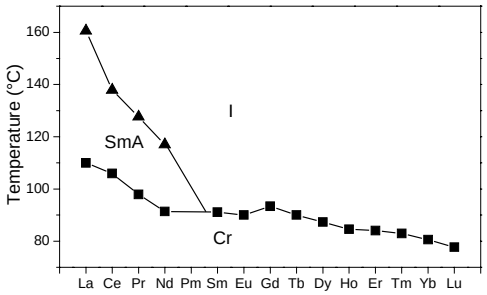

Figure 3-11 Phase diagram for the lanthanide(III) dodecanoates

The mesophases can be considered as semi-solid compounds, the alkyl chains exhibiting a molten behaviour, while to some extent the ionic part of the structure remains intact. Consequently, a sharp melting point is not observed for the lanthanide(III) dodecanoates, but rather a melting range. Not all the alkyl chains melt at the same temperature. This became evident when X-ray diffractograms of the compounds forming a mesophase were recorded close to their melting points. Such X-ray diffractograms show more peaks than those of the solid phase or of the mesophase and it turned out that they were in fact a superposition of these respective diffractograms.

The crystallisation peak in the cooling run is rather broad. The alkyl chains do not all crystallise at the same temperature, so the compounds become solid over a broad temperature range. Moreover, no complete crystallisation occurs. The alkyl chains do not rearrange to the *all trans* conformation when cooling from the isotropic phase.

The layer structure is gradually lost in the compounds that form a mesophase, whereas it is lost much more abruptly in the compounds that melt without forming a mesophase. It must be emphasized that in the compounds forming a mesophase, the layer structure breaks down at the clearing point, whereas in the case of the non-mesogenic compounds total break-down of the layer structure occurs only at the melting point.

The effect of the lanthanide(III) ion on the thermal properties is significant for the lanthanide(III) alkanoates. Although it is often observed that the transition temperatures depend on the size of the lanthanide ion [15], the effect is less pronounced than for these compounds. A possible explanation is the more or less polymeric structure of lanthanide(III) carboxylates (see Figure 3-6), in contrary to for example lanthanide(III) Schiff's bases complexes where the layered structure is built by discrete molecules [16].

However, it seems that the overall thermal behaviour of lanthanide(III) dodecanoates can be divided in two groups. The first group (Ln = La – Eu) shows a fast decrease of the melting point per lanthanide ion (average decrease is 2.86°C per lanthanide ion). This is a factor 1.5 larger than in the case of the second part of the lanthanide series (average decrease is 1.88°C per lanthanide ion). This can be related to the size of the lanthanide ion and the number of f-electrons.
The ionic radius of the lanthanide ions decreases exponential with the number of f-electrons. This means that the difference in the effect of the ionic size and hence the difference in thermal behaviour of two neighbouring lanthanide ions decreases through the lanthanide series. Hence the average difference in temperature between two successive lanthanide ions is less in the second half of the lanthanide series than in the first half. The difference in thermal behaviour between the first and the second half of the lanthanide series must be related to the respectively less – than – half and more – than – half filled f-shell.

3.3.2 Influence of the Chain Length on the Thermal Behaviour of Lanthanide(III) Alkanoates

As was pointed out in 3.3.1 , the lanthanide ion strongly influences the thermal behaviour of lanthanide(III) dodecanoates. It is evident that also the chain length can influence the thermal behaviour of the complex. Therefore, lanthanide(III) alkanoates with different chain lengths were synthesised and their thermal behaviour was investigated.

3.3.2.1 $La(C_xH_{2x+1}CO_2)_3$, $Ce(C_xH_{2x+1}CO_2)_3$ and $Pr(C_xH_{2x+1}CO_2)_3$

First the thermal behaviour of the lanthanum(III) alkanoates is described. The thermal behaviour of the cerium(III) and praseodymium(III) alkanoates is analogous. A short comparison of these three series will be given.

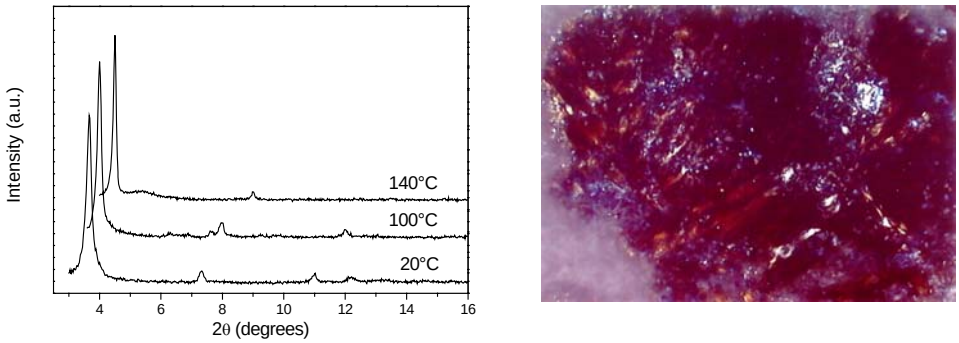

Figure 3-12 X-ray diffractogram of lanthanum(III) octanoate at room temperature (20°C), in mesophase M (100°C) and in the smectic A phase (140°C) (left) and texture of the mesophase M of $La(C_5H_{11}CO_2)_3$ at 98°C

The DSC thermograms of the homologous series $La(C_xH_{2x+1}CO_2)_3$ (x = 4 – 19) show several phase transitions. The shorter members (x = 4 – 9) exhibit three phase transitions (whereby the enthalpy of the second and of the third transition are much lower as of the first one), suggesting that several mesophases are present.

Lanthanum(III) undecanoate and the higher homologues show only two peaks in their DSC curves (see DSC thermogram of $La(C_{11}H_{23}CO_2)_3$, Figure 3-8), suggesting a mesophase.

The presence of mesophases was investigated by thermo-optical microscopy. Most of the compounds soften before they exhibit birefringence at the melting point. Except for lanthanum(III) butyrate monohydrate which does not exhibit any mesomorphism, all the compounds of the series $La(C_xH_{2x+1}CO_2)_3$ (x = 4 – 19) are liquid crystalline. The shorter ones (lanthanum(III) pentanoate to decanoate) show two mesophases. The first mesophase, labelled as M, has a very high viscosity and the texture contains star-like regions on a black background (Figure 3-12). The high temperature mesophase (i.e. the only mesophase in the lanthanum(III) undecanoate-eicosanoate series) is less viscous and has a texture similar to the one reported by Marques for cerium(III) alkanoates [5]. Specifically the texture has a grainy appearance, with a white-yellow zone on a dark background (see Figure 3-9). The results from thermo-optical microscopy confirm the existence of two mesophases as was already mentioned from DSC-measurements.

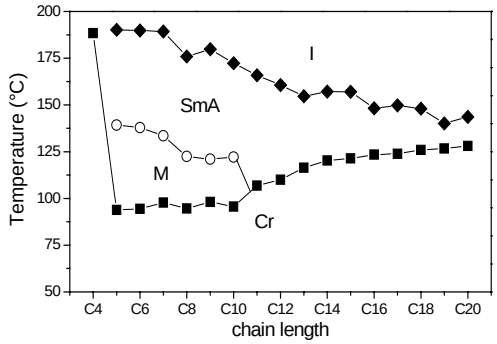

Figure 3-13 Phase diagram of $La(C_xH_{2x+1}CO_2)_3$

Whereas in the crystalline state the alkyl chains are totally extended, a distinct decrease of the *d* spacing can be seen in the crystal to mesophase M transition (Figure 3-13). This is an indication for a bilayer structure with partially molten alkyl chains but with restricted motions of the lanthanide ions. However, a rearrangement of the ionic layer and the carboxylate groups to form a structure that is more stable at higher

temperatures may also be expected. This low temperature mesophase M is observed for the shorter chain homologures (lanthanum(III) pentanoate to decanoate).
A second decrease of the *d* spacing is observed for the mesophase M to smectic A phase transition. This is the only mesophase for the long chain homologues. Here the alkyl chains are completely molten and the lanthanide ions can rotate freely through the layer. The temperature dependence of the *d* spacing confirms the existence of a smectic A phase. For the long chain homologues, the temperature dependence of the *d* spacing is analogous as described for the mesogenic lanthanide(III) dodecanoates (see 3.3.1). These compounds show a smectic A phase.
At the clearing point, most of the structure is lost, and a structure with random domains is formed.

The complete series of synthesized lanthanum(III) alkanoates exhibits mesomorphism except for the butyrate homologue, although there is a marked influence of the chain length on the transition temperatures. Whereas the melting point increases at increasing chain length, the clearing point decreases. The length of the alkyl chain causes the increase of the melting temperature. The longer the alkyl chain the more thermal energy is required to melt the alkyl chain. The decrease of the clearing point at increasing chain lengths can be attributed to less favourable interactions between the molten alkyl chains for the long chain homologues.
A second influence of the chain length is the existence of a second mesophase M for the shorter lanthanum(III) alkanoates. In Figure 3-13 the phase diagram of the lanthanum(III) alkanoates is given.

Also for the $Ce(C_xH_{2x+1}CO_2)_3$ series the influence of the chain length on the transition temperatures and on the occurrence of a second mesophase is observed. Although we do not have any X-ray diffractograms at high temperatures of these compounds, their thermal behaviour observed in DSC and thermo-optical microscopy are comparable with the thermal behaviour of lanthanum(III) alkanoates. So we propose for this mesophase a bilayer structure with partially molten alkyl chains, but rotation through the two-dimensional network structure of the ionic layer is restricted. This is in

contrast to the SmA phase where the lanthanide ions can rotate in the ionic layers. The M ↔ SmA phase was here also reversible in the DSC measurements.
The phase behaviour here described, confirms the results of Marques for Ce(III) alkanoates with even chain lengths [5].

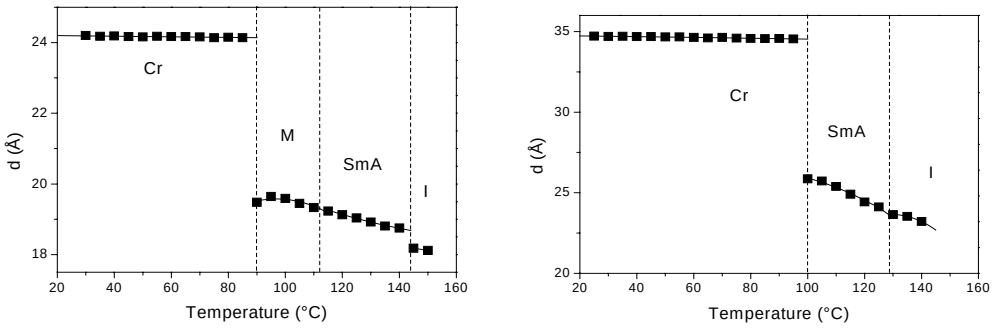

Figure 3-14 Change of the *d* spacing of praseodymium(III) octanoate (left) and of praseodymium(III) dodecanoate as a function of temperature

The influence of the chain length on the thermal behaviour of praseodymium(III) alkanoates is largely the same as observed for the series $La(C_xH_{2x+1}CO_2)_3$ and $Ce(C_xH_{2x+1}CO_2)_3$. The melting point increases with increasing chain length, whereas the clearing point decreases.
The occurrence of a second mesophase for shorter chain lengths (praseodymium(III) hexanoate to nonanoate) is also observed in this series. This mesophase is detected by DSC and by thermo-optical microscopy. However, there is no change in *d* spacing in the X ray diffractograms at the transition temperature (Figure 3-14), although we observed a marked decrease in viscosity when going from mesophase M to the SmA phase. Because we observed a similar phase transition for the lanthanum(III) alkanoates and because the M ↔ SmA transition is reversible in DSC measurements, we assigned the label M hereon.

The mesophase behaviour of the series $La(C_xH_{2x+1}CO_2)_3$, $Ce(C_xH_{2x+1}CO_2)_3$ and $Pr(C_xH_{2x+1}CO_2)_3$ are very similar. However, the lanthanide ion influences the thermal behaviour of these three series in the sense that the transition temperatures depend on

the ionic size. The larger the lanthanide ion is, the higher the clearing point and the larger the mesophase stability.

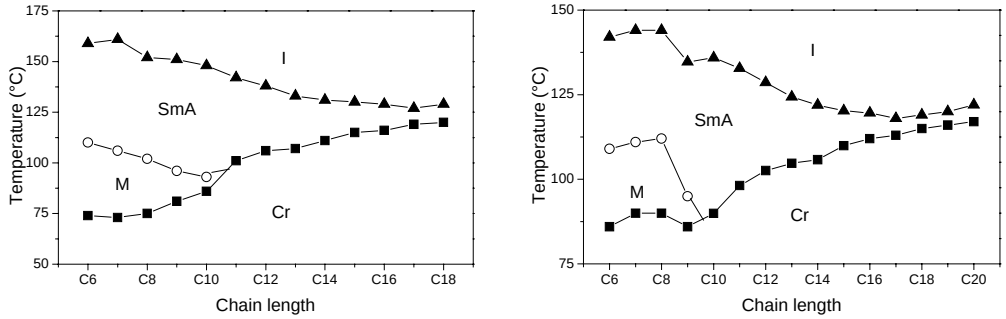

Figure 3-15 Phase diagram of $Ce(C_xH_{2x+1}CO_2)_3$ (left) and of $Pr(C_xH_{2x+1}CO_2)_3$

We do not observe an odd-even effect in the transition temperatures, although this is often observed for liquid crystals. Lanthanide(III) alkanoates are bilayered structures. This means that on both sides of the ionic lanthanide layer alkyl chains are placed. So, the overall number of carbon atoms in this bilayered structure is always even, and no odd-even effect occurs.

The transition temperatures and enthalpies of these three series are listed in Table 1.4-3 - Table 1.4-5, Appendix 1.

3.3.2.2 $Nd(C_xH_{2x+1}CO_2)_3$

The DSC thermograms of the series $Nd(C_{11}H_{23}CO_2)_3$ - $Nd(C_{14}H_{29}CO_2)_3$ reveal the presence of one mesophase. Neodymium(III) butyrate monohydrate has a single high melting point. For the series $Nd(C_4H_9CO_2)_3$ - $Nd(C_{10}H_{21}CO_2)_3$ more than one mesophase is observed. The low temperature mesophase of the short chain homologues has a high viscosity and even the high temperature mesophase (i.e. the unique mesophase in the $Nd(C_{11}H_{23}CO_2)_3$ - $Nd(C_{14}H_{29}CO_2)_3$ series) is not very fluid.

The behaviour of these compounds is thus very similar as described in 3.3.2.1 for lanthanum(III), cerium(III) and praseodymium(III) alkanoates.

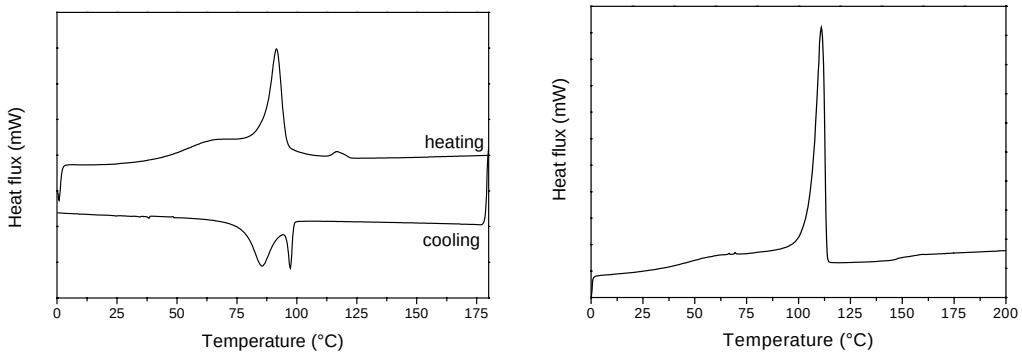

Figure 3-16 DSC thermogram of $Nd(C_{11}H_{23}CO_2)_3$ (first heating and cooling cycle) (left), and of $Nd(C_{16}H_{33}CO_2)_3$ (first heating cycle); endothermic peaks are pointing upwards

The main difference of the thermal behaviour of neodymium(III) alkanoates is that no mesophase is observed for neodymium(III) hexadecanoate and longer homologues in contrary to the presence of at least one mesophase for the entire series of lanthanum(III), cerium(III) and praseodymium(III) alkanoates. This due to a competition between the melting of the alkyl chains and break-down of the ionic layer. In Figure 3-17 the phase diagram of the series $Nd(C_xH_{2x+1}CO_2)_3$ is given.

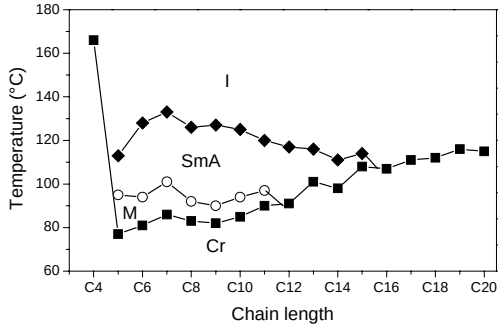

Figure 3-17 Phase diagram of the series $Nd(C_xH_{2x+1}CO_2)_3$

3.3.2.3 $Sm(C_xH_{2x+1}CO_2)_3$ and $Eu(C_xH_{2x+1}CO_2)_3$

In the series of the lanthanide(III) dodecanoates we found that only the first four lanthanide(III) dodecanoates with a large ionic radius (i.e. La, Ce, Pr and Nd) are mesomorphic. But as pointed in 3.3.2.1 and 3.3.2.2 the phase behaviour and the transition temperatures of lanthanide(III) alkanoates also depend on the length of the alkyl chain. Therefore it was interesting to find out if a mesophase could be formed in the series $Sm(C_xH_{2x+1}CO_2)_3$ and $Eu(C_xH_{2x+1}CO_2)_3$ where $x < 11$.

The DSC and thermo-optical microscopy measurements of the short homologues of these series pointed out that no mesophase was present, although the melting temperature depends on the chain length, i.e. the longer the alkyl chain, the higher the melting temperature.

In Figure 3-18 the phase diagram of $Sm(C_xH_{2x+1}CO_2)_3$ and of $Eu(C_xH_{2x+1}CO_2)_3$ is given.

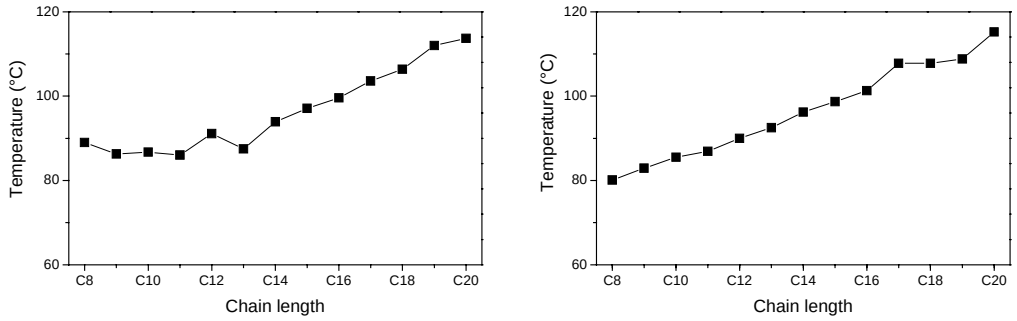

Figure 3-18 Phase diagram of $Sm(C_xH_{2x+1}CO_2)_3$ (left) and of $Eu(C_xH_{2x+1}CO_2)_3$

3.3.3 Conclusion

As showed in 3.3.1 and 3.3.2 the thermal behaviour of lanthanide(III) alkanoates depends on the size of the lanthanide ion and on the length of the alkyl chain.

The effect of the lanthanide ion can be explained by taking into account unfavourable electrostatic interactions between the carboxylate groups. As the ionic radius of the

lanthanide cation decreases, the distance between the carboxylate groups on either side of the plane containing the lanthanide ions also decreases. The amplitude of the thermal vibrations increases on increasing temperature and thereby induces unfavourable electrostatic interactions (repulsions) between the carboxylate groups, not only between those of the two opposing layers, but also between adjacent carboxylate groups within the same layer. When the repulsive forces between the negative charges are stronger than the attractive forces between the negative (carboxylate groups) and positive (lanthanide ions) charges, the bilayer structure is no longer stable and breaks down. In this case, a rearrangement of the carboxylate groups and lanthanide ions to obtain a more stable solid structure (i.e. a crystal - crystal transition) might be expected. However, melting of the compounds is observed. The alkyl chains have sufficient thermal energy for their all trans conformation to be lost when the layer structure breaks down.

This theory explains the decrease of the melting point within the lanthanide series for a given chain length. The smaller the lanthanide ion, the more unstable the layer structure becomes, and hence less thermal energy is required to break down the solid state structure.

A mesophase is formed, when, at the melting point of the alkyl chains, the electrostatic attraction between the lanthanide ions and the carboxylate groups is still sufficiently high to maintain a layer structure. This is the case for lanthanum(III), cerium(III), praseodymium(III) and neodymium(III) compounds.

Also the clearing point decreases over the lanthanide series. Heating does not only affect the thermal vibrations of the carboxylate groups in the crystalline phase, but also in the mesophase. The smaller the lanthanide ion, the lower the temperature whereby the ionic layer of the mesophase breaks down.

The metal soaps are converted to an isotropic structure with random domains after the clearing point for the mesogenic lanthanide(III) dodecanoates and after melting for the non-mesogenic compounds.

We also observed an increase of the melting point and a decrease of the clearing point at increasing chain length. The increase in melting point can be dedicated to the length of the alkyl chain and the stronger Van der Waals interactions for the longer alkyl chains, hence more thermal energy is required to melt the chains. The decrease in clearing point is caused by stronger unfavourable interactions between the molten alkyl chains in the mesophase. Hence the compounds with long alkyl chains rearrange to a less-ordered structure at lower temperatures.

The fact that only the first three lanthanides (La, Ce and Pr) exhibit a mesophase across the complete homologous series ($4 \leq x \leq 19$), and that the neodymium series does not show mesomorphism for the longer chain lengths, can be explained by taking into account both the effect of the lanthanide ion and the chain length. Whereas for lanthanum(III), cerium(III) and praseodymium(III) alkanoates the ionic radius is sufficiently large to reduce unfavourable electrostatic interactions between the carboxylate groups (and thus the melting of the alkyl chains is the major factor determining the thermal properties of the compounds), for neodymium soaps there is a competition between the stabilisation of the ionic layers and melting of the alkyl chains. For the shorter alkyl chains, their melting is the determining factor, whereas for the longer soaps the thermal energy required to melt the alkyl chains is that high that the ionic layer structure breaks down before the alkyl groups are completely molten.

Lanthanum(III) and neodymium(III) butyrate are not liquid crystalline. The alkyl chain is not long enough to form a stable mesophase, although the overall structure is very stable (cfr. their high melting points). Such a different mesophase behaviour for short chain homologues is also observed for copper soaps. Copper(II) butyrate forms a rectangular discotic mesophase, whereas a hexagonal discotic mesophase is observed for the longer homologues. In the case of copper(II) butyrate the alkyl chain is too short to fill the intercolumnar space efficiently [17].

3.4 Optical Properties of Vitrified Rare-Earth Soaps

3.4.1 Synthesis and Characterisation

The lanthanide(III) octadecanoates (Ln = La, Pr, Nd, Sm, Eu, Dy, Ho, Er, Tm) were synthesised by a metathesis reaction between the corresponding hydrated lanthanide nitrate and sodium octadecanoate. The elemental analysis results are given in Table 1.1-2, Appendix 1.

The thermal behaviour of these lanthanide(III) octadecanoates was investigated by DSC and thermo-optical microscopy. As was pointed out in 3.3 , only a mesophase is present for lanthanum(III), cerium(III) and praseodymium(III) octadecanoate. The complexes with the heavier lanthanide ions (i.e. Nd – Lu) are not mesogenic. A competition between stabilisation of the ionic layer and melting of the alkyl chains explains the non-mesogenic behaviour of these compounds. The overall thermal properties are comparable to these of lanthanide(III) dodecanoates. In Figure 3-19 the phase diagram of the series $Ln(C_{17}H_{35}CO_2)_3$ is given.

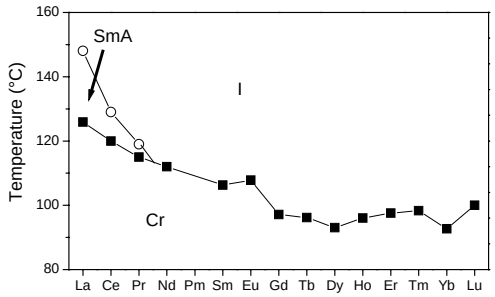

Figure 3-19 Phase diagram of the series $Ln(C_{17}H_{35}CO_2)_3$

The glass samples were prepared by melting the compounds in a mould, which was placed on a microscope cover glass. The mould consisted of an aluminium plate of 10x10x1mm, with a hole of 4 mm diameter. The microscope slide glass and the mould were heated on a heating plate. After melting, a second microscope cover glass was placed on top of the mould, so that a sample of uniform thickness was obtained. The molten sample was vitrified by quench cooling in a dry ice/acetone mixture.

In contrast to common inorganic glasses, the lanthanide soaps are first synthesised to a vitreous state by melting and cooling. Glasses of a good quality are free of crystallites and air bubbles. The tendency to crystallise increases over the lanthanide series. Glasses of the lighter lanthanides can be obtained even when the cooling process is relatively slow, whereas glasses of the heavier lanthanides can be obtained in general only with quench cooling. No glasses free of crystallites could be prepared for thulium(III) octadecanoate, neither of lanthanum(III) octadecanoate although this is the first element of the lanthanide series. Air bubbles could be driven out of the melt by prolonged heating of the molten compound.

3.4.2 Optical Properties

The optical absorption spectra of the trivalent lanthanide ions in glasses are characterised by narrow, weak absorption bands. The absorption spectra of neodymium(III) octadecanoate and holmium(III) octadecanoate are given in Figure 3-20. Each transition corresponds to a transition between two spin-orbit coupling levels. The majority of the transitions are induced electric dipole transitions, although some magnetic dipole transitions are observed. The dipole strengths *D* of the transitions (expressed in D^2) were extracted from the absorptions spectrums, using Equation 3-2

Equation 3-2

$$D = \frac{1}{108.9Cd}\int \frac{A(\bar{\nu})}{\bar{\nu}} d\bar{\nu}$$

where *C* is the concentration of the lanthanide ion (mol L^{-1}), d is the optical path length (cm), A is the absorbance ($A = -\log(I/I_0)$) and ν is the wavelength number (cm^{-1}). The absorbance is related to the molar absorptivity ε via Lambert-Beer's law: $A = C\varepsilon d$. The dipole strength of a magnetic dipole transition can be calculated by using the 4f-free ion wave functions only.

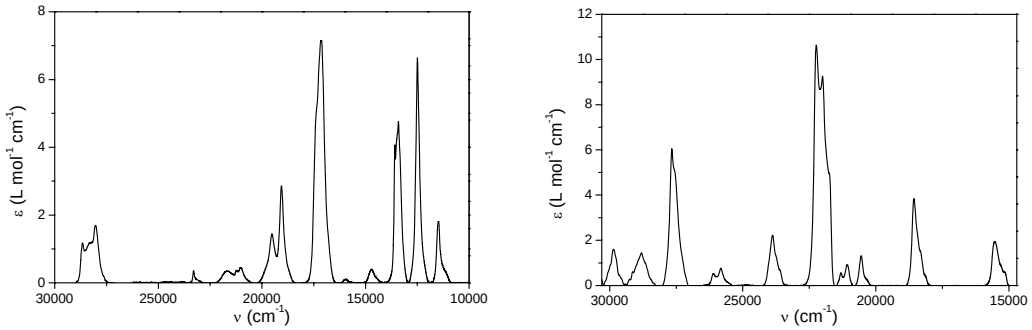

Figure 3-20 Absorption spectrum of vitrified neodymium(III) octadecanoate (left) and holmium(III) octadecanoate

However, for the calculation of the dipole strengths of the induced electric dipole transitions, parametrisation is necessary. In the framework of the Judd-Ofelt theory [18 - 20] the dipole strengths of induced electric dipole transitions can be described by three phenomenological intensity parameters Ω_λ ($\lambda = 2, 4, 6$):

Equation 3-3

$$D = \frac{10^{36}}{2J+1}\frac{\left(n^2+2\right)^2}{9n}e^2\sum_{\lambda=2,4,6}\Omega_\lambda\left|\left\langle J\left\|U^{(\lambda)}\right\|J'\right\rangle\right|^2$$

The factor 10^{36} is used for conversion between D^2 and esu^2 cm^2($1D = 10^{-18}$esu cm). The degeneracy of the ground state is equal to *2J + 1*. The factor $(n^2 + 2)/9n$ takes into account that the lanthanide ion is not in a vacuum, but in a dielectric medium (n is the refractive index of the glass). The refractive index was found to be virtually independent of the lanthanide ion and its value is 1.48. Because of the low dispersity of such compounds, no wavelength dependence of the refractive index was taken into account. Finally, the $\left|\left\langle J\left\|U^{(\lambda)}\right\|J'\right\rangle\right|^2$ are the squared reduced matrix elements. We used the reduced matrix elements reported by Carnal [21 - 24]. In the case of overlapping transitions, we made a summation of the appropriate matrix elements [20]. The Ω_λ parameters are determined via a least-squares fit, minimising the sum of the squares of the differences between experimental and calculated dipole strengths.

The results of intensity calculations are summarised for neodymium(III) and holmium(III) octadecanoate in Table 1.5-1 and Table 1.5-2, Appendix 1. The spectral data of the other lanthanide(III) octadecanoates were treated in a similar way. The Judd-Ofelt intensity parameters of the glasses are given in Table 3.4-1.

Table 3.4-1 Judd-Ofelt intensity parameters of vitrified lanthanide(III) octadecanoates, $[Ln(C_{17}H_{35}COO)_3]$

Ln(III)	Ω_2 /10^{-20} cm^2	Ω_4 /10^{-20} cm^2	Ω_6 /10^{-20} cm^2
Nd(III)	3.63±0.46	4.69±0.67	5.69±0.30
Sm(III)	4.19±1.05	4.99±0.41	2.91±0.25
Eu(III)[a]	17.96	2.93	1.71
Gd(III)	---[b]	---[b]	5.43±0.05
Dy(III)	6.73±0.67	1.49±0.66	2.72±0.45
Ho(III)	6.44±0.30	3.07±0.45	2.21±0.27
Er(III)	6.50±1.00	1.83±1.48	1.44±0.90

[a] The Judd-Ofelt parameters for europium(III) octadecanoate have been determined using three transitions only: $^5D_2 \leftarrow {}^7F_0$, $^5L_6 \leftarrow {}^7F_0$ and $^5D_4 \leftarrow {}^7F_0$. Therefore no error on the parameters can be given.
[b] Indeterminate

Reliable sets of Judd-Ofelt intensity parameters could be determined for the vitreous samples containing neodymium, samarium, europium, dysprosium, holmium and erbium. The error on the parameters of the praseodymium sample was of the same size or even larger than the actual value of the parameters themselves. Therefore no intensity results for praseodymium(III) octadecanoate are given. It is well known that the Judd-Ofelt theory often fails for trivalent praseodymium [20]. Due to the lack of experimental dipole strengths, for gadolinium(III) octadecanoate only a reliable value could be determined for the Ω_6 parameter, and no errors could be determined for the intensity parameters of europium(III) octadecanoate.

The values of the Ω_4 and Ω_6 parameters of the heavy lanthanides (after gadolinium) are smaller than the values of the lighter lanthanides. This is due to the contraction of the 4f-shell over the lanthanide series and subsequently smaller values of the radial

integrals $\langle r^4 \rangle$ and $\langle r^6 \rangle$ in the expressions of the Judd-Ofelt intensity parameters [20]. An opposite trend is observed for the Ω_2 parameter: this parameter is smaller for the lighter lanthanides than for the heavier lanthanides. The Ω_2 parameter describes the intensity of the so-called hypersensitive transitions. The trend for the parameters is comparable with what is observed for lanthanide ions in many oxide glasses: Ω_2 of a comparable size of Ω_4 and Ω_6 for the elements in the beginning of the lanthanide series, and a much larger value of Ω_2 in comparison to Ω_4 and Ω_6 for the elements at the end of the lanthanide series. The large values of the Ω_2 parameter of europium(III) octadecanoate can be related to the high intensity of the $^5D_0 \rightarrow {}^7F_2$ transition in the absorption spectrum. Large values for the Ω_6 parameter of Eu(III) were also found in the cases of $Eu(dpa)_3^{3-}$ in water [25], Eu(III) in germanate glass [26], $Eu(picNO)_3$Terpy [27], Eu(III) in $LiNO_3$-KNO_3 melt [28] and $Eu(dbm)_3 \cdot 3H_2O$ powder [29].

Because the intensities of the f-f transitions are comparable with the behaviour of lanthanide ions in oxide glasses (in which oxygen atoms are in the first coordination sphere of the lanthanide ion), we can propose that the spectroscopic behaviour of the lanthanide(III) soaps are mainly determined by the oxygen atoms in the first coordination sphere of the lanthanide ion, rather than by the long alkyl chains in the bulk of the sample. This is illustrated once more by the comparison of the Ω_4 and Ω_6 parameters of neodymium(III) octadecanoate: the experimental ratio $\Omega_4/\Omega_6 = 1.21$. This value is close to the ratio $\Omega_4/\Omega_6 = 1.12$ which Binnemans and Görller-Walrand found by analysis of the literature data of more than 200 Nd(III) containing inorganic glass samples [30]. For neodymium(III) coordination compounds this ratio is in general much higher [20].

Upon irradiation with ultraviolet light, visible photoluminescence was observed for the samarium, europium and dysprosium compounds. The luminescence spectrum of europium(III) octadecanoate is shown in Figure 3-21. Its luminescence colour is bright red. All the transitions start from the $^5D_0$ level. The $^5D_0 \rightarrow {}^7F_J$ (J = 0 - 4) transitions

exhibit some fine-structure due to the crystal field splitting of the ^7F_J levels. However, it is not possible to determine the local structure around the europium(III) ion in the glass matrix, because the crystal-field transitions are not well resolved due to the inhomogeneous line-broadening. The most intense transition is the hypersensitive transition $^5D_0 \rightarrow {}^7F_2$. The intensity ratio $I(^5D_0 \rightarrow {}^7F_2)/I(^5D_0 \rightarrow {}^7F_1)$ is 2.91. It is known that the intensity of magnetic dipole transitions are, within the approximation of the intermediate coupling scheme, independent of the environment of the lanthanide ion [31].

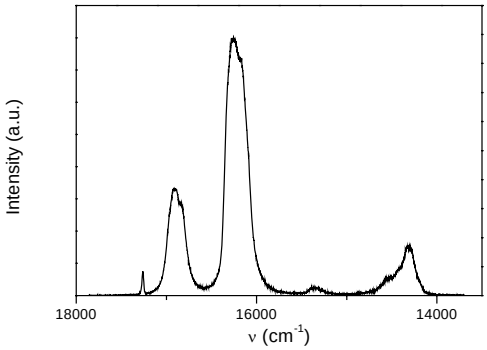

Figure 3-21 Luminescence spectrum of vitrified europium(III) octadecanoate at room temperature

References

[1] K. Binnemans, C. Görller-Walrand *Chem. Phys. Lett.* **235** (1995) 163.

[2] R.A. Meiklejohn, R.J. Meyer, S.M. Aronovic, H.A. Schuette, V.W. Meloch *Anal. Chem.* **29** (1957) 329.

[3] D. Saperstein *J. Phys. Chem.* **91** (1987) 2922.

[4] G.B. Deacon, R.J. Phillips *Coord. Chem. Rev.* **22** (1980) 227.

[5] E. F. Marques, H. D. Burrows, M. da Graça *J. Chem. Soc., Faraday Trans.* **94** (1998) 1729.

[6] R. D. Shannon *Acta Crystalllogr.* **A32** (1976) 751.

[7] A. Skoulios, V. Luzatti *Nature* **183** (1959) 1310.

[8] A. Ouchi, Y. Suzuki, Y. Okhi, Y. Koizumi *Coord. Chem. Rev.* **92** (1988) 29.

[9] D. Deiters, G. Meyer *Z. Anorg. Allg. Chem.* **622** (1996) 325.

[10] K. N. Mehrotra, A. S. Gahlaut *J. Indian Chem. Soc.* **65** (1987) 309.

[11] K. N. Mehrotra, M. Chauhan, R. K. Shukla *Monatsh. Chem.* **120** (1989) 1063.

[12] K. N. Mherotra, R. K. Shukla, M. Chauhan *Bull. Chemm. Soc. Jpn.* **68** (1995) 1825.

[13] E. F. Marques, H. D. Burrows, M. da Graça Miguel *J. Chem. Soc. Faraday Trans.* **94** (1998) 1729.

[14] J. M. Seddon *Structural Studies of Liquid Crystals by X-ray diffraction,* in *Handbook of Liquid Crystals* (Eds.: D. Demus, J. Goodby, G. W. Gray, H. W. Spiess, V. Vill) Wiley VCH, Wienheim **1998** Vol.1, p. 635-679.

[15] K. Binnemans, R. Van Deun, D. W. Bruce, Y. G. Galyametdinov *Chem.Phys.Lett.* **300** (1999) 509.

[16] K. Binnemans, Y. G. Galyametdinov, R. Van Deun, D. W. Bruce, S. R. Collinson, A. P. Polishchuk, I; Bikchantow, W. Haase, A. V. Prosvirin, L. Tinchurina, I. Litvinov, A. Guboijdullin, A. Rakhmatullin, K. Uytterhoeven, L. Van Meervelt *J. Am. Chem. Soc.* **122** (2000) 4335.

[17] A. M. Giroud-Godquin, J. C. Marchon, D. Guillon, A. Skoulios *J. Phys. Lett.* **45** (1984) L681.

[18] B. R. Judd *Phys. Rev.* **127** (1962) 750.

[19] G. S. Ofelt *J. Chem. Phys.* **37** (1962) 511.

[20] C. Görller-Walrand, K. Binnemans *Handbook on the Physics and Chemistry of Rare Earths* (ed. K. A. Gschneider, L. Eyring) North-Holland, Amsterdam vol. 25, ch. 167, p. 101, **1998**.

[21] W. T. Carnall, P. R. Fields, K. Rajnak *J. Chem. Phys.* **49** (1968) 4424.

[22] W. T. Carnall, P. R. Fields, K. Rajnak *J. Chem. Phys.* **49** (1968) 4443.

[23] W. T. Carnall, P. R. Fields, K. Rajnak *J. Chem. Phys.* **49** (1968) 4447.

[24] W. T. Carnall, P. R. Fields, K. Rajnak *J. Chem. Phys.* **49** (1968) 4450.

[25] K. Binnemans, K. Van Herck and C. Görller-Walrand, *Chem. Phys. Lett*. **266** (1997) 297.

[26] R. Reisfeld and J. Hormadaly, *J. Chem. Phys*. **64** (1976) 3207.

[27] G.F. de Sa, F.R.G. e Silva and O.L. Malta, *J. Alloys Compds* **207/208** (1994) 457.

[28] W.T. Carnall, J.P. Hessler and F. Wagner, *J. Phys. Chem.* **82** (1978) 2152.

[29] A.F. Kirby and R.A. Palmer, *Inorg. Chem.* **20** (1981) 4219.

[30] K. Binnemans and C. Görller-Walrand, *J. Phys.: Condens. Matter*. **10** (1998) L167.

[31] C. Görller-Walrand, L. Fluyt, A. Ceulemans, W. T. Carnall *J. Chem. Phys.***95** (1991) 3099.

Chapter 4 Binary Mixtures of Lanthanide(III) Dodecanoates

As described in 3.3 we found that the size of the trivalent lanthanide ion has a critical effect on the transition temperatures in the sense that a mesophase can only be formed with the lighter lanthanide elements with a large ionic radius (*i.e.* La(III), Ce(III), Pr(III) and Nd(III)).

Therefore it was interesting to find out if we could induce mesomorphism in non-mesogenic lanthanide(III) soaps. Till now, information about mesophase induction is scarce. High isotropic pressure has been proved to induce mesomorphism [1] and in particular to induce liquid-crystalline behaviour in compounds that do not form liquid crystalline phases at atmospheric pressure [2]. Levelut published in 1981 the induction of polymorphism in a binary mixture of two liquid crystals [3]. Mirnaya reported on mesophases of binary alkaline salt systems of carboxylic acids [4] whereas Cheda described binary phase diagrams of lead(II) alkanoates and *n*-alkanoic acids [5].

Here we describe the synthesis and thermal properties of mixtures of lanthanum(III) dodecanoate with europium(III), neodymium(III), terbium(III), holmium(III) and ytterbium(III) dodecanoate with different compositions.

4.1 Synthesis and Characterisation

The series of $[La_xEu_{1-x}(C_{11}H_{23}COO)_3]$ (x is the mole fraction of lanthanum in the mixtures) was synthesized by a metathesis reaction between the sodium salt of dodecanoic acid and aqueous solutions prepared from desired amounts of lanthanum(III) and europium(III) nitrate hexahydrate, respectively. The reaction medium is an aqueous ethanol solution (water:ethanol 1:1). The exact concentrations

of the lanthanide solutions were determined by titration with EDTA as complexing agent and a mixed indicator (45 ml 0.5% sodium alizarine sulfate plus 15 ml 0.1% methylene blue). After synthesis the soaps were filtered off, washed carefully with water, ethanol and acetone. The soaps were dried for 24 hours in vacuum at 40°C.
The mixtures of lanthanum with the other lanthanides (i.e. neodymium, terbium, holmium and ytterbium) were prepared in the same way.

The carbon and hydrogen content of the compounds was determined by CH elemental analysis. The analysis results are consistent with an alkanoic acid to lanthanide(III) ratio of 3:1, but also indicate that under the given reaction conditions the compounds can not be obtained in a total anhydrous form. Most of the soaps are monohydrates, $[La_xLn_{1-x}(C_{11}H_{23}COO)_3]\cdot H_2O$. The degree of hydration does not depend on the drying conditions. However, thermogravimetric study showed that the water molecules are lost before or at the melting point. The amount of water calculated by thermogravimetry is close to 1, which is in agreement with the CH results. The analysis results are given in Table 2.1-1 - Table 2.1-5, Appendix 2.

Exptl. for $[La_{0.725}Eu_{0.275}(C_{11}H_{23}COO)_3]\cdot H_2O$: Experimental for C: 57.09%, for H: 9.70%; Calculated for C: 57.01%, for H: 9.44%.

4.2 Thermal Behaviour of $[La_xLn_{1-x}(C_{11}H_{23}COO)_3]$

4.2.1 $[La_xEu_{1-x}(C_{11}H_{23}COO)_3]$

All the compounds of the series $[La_xEu_{1-x}(C_{11}H_{23}COO)_3]$ with $x \geq 0.40$ exhibit in the DSC-curve multiple melting phenomena, indicating the presence of a mesophase. This is in contrast with the pure non-mesogenic europium(III) dodecanoate, which shows in the DSC-thermogram only one phase transition, i.e. melting. However, the mesogenic

lanthanum(III) dodecanoate exhibits a comparable DSC curve as the compounds of the series $[La_xEu_{1-x}(C_{11}H_{23}COO)_3]$. In Figure 4-1 the DSC thermogram of $[La_{0.55}Eu_{0.45}(C_{11}H_{23}COO)_3]$ is shown (first heating and cooling cycle). Both peaks are quite distinct and the enthalpy change of the first transition is much higher as that of the second, indicating the formation of a mesophase.

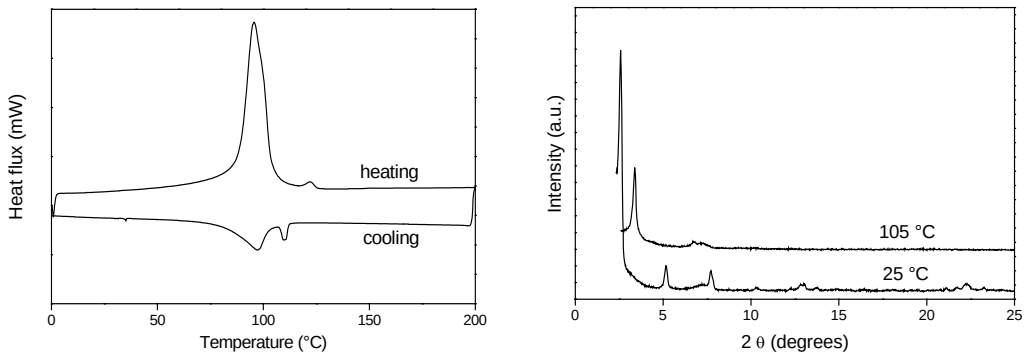

Figure 4-1 DSC thermogram of $[La_{0.55}Eu_{0.45}(C_{11}H_{23}CO_2)_3]$, first heating and cooling cycle, endothermic peaks are pointing upward (left) and X-ray diffractogram of $[La_{0.60}Eu_{0.40}(C_{11}H_{23}CO_2)_3]$ at room temperature and in the mesophase

The fact that in these compounds both melting and clearing points can be observed, means that mesomorphism is induced in a non-mesogenic compound (i.e. europium(III) dodecanoate) by mixing it with the mesogenic lanthanum(III) dodecanoate.

Although the compounds with lower lanthanum(III) content ($x < 0.40$) do not exhibit two or more peaks in their DSC-thermograms, we expected a mesophase for these compounds. Indeed, plotting the melting and clearing temperatures as a function of the lanthanum concentration gives two straight lines crossing at a mole fraction of lanthanum(III) of ca. 0.04. This means that all the compounds from the series $[La_xEu_{1-x}(C_{11}H_{23}COO)_3]$ with $x \geq 0.04$ must be mesomorphic. The fact that we do not see a clearing peak in the DSC-thermogram can be attributed to a very small heat exchange at the phase transition and to overlap between the melting and the clearing peak.

It should be noticed that although the compounds are not anhydrous, the presence of water molecules does not influence the lamellar structure and therefore not the mesophase behaviour. This is due to the fact that the water molecules are situated in the ionic layer of these compounds and the mesomorphic behaviour is mostly determined by the melting of the alkyl chains. However, the presence of water molecules affects the melting enthalpy, but not the transition temperature. In the first heating run the melting peak is rather broad and the enthalpy is much higher than in the second heating run because of the loss of water molecules.

The mesomorphic properties of these compounds have been investigated by hot-stage polarized optical microscopy. In this way it was possible to determine the complete phase diagram of the series $[La_xEu_{1-x}(C_{11}H_{23}COO)_3]$. The obtained textures had a grainy appearance with white-yellow zones on a dark background. They look very similar to those for lanthanide(III) dodecanoates, which exhibit a SmA phase. The exact mesophase could only be determined by high-temperature X-ray diffraction.

The X-ray diffractogram of $[La_{0.60}Eu_{0.40}(C_{11}H_{23}COO)_3]$ at room temperature and in the mesophase is given in Figure 4-1. Up to 4 peaks were observed in the low-angle region of the X-ray powder diffractogram of the solid mixed lanthanum-europium alkanoates, with the peak at the smallest angle bearing by far the highest intensity. The *d* spacing values are in the ratio 1:1/2:1/3….1/*n*. These diffraction peaks correspond to the successive (00*l*) reflections, and indicate the presence of a lamellar structure. The polar groups of the lanthanide(III) alkanoates are localized in infinite, parallel and equidistant planes. These planes are separated from each other by a bilayer of alkyl chains in the *all trans* conformation. The interplanar layer spacing *d* corresponds to the distance between two successive layers of lanthanide(III) ions. So the overall structure of binary lanthanide(III) dodecanoate mixtures is the same as the normal lanthanide(III) alkanoate structure. Hence we may make the same assumptions between structure and thermal behaviour as we have done for the normal lanthanide(III) alkanoates.

In the mesophase, the lamellar bilayer structure is retained, but a distinct decrease in *d* spacing is observed at the solid-mesophase transition (see Figure 4-1). This indicates that the alkyl chains lose their *all trans* conformation and that some kind of curling occurs. The temperature dependence of the *d* spacing in the mesophase (decrease of *d* spacing at increasing temperatures) corresponds to the behaviour expected for a smectic A phase (Figure 4-2) [6]. At the clearing point most structure is lost and an isotropic phase is formed.

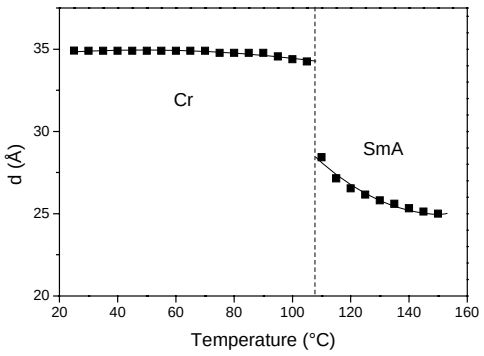

Figure 4-2 Change of the *d* spacing of $[La_{0.95}Eu_{0.5}(C_{11}H_{23}CO_2)_3]$ as a function of the temperature

The whole series of $[La_xEu_{1-x}(C_{11}H_{23}COO)_3]$ whereby $x \geq 0.04$ exhibits a smectic A phase, although there is a marked influence of the composition of the mixed complexes on the transition temperatures (Figure 4-3). Both melting and clearing point increase with increasing mole fraction of lanthanum(III), but the mesophase stability increases at increasing lanthanum(III) concentration. The more stabilising lanthanum(III) is added, the more the ionic layer will be stabilised and the larger the mesophase range.

It was possible to fit the data linearly. This resulted in two straight lines with rather good R-values (linear regression for the melting point: $T_m = 80.21 + 29.59x$, R = 0.991; linear regression for the clearing point: $T_c = 78.44 + 79.18x$, R = 0.997). The fitted lines cross at 3.6 mole % lanthanum(III). So a very small amount of lanthanum(III) dodecanoate has to be added to induce mesomorphism in the non-mesogenic europium(III) dodecanoate.

The transition temperature for pure lanthanum(III) dodecanoate obtained by this fitting procedure agrees very well to the experimental values reported in 0.

This is not the case for the pure europium(III) compound (fitted temperature 81°C, experimental temperature 90°C). There are probably special effects at low lanthanum(III) concentrations, so that the transition temperatures do not depend linearly on the composition of the compounds and the fitted and experimental temperature do not agree.

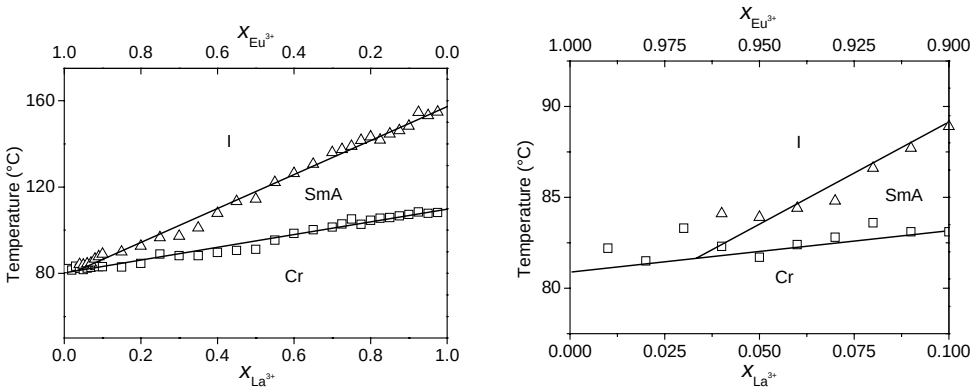

Figure 4-3 Phase diagram of the series $[La_xEu_{1-x}(C_{11}H_{23}CO_2)_3]$ as a function of the lanthanum content (left) and detail hereof

4.2.2 $[La_xNd_{1-x}(C_{11}H_{23}COO)_3]$

Although neodymium(III) dodecanoate is mesogenic (Cr · 91 · SmA · 117 · I), the stability range of the mesophase is much lower as for the lanthanum(III) dodecanoate.

We tried to obtain a higher mesophase stability by adding small amounts of lanthanum(III) dodecanoate, but this did not work. Also for higher lanthanum(III) content the stability of the mesophase is lower than can be expected from the *additivity law*, that is $T_c = T_1 + x_2(T_2 - T_1)$ [7]. T_c is the clearing point of the binary mixture, T_1 and T_2 are the clearing points of both components of the mixtures and x_2 is the mole percent of the second component. This is in contrast to the observations of Mirnaya who describes binary mixtures of ionic mesogenic systems with short alkyl chains [4].

The fact that our compounds have lower clearing points than expected, can be assigned to the long alkyl chains in the mixed lanthanum(III)-neodymium(III) dodecanoates. In lanthanide(III) alkanoates phase transitions are a competition between electrostatic interactions in the ionic layer and melting of the alkyl chain, whereas for short chain homologues (as described by Mirnaya) the alkyl chains have a minor influence on the phase transitions.

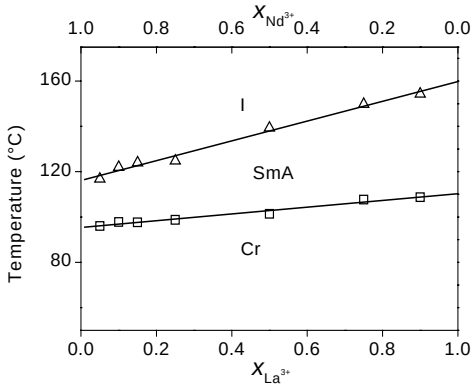

Figure 4-4 Phase diagram of the series $[La_xNd_{1-x}(C_{11}H_{23}CO_2)_3]$ as a function of the lanthanum content

4.2.3 $[La_xTb_{1-x}(C_{11}H_{23}COO)_3]$, $[La_xHo_{1-x}(C_{11}H_{23}COO)_3]$ and $[La_xYb_{1-x}(C_{11}H_{23}COO)_3]$

Additionally, phase diagrams of $[La_xTb_{1-x}(C_{11}H_{23}COO)_3]$, $[La_xHo_{1-x}(C_{11}H_{23}COO)_3]$ and $[La_xYb_{1-x}(C_{11}H_{23}COO)_3]$ have been investigated. It can clearly be seen that mesomorphism is induced by mixing the non-mesogenic compounds terbium(III), holmium(III) and ytterbium(III) dodecanoate with the mesogenic lanthanum(III) dodecanoate, but the amount of lanthanum(III) dodecanoate necessary to induce mesomorphism is much higher than for the lanthanum-europium mixtures.

All the data can be fitted easily, so we were able to deduce the lanthanum(III) content whereby the mixed lanthanum-lanthanide complexes form mesophases. Whereas for lanthanum-europium mixtures not more than 4 mole percent lanthanum(III) was necessary for mesophase induction, the minimum lanthanum(III) content increases to

42 % for lanthanum-terbium, 47 % for lanthanum-holmium and 48 % for lanthanum-ytterbium mixtures. (see Figure 4-4 - Figure 4-5)

The transition temperatures and enthalpies of all the compounds described in this work can be found in Table 2.2-1 - Table 2.2-5, Appendix 2.

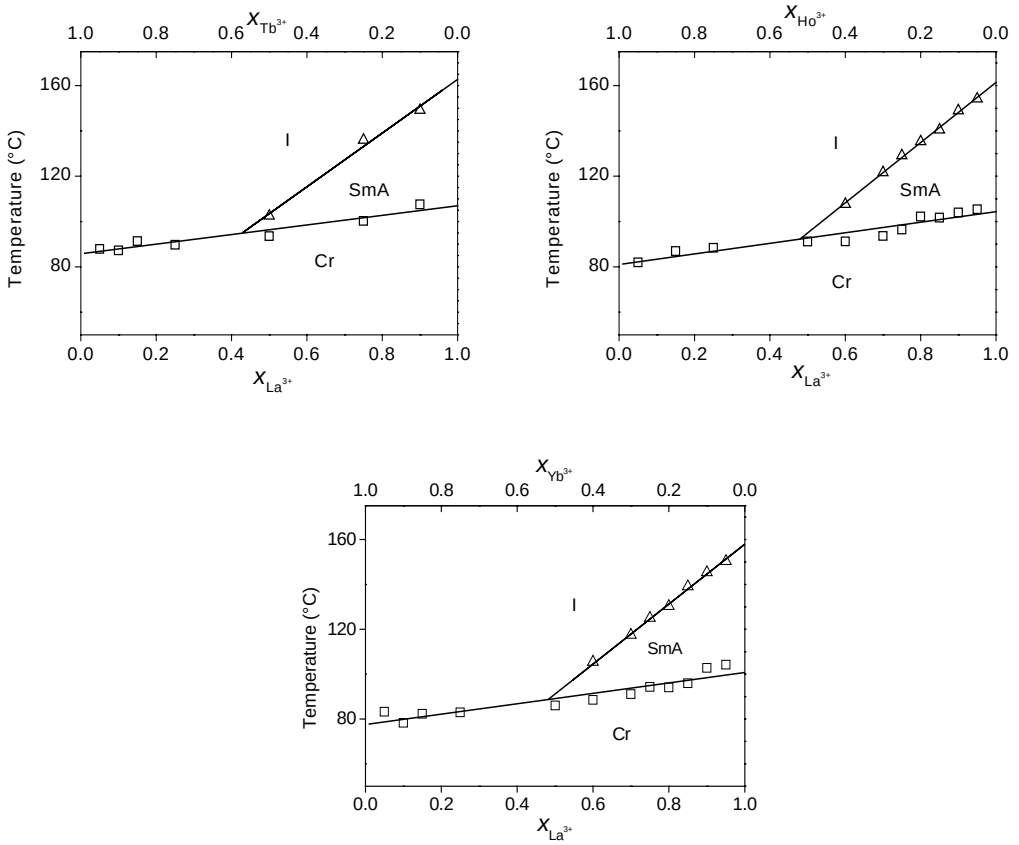

Figure 4-5 Phase diagram of the series $[La_xTb_{1-x}(C_{11}H_{23}CO_2)_3]$ (upperleft), $[La_xHo_{1-x}(C_{11}H_{23}CO_2)_3]$ and of $[La_xHo_{1-x}(C_{11}H_{23}CO_2)_3]$ as a function of the lanthanum content

4.2.4 Conclusion

The results of this experiment confirm the theory on the effect of the ionic radius on the stability of a mesophase. The smaller the lanthanide ion, the more unfavourable the electrostatic interactions between the carboxylate groups become and the easier the layer structure of the lanthanide ions breaks down. This results in lower transition temperatures.

Adding a lanthanide(III) ion with a large ionic radius reduces the unfavourable interactions that much that a mesophase can occur. Whereas the ionic radius of the europium ion is only just too small to form a stable mesophase, adding small amounts of lanthanum is enough to form a smectic A phase. The more stabilizing lanthanum(III) is added, the more the mesophase will be stabilized and the higher mesophase stability will be. We were thus able to induce a mesophase in mixtures of lanthanum(III) dodecanoate with europium(III), terbium(III), holmium(III) and ytterbium(III).

There is a marked influence of the lanthanide ion on the stability of the induced mesophase.

Whereas for La(III) – Eu(III) mixtures only 4 mole percent lanthanum is necessary to induce a mesophase, for La(III) – Tb(III) mixtures this increases to 42% , to 47% for lanthanum(III) – holmium(III) mixtures and to 48% for lanthanum(III) – ytterbium(III) mixtures. These experiments show again the relation between the formation of a mesophase and the ionic radius of the lanthanide ions which was found for the lanthanide(III) dodecanoates.

References

[1] J. Robberecht *Bull. Soc. Chim. Belg.* **47** (1938) 597.

[2] R. Shasidar, S. Chandrasekhar *J. Phys. Coll.* **36** (1985) C1-48.

[3] A. M. Levelut, R. J. Tarento, F. Harodouin, M. F. Achard, G. Sigaud *Phys. Rev. A*, **24** (1981) 2180.

[4] T. A. Mirnaya, V. D. Prisyazhnyi, V. A. Shcherbakov *Russ. Chem. Rev.* **58** (1989) 821.

[5] J. A. R. Cheda, M. Fernandez-Garcia, M. V. Roux, C. Turrion *Pure Appl. Chem.* **64** (1992) 65.

[6] J. M. Seddon, *Structural Studies of Liquid Crystals by X-ray Diffraction,* in *Handbook of Liquid Crystals Vol.1* (Eds. D. Demus, J. Goodby, G. W. Gray, H.-W. Spiess, V. Vill), VCH-Wiley, Weinheim, Chapt. 13 **1998**.

[7] G. W. Gray *Molecular Structure and the Properties of Liquid Crystals,* Academ. Press, London-NewYork **1962**.

Chapter 5 Lanthanide(III) Complexes of n-Alkanoic Acids and 1,10-phenanthroline

A neutral ligand can be used to induce a mesophase and stabilisation of the lanthanide – ligand interaction [1 - 2]. With the synthesis of adducts of lanthanide(III) alkanoates with 1,10-phenanthroline we tried to stabilise the ionic lanthanide layer so that possibly a mesophase can be found for lanthanide(III) alkanoates which normally do not show any mesomorphism.

Lebedev was the first to describe in 1995 the synthesis of binary complexes of lanthanide(III) ions with carboxylic acids and 1,10-phenanthroline [3]. The group of Legendiewicz studied [$Eu(C_5H_{11}CO_2)_3$·1,10-phenanthroline] thoroughly because of its strong luminescence [4 - 6].

5.1 Synthesis and Characterisation

1,10-phenanthroline and the carboxylic acid were dissolved in pure dry ethanol. The solution was heated till boiling. An equivalent amount of NaOH in ethanol was added dropwise.

The lanthanide(III) nitrate salt was dissolved in pure ethanol and heated. The hot lanthanide(III) solution was added dropwise to the 1,10-phenanthroline – carboxylate solution. The solution of this mixture must be clear; when a precipitate is formed, the solution must be decanted. The remaining solution was refluxed during 1h.

Hereafter the hot solution was cooled down immediately in the refrigerator (-25°C). After 2 days the precipitate was filtered off, washed with pure ethanol and dried in vacuum.

The compounds were recrystallised from pure dry ethanol. The dissolved product is decanted and the insoluble rest is thrown away. The hot solution was put in the refrigerator for 2 days. The compounds were filtered off after 2 days, washed with pure ethanol and dried in vacuum.
When crystals for X-ray analysis were grown, the crystallisation took place at room temperature.
It was not possible to synthesize adducts with all the lanthanide ions or with all the chain lengths like the normal lanthanide(III) alkanoates. First, the size of the lanthanide ion determines the adduct formation. When the lanthanide ion is too large (e.g. La^{3+}) the cavity in the 1,10-phenanthroline group is too small for the lanthanide ion and the adduct does not form. When the lanthanide ion is too small (e.g. Lu^{3+}) it is very difficult to synthesize the adduct because the 1,10-phenanthroline cavity is too large. Secondly, the length of the alkyl chain influences the complex formation because adducts are only formed in solution. The longer the alkyl chain, the worse the lanthanide(III) alkanoate dissolves in ethanol and the lanthanide(III) alkanoate precipitates before adduct formation takes place.
Both factors (i.e. the lanthanide ion size and the alkyl chain length) determine if an adduct can be formed with a certain lanthanide ion and a given carboxylic acid.
No complexes of Ce(III) ware synthesised, because of unexpected oxidation of the reagents during synthesis.

In general the compounds are obtained as needle like crystals (x = 5 – 8) or as crystalline powders (x = 9 – 11), with the typical colour of the trivalent lanthanide ion.

The purity of all the compounds is checked with elemental analysis. Reliable analytical data could only be obtained after purification of the adducts by recrystallisation. In Table 3.1-1 -Table 3.1-3, Appendix 3 the CHN results are given.

Exptl. [$Ho(C_{11}H_{23}CO_2)_3$·1,10-phenanthroline]: Experimental for C: 59.40%, for H: 7.88%, for N: 3.12%; Calculated for C: 59.98%, for H: 8.28%, for N:2.91 %

5.2 Crystal Structure of [$Tb(C_5H_{11}CO_2)_3$·1,10-phenanthroline], [$Nd(C_5H_{11}CO_2)_3$·1,10-phenanthroline] and [$Nd(C_7H_{15}CO_2)_3$·1,10-phenanthroline]

5.2.1 [$Tb(C_5H_{11}CO_2)_3$·1,10-phenanthroline] and [$Nd(C_5H_{11}CO_2)_3$·1,10-phenanthroline]

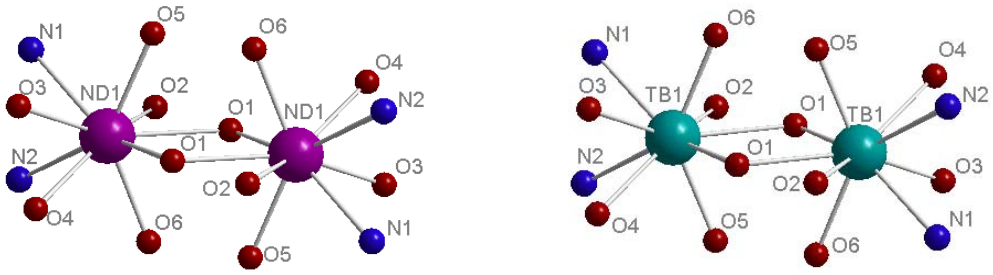

Figure 5-1 Coordination of the lanthanide ions (first coordination sphere)

Both compounds crystallise in the space group $P2_1/n$ (No. 14). The unit cell of the crystal structure of [$Tb(C_5H_{11}CO_2)_3$·1,10-phenanthroline] is built by four molecules, i.e. two dimers, so a better formula of this compound is [$Tb(C_5H_{11}CO_2)_3$·1,10-phenanthroline]$_2$. In these dimers both terbium atoms are nine-coordinated (see Figure 5-1). Each atom is surrounded by seven oxygen atoms of carboxylate groups and by two nitrogen atoms of one phenanthroline group. The terbium atoms are held together by two bidentate bridging and two tridentate chelating carboxylate groups. Further coordination of each terbium atom occurs by one bidentate chelating carboxylate and one phenanthroline group. These phenanthroline groups are placed straight in front of the terbium dimer parallel to the *bc*-plane. The alkyl chains of the bidentate and tridentate chelating carboxylate groups are placed perpendicular to the plane of the phenanthroline groups, the bidentate bridging ones are placed in a parallel way (see Figure 5-2).

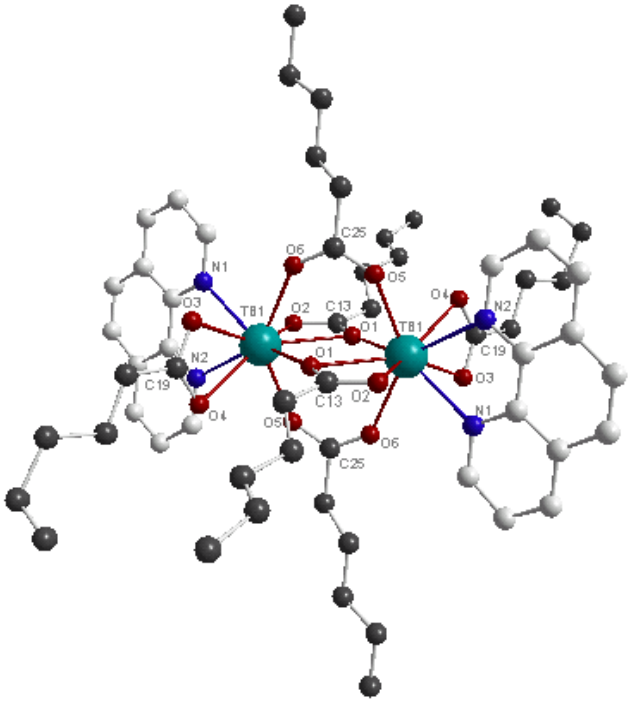

Figure 5-2 Structure and bonds in the dimer of [Tb($C_5H_{11}CO_2$)$_3$·1,10-phenanthroline]; hydrogen atoms have been omitted for clearness

These compounds show two main differences with the normal lanthanide(III) alkanoates. First, these compounds do not form infinite layers where all the lanthanide ions are connected by carboxylate groups, secondly not all the alkyl chains are in *all trans* conformation, namely the last carbon atom of the bidentate chelating carboxylate alkyl chain is in *cis* conformation. The entire dimer is spherical what implicates some important features for the thermal behaviour of this kind of compounds. (*see further)*

The crystal structures of [Tb($C_5H_{11}CO_2$)$_3$·1,10-phenanthroline] and [Nd($C_5H_{11}CO_2$)$_3$·1,10-phenanthroline] are isomorphic. So there is no clear evidence that the lanthanide ion plays an important role by the formation of the structure, although one should expect a different structure because of the difference in ion size. Moreover [Eu($C_5H_{11}CO_2$)$_3$·1,10-phenanthroline], which is known in the literature, crystallises in the same space group [3].

To interpret the 3-dimensional structure only the coordination polyhedra of the terbium dimers are shown (see Figure 5-3 - Figure 5-5).

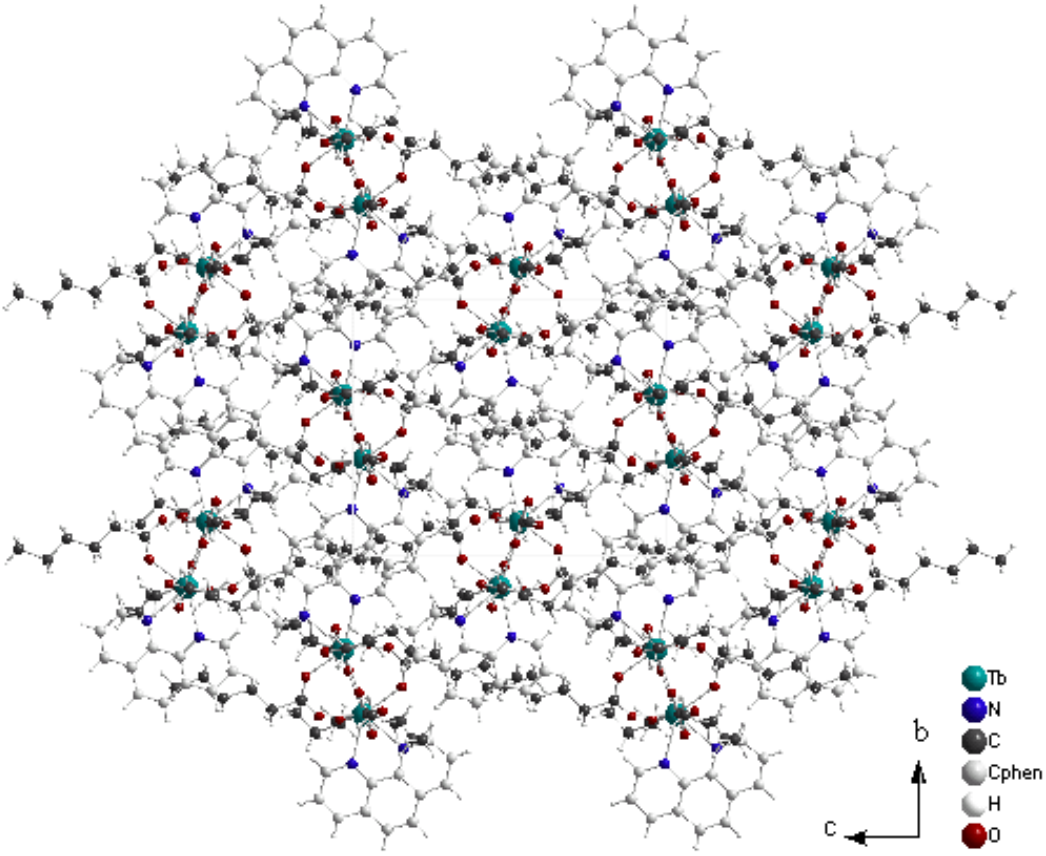

Figure 5-3 [$Tb(C_5H_{11}CO_2)_3$·1,10-phenanthroline], view down the *a*-axis

Although no layered structure is formed, dimers are placed in rows along each of the three axes. Along the *a*-axis the dimers are placed stepwise oblique. The orientation of two neighbouring rows is opposite and the dimers of one row are shifted down in regard to the next row. Along the *b*-axis the rows of dimers form oblique sheets following the diagonal of the unit cell (see Figure 5-4). The rows in these sheets are orientated in such a way that the dimer rows are alternating orientated. Also along the *c*-axis the dimers are placed in rows. Just like in the other directions these rows form sheets but the dimers of two following sheets are orientated in a different way (see Figure 5-5).

Crystallographic data can be found in Table 5.2-1, selected bond lengths and angles of [$Tb(C_5H_{11}CO_2)_3$·1,10-phenanthroline] in Table 3.2-1, Appendix 3.

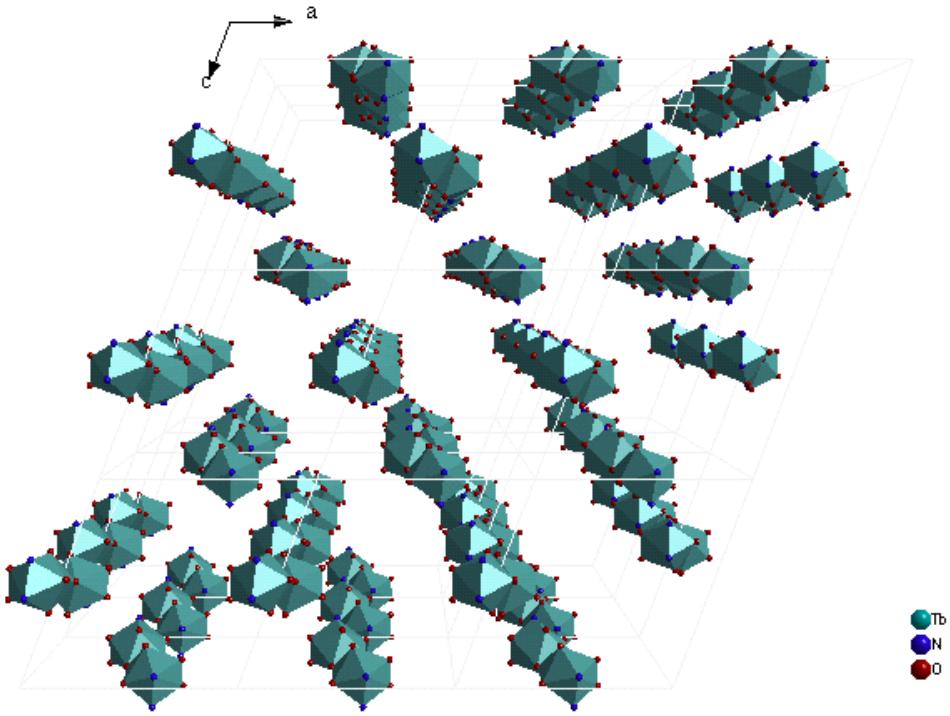

Figure 5-4 [$Tb(C_5H_{11}CO_2)_3$·1,10-phenanthroline], coordination polyhedra of terbium ions, view down the *b*-axis

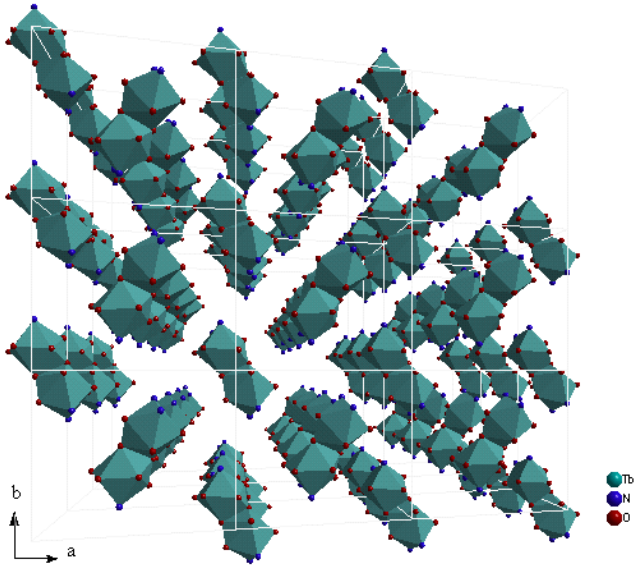

Figure 5-5 [$Tb(C_5H_{11}CO_2)_3$·1,10-phenanthroline], coordination polyhedra of terbium ions, view down the *c*-axis

5.2.2 [Nd($C_7H_{15}CO_2$)$_3$·1,10-phenanthroline]

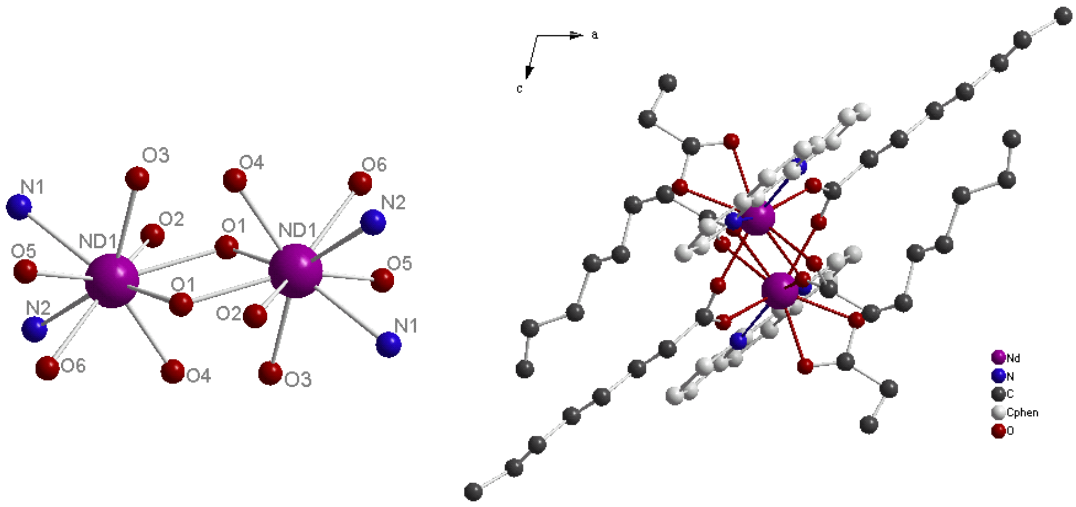

Figure 5-6 First coordination sphere and structure of the dimers of [Nd($C_7H_{15}CO_2$)$_3$·1,10-phenanthroline], not all the carbon atoms of the bidentate chelating carboxylate group were found

[Nd($C_7H_{15}CO_2$)$_3$·1,10-phenanthroline], which crystallises in the space group C2/n (No. 15), has a unit cell with eight molecules, i.e. 4 dimers. Although the alkyl chain of this compound possesses just two carbon atoms more than the structures described in 5.2.1 , the structure of the dimer is different. The main difference is the conformation of the alkyl chains rather than the first coordination sphere of the lanthanide ions. Just like the other compounds three different kinds of carboxylate groups are present: one bidentate bridging, one bidentate and one tridentate chelating carboxylate. But, whereas for the lanthanide(III) hexanoate phenanthroline complexes two alkyl chains are perpendicular to the phenanthroline groups, only one is present for this neodymium(III) octanoate phenanthroline complex. The other two alkyl chains are placed parallel to this plane. This means that one of both alkyl chains is not in *all trans* conformation but in *cis*. The folding occurs on the second carbon atom. So only the bidentate bridging and the bidentate chelating carboxylate alkyl chain are totally stretched (see Figure 5-6). This folded alkyl chain and the fact that the overall dimer structure is spherical strongly influences the thermal properties.

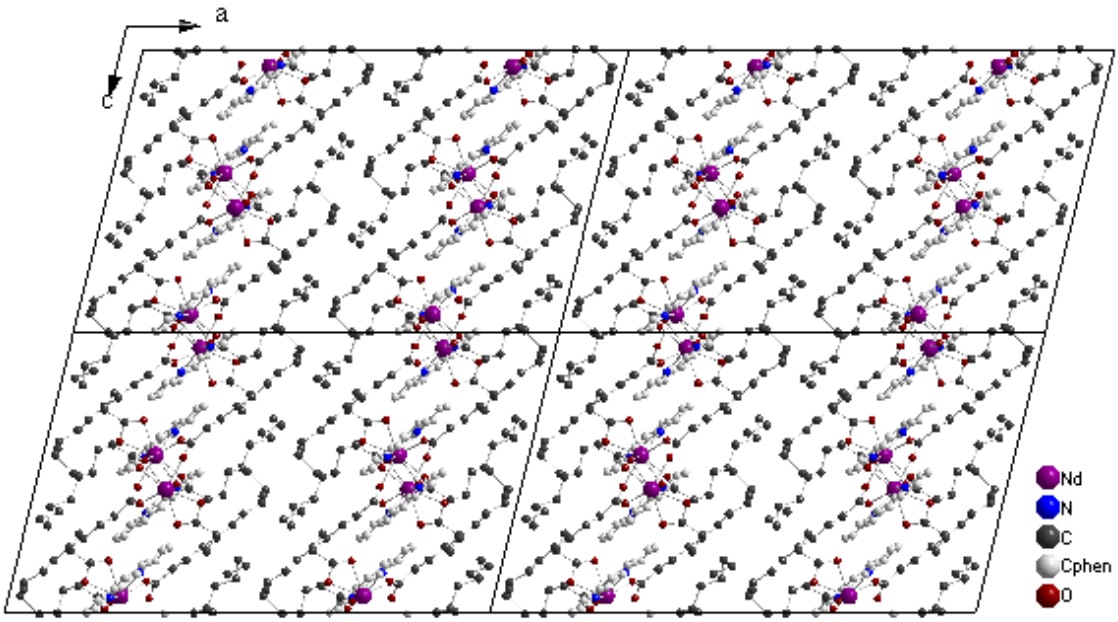

Figure 5-7 [$Nd(C_7H_{15}CO_2)_3$·1,10-phenanthroline], view down the *b*-axis

Another difference with [$Ln(C_5H_{11}CO_2)_3$·1,10-phenanthroline] complexes is the three-dimensional structure. Whereas for the hexanoate phenanthroline complexes along the three unit cell axes rows of dimers are built, here this is only the case along the *a* and *b*-axis. (see Figure 5-7 - Figure 5-9). Along *b* rows form sheets parallel to *c*. The molecules in two neighbouring rows in one sheet are oppositely oriented.
Along the *a*-axis the rows are placed stepwise, whereby one row is shifted down in regard to the second one. The rows form sheets parallel to the *ab* plane.
Along the *c*-axis the molecules form undulating sheets in the *bc* plane. No real dimer rows are present, because two following rows are penetrated into each other.

It was very difficult to dissolve the structure of this last compound. First, the number of reflections was very low; secondly the temperature factors of the carbon atoms of the alkyl chains were very large and the atoms could hardly be found. Especially, we did not find all the carbon atoms of the bidentate chelating carboxylate groups. This can be attributed to the fact that this chain has much space to move, so a badly ordered crystal is formed.

However, because the structure of the neodymium(III) octanoate 1,10 phenanthroline is different from the hexanoate complex, we decided to mention the structure here, mostly because the thermal behaviour of this kind of compounds is largely influenced by the structure.

Crystallographic data are listed in Table 5.2-2.

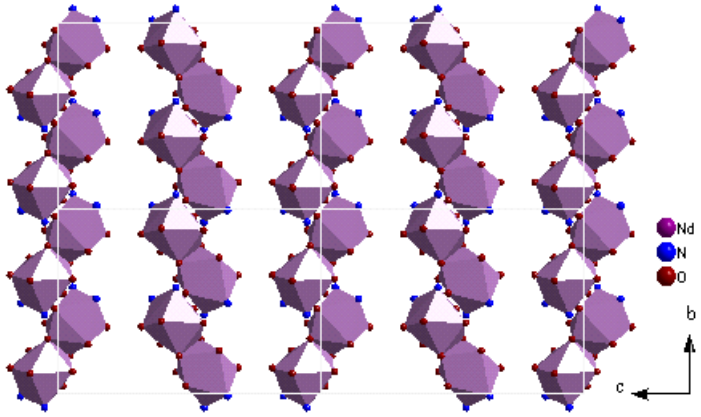

Figure 5-8 [$Nd(C_7H_{15}CO_2)_3 \cdot$1,10-phenanthroline], view down the *a*-axis

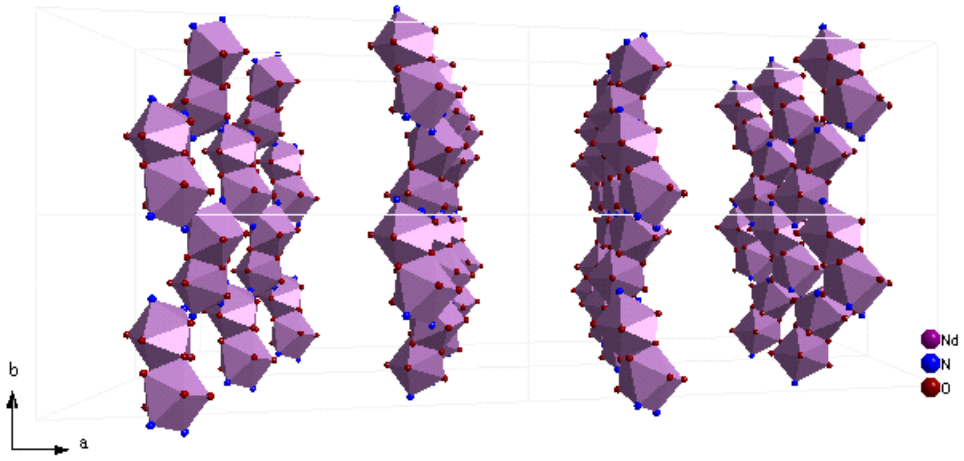

Figure 5-9 [$Nd(C_7H_{15}CO_2)_3 \cdot$1,10-phenanthroline], view down the *c*-axis

Table 5.2-1 Summary of crystallographic data for [$Tb(C_5H_{11}CO_2)_3$·1,10-phenanthroline]

Emperical Formula	$C_{120}H_{164}N_8O_{24}Tb_4$
Fw	2736.96
Space Group (No.)	$P2_1/n$ (No.14)
Unit Cell Dimensions (Å, °)	a = 16.111 (6)
	b = 12.683 (3)
	c = 16.632 (7)
	α = 90.00
	β = 110.84 (4)
	γ = 90.00
V ($Å^3$)	3176.3 (19)
Z	1
D_{calc} (g cm^{-1})	1.431
T (K)	293 (2)
λ (Å)	0.7107 (Mo-Kα graphite)
θ limits (deg)	2.07-24.09
μ (mm^{-1})	2.138
No. of Parameters	352
F (000)	1392
Reflections collected/unique	24944/4916 [R_{int} = 0.0899]
Goodness-of-fit on F^2	0.836
Final R indices [$I_0 > 2\sigma(I_0)$]	R_1 = 0.0377, wR2 = 0.0765
R indices (all data)	R_1 = 0.0870, wR2 = 0.0765

Table 5.2-2 Summary of crystallographic data for [$Nd(C_7H_{15}CO_2)_3$·1,10-phenanthroline]

Emperical Formula	$C_{288}H_{80}N_{16}Nd_8O_{48}$
Fw	5684.96
Space Group (No.)	C2/n (No. 15)
Unit Cell Dimensions (Å, °)	a = 31.861(10)
	b = 12.906(3)
	c = 18.958(5)
	α = 90.00
	β = 103.90(3)
	γ = 90.00
V ($Å^3$)	7567(3)
Z	1
D_{calc} (g cm^{-1})	1.248
T (K)	293 (2)
λ (Å)	0.7107 (Mo-Kα graphite)
θ limits (deg)	1.71 - 21.04
μ (mm^{-1})	1.318
No. of Parameters	186
F (000)	2783
Reflections collected/unique	4005/626
Goodness-of-fit on F^2	0.594
Final R indices [$I_0 > 2\sigma(I_0)$]	R_1 = 0.3563, wR2 = 0.2905
R indices (all data)	R_1 = 0.0944, wR2 = 0.1907

5.3 Thermal Behaviour of [$Ln(C_xH_{2x+1}CO_2)_3$·1,10-phenanthroline]

It was clear from the first DSC measurements that the thermal properties of adducts of lanthanide(III) alkanoates with 1,10-phenanthroline are completely different from these of the pure alkanoates. The melting point is much higher and the transition peaks are much smaller. We investigated the influence of the lanthanide ion on the series [$Ln(C_5H_{11}CO_2)_3$·1,10-phenanthroline] and of [$Ln(C_{11}H_{23}CO_2)_3$·1,10-phenanthroline] and of the chain length on the series [$Eu(C_xH_{2x+1}CO_2)_3$·1,10-phenanthroline].
Transition temperatures and enthalpies are listed in Table 3.3-1 - Table 3.3-3, Appendix 3.

5.3.1 Influence of the Lanthanide ion on the Thermal Behaviour of [$Ln(C_xH_{2x+1}CO_2)_3$·1,10-phenanthroline]

5.3.1.1 [$Ln(C_5H_{11}CO_2)_3$·1,10-phenanthroline]

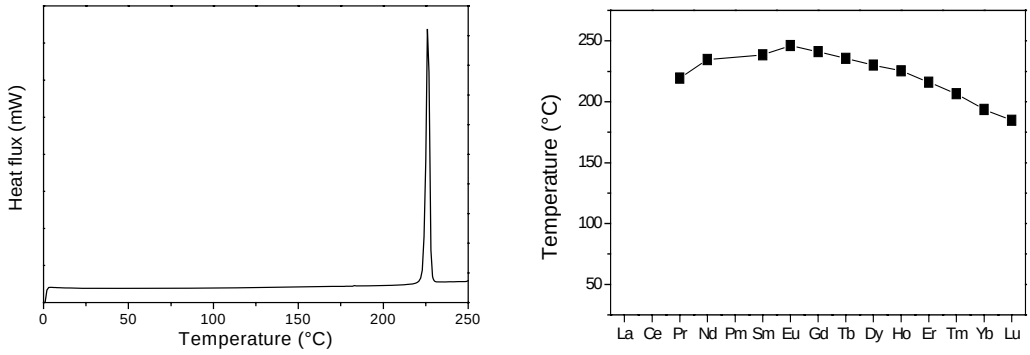

Figure 5-10 DSC thermogram of [$Nd(C_5H_{11}CO_2)_3$·1,10-phenanthroline] (left) and effect of the lanthanide ion on the transition temperatures

There is a single melting peak above 180°C for all compounds of the series [$Ln(C_5H_{11}CO_2)_3$·1,10-phenanthroline] (see Figure 5-10). The temperature increases

from praseodymium to europium and decreases from europium to lutetium (see Figure 5-10). It is possible that the interaction between the europium ion and the phenanthroline group is ideal, whereas for the larger or smaller lanthanide ions this interaction is less favourable, so the structure will break down at lower temperatures. At the melting point the compounds are transformed in an isotropic liquid. This became evident from XRD measurements at high temperatures. No peak is observed after melting, so a totally isotropic phase must be formed.

There is no evidence for mesomorphism, neither in DSC, neither in thermo-optical microscopy, nor in X-ray diffraction at high temperatures.
The high melting point and the absence of a mesophase are in contrast with the normal lanthanide(III) alkanoates where at least one mesophase is present when Ln = La, Ce, Pr and Nd and where the melting point is much lower. The reason for the absence of any mesomorphism can be related to the structure of the complexes. Lanthanide(III) hexanoate phenanthroline adducts are more or less spherical dimeric compounds. There is no interaction between the dimers. Hence, it is rather logical that these compounds do not form a mesophase because molecular anisotropy is a condition for the existence of a mesophase.

5.3.1.2 [Ln($C_{11}H_{23}CO_2$)$_3$·1,10-phenanthroline]

These compounds show a complex phase behaviour. In DSC and thermo-optical microscopy two phase transitions occur before complete melting (see Figure 5-11). These transitions are crystal - crystal transitions because in microscopy only some birefringence appears, but the compounds do not show any fluidity. Except for this the enthalpies of all the transitions are comparable. If the compounds were mesomorphic, the clearing enthalpy would be much smaller than the other phase transitions. One of both phase transitions can be seen in X-ray diffraction at high temperatures. This phase transition can unambiguously be related to the crystal structure of this compound.

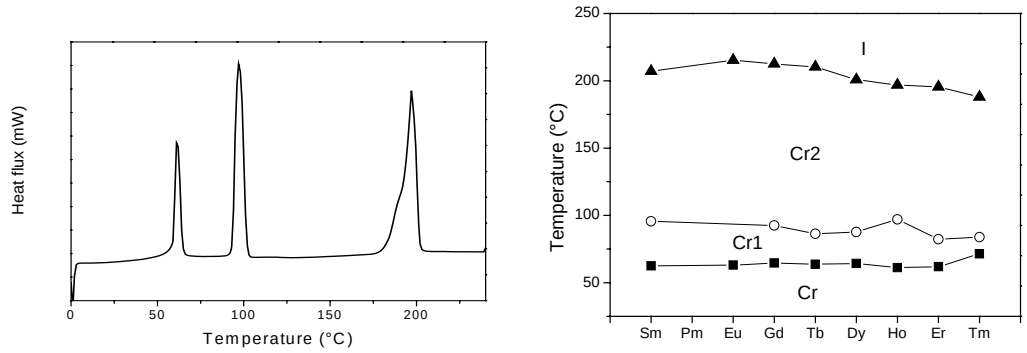

Figure 5-11 DSC thermogram of [Ho($C_{11}H_{23}CO_2$)$_3$·1,10-phenanthroline] (left) and effect of the lanthanide ion on the transition temperatures

First suppose that all the compounds of the series [Ln($C_xH_{2x+1}CO_2$)$_3$·1,10-phenanthroline] with $x \geq 7$ show more or less the same structure and more specific the same dimer structure (this approach fits very well for the Ln($C_xH_{2x+1}CO_2$)$_3$ series). In this case there always is an alkyl chain that is not totally stretched. By heating, the alkyl chains move more and more. At a given temperature, the folding of the chain is not longer stable and the chain will rearrange to an *all trans* conformation. At this point a phase transition occurs. It is possible that at higher temperatures a rearrangement occurs.

5.3.2 Influence of the Chain Length on the Thermal Behaviour of the Series [Eu($C_xH_{2x+1}CO_2$)$_3$·1,10-phenanthroline]

It was also interesting to investigate the influence of the chain length on the thermal behaviour. Therefore the series [Eu($C_xH_{2x+1}CO_2$)$_3$·1,10-phenanthroline] was synthesised. We also tried to synthesise compounds with $x > 11$, but they could not be obtained as pure products.

The chain length has an influence on the transition temperatures. The melting point decreases with increasing chain length (but less than for the normal alkanoates). The

temperature of the crystal – crystal transition increases slightly with increasing chain length and an odd - even effect seems to occur (see Figure 5-12). This odd - even effect arises from the structure of the adducts. These complexes do not form bilayers, but dimers. So the number of carbon atoms can be odd.

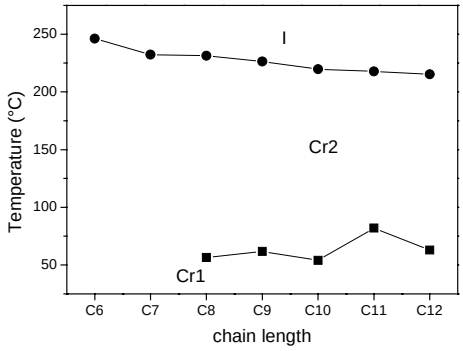

Figure 5-12 Effect of the chain length in the series [Eu($C_xH_{2x+1}CO_2$)$_3$·1,10-phenanthroline]

[Eu($C_5H_{11}CO_2$)$_3$·1,10-phenanthroline] and [Eu($C_6H_{13}CO_2$)$_3$·1,10-phenanthroline] show only one single phase transition (i.e. melting). When the alkyl chain is longer, at least two phase transitions are visible which can be related to a difference in structure (see 5.3.1.2).

5.3.3 Conclusion

It is clear that the introduction of a phenanthroline group in lanthanide(III) alkanoates has a pronounced effect not only on the thermal behaviour, but also on the synthesis and structure of the complexes.

The basic idea behind the preparation of this type of compounds was the stabilisation of the ionic lanthanide layer so that the smaller lanthanide(III) ions (from which the normal alkanoates do not show mesomorphism because they are too small) show mesomorphism.

The stabilisation of the ionic layer was successful (cfr. high melting temperatures) but none of the compounds is mesomorphic, neither the complexes with the lanthanide(III) ions that normally show a mesophase. This can be contributed to the fact that the compounds do not show any anisotropy, but they form more or less spherical dimers. There is a rigid centre present and there are flexible chains, but these chains point in all directions and can not be orientated in an anisotropic way, nor can the dimers be oriented in layers of columns because there is no interaction between them. However, several phase transitions occur for the longer chain length complexes. This can be attributed to the conformation of the alkyl chains in the adduct structure.
The thermal behaviour of the adducts is different from the thermal behaviour of the normal lanthanide(III) alkanoates. These compounds show a crystal – crystal transition before they melt to an isotropic liquid. These phase transitions can be related to the crystal structure of the compounds. The thermal behaviour of lanthanide(III) alkanoates is related to a certain degree of melting of the alkyl chains. Moreover the normal lanthanide(III) alkanoates do not form a real isotropic liquid, but rather isotropic random domains.

The dimeric structure of these adducts are not the only known dimers of lanthanide(III) carboxylates. Lossin and Meyer discovered the crystal structure of $[Sm(CH_3CO_2)_3 \cdot (H_2O)_2] \cdot CH_3CO_2H$. [7]. The dimer unit of this compound is built in the same way as lanthanide(III) alkanoate phenanthroline adducts. In this acetic acid adduct of samarium acetate dihydrate, the lanthanide ions are coordinated by a bidentate chelating, a bidentate bridging and a tridentate carboxylate group. Two water molecules complete the coordination of the lanthanide ions. The overall dimer structure is the same as we found for lanthanide(III) alkanoate phenanthroline complexes.

References

[1] A. M. Giroud-Godquin *Coord. Chem. Rev.* **180** (1998) 1485.

[2] K. Binnemans, K. Lodewyckx *Angew. Chem. Int. Ed* .**40** (2001) 242

[3] M.A. Poraikoshits, A. S. Antsyshkina, G. G. Sadikov, E. N. Lebedeva, S. S. Korovin, R. N. Shchelokov, V. G. Lebedev *Russian J. Inorg. Chem.* **40** (1995) 748.

[4] J. Legendziewicz *Acta Phys. Pol. A* **90**(1996) 127.

[5] V. Tsaryuk, J. Legendziewicz, V. Zolin, J. Sokolnicki, R. Szostak, L. Puntus *J. All. Comp.* **323** (2001) 661.

[6] J. Legendziewicz, V. Tsaryuk, V. Zolin, E. Lebedeva, M. Borzechowska, M. Karbowiak *New J. Chem.* **25** (2001) 1037.

[7] A. Lossin, G. Meyer *Z. Naturforsch.* **47b** (1991) 179.

Chapter 6 Lanthanide(III) Complexes of 4-Alkoxybenzoic Acids

The synthesis and characterisation of these ligands is well known. Mostly these compounds are used as starting products of mesomorphic compounds [1 - 4]. However they also can be used as ligands themselves because of their carboxylate function. It must be said that much less information is available on lanthanide(III) benzoates [5 - 8].

6.1 Synthesis and Characterisation

6.1.1 Synthesis and Characterisation of the Ligands

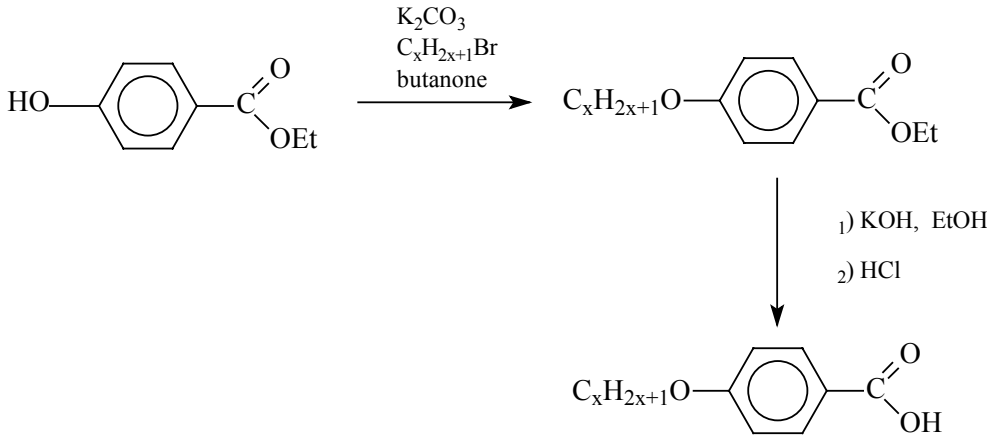

Scheme 6-1 Synthesis of 4-alkoxybenzoic acids

4-alkoxybenzoic acids were prepared via a Williamson-ether synthesis. Here the *n*-bromoalkane reacted with a mixture of ethyl-4-hydroxybenzoate and potassium

carbonate with potassium iodide as catalyst and 2-butanone as solvent. This was followed by saponification of the ester and workup in acidic solution. Hereafter the compounds were recrystallised from pure ethanol.

In this way the following 4-alkoxybenzoic acids were synthesized: 4-butyloxybenzoic acid, 4-hexyloxybenzoic acid, 4-octyloxybenzoic acid, 4-nonyloxybenzoic acid and 4-decyloxybenzoic acid.
CH analysis was used for the characterisation of these compounds. Calculated and experimental values for the carbon and hydrogen content are given in Table 4.1-1, Appendix 4.

Exptl. for $C_6H_{13}OC_6H_4CO_2H$: Experimental for C: 70.32%, H: 8.50%;
Calculated for C: 70.24%, H: 8.11%.

6.1.2 Synthesis and Characterisation of the Complexes

The synthesis method of the complexes was the same as for the normal lanthanide(III) carboxylates, i.e. via a metathesis reaction. To a solution of a 4-alkoxybenzoic acid in ethanol an equivalent amount of NaOH was added. To this sodium salt an aqueous solution of the desired lanthanide(III) nitrate was added dropwise. The metal complex immediately precipitated. After stirring for 1h the precipitate was filtered off and dried in vacuum.
We have tried to synthesize complexes with the different 4-alkoxybenzoic acids and with all the lanthanide ions except of the radioactive Pm and of Ce because of oxidation reactions. The compounds were obtained as waxy parchment art fragments with the colour of the lanthanide ion.

The purity was checked by CH analysis. The compounds were obtained as di- or tri-hydrates. In Appendix 4 (Table 4.1-2 - Table 4.1-6) the CH results are given for all the synthesized products.
The voluminous head groups of the ligands can explain the high degree of hydration of these complexes. This causes much space in the first and second coordination sphere of the lanthanide(III) ions where water molecules can be placed.

Exptl. for $Gd(C_6H_{13}OC_6H_4CO_2)_3.3H_2O$: Experimental for C: 53.66%, for H: 6.40%; Calculated for C: 53.53%, for H: 6.56%.

6.2 Thermal Behaviour

Whereas the normal lanthanide(III) alkanoates show a rather simple thermal behaviour, lanthanide(III) 4-alkoxybenzoates do not. Although the DSC-thermograms of the first heating cycle do not differ that much from the normal lanthanide(III) alkanoates, the thermal behaviour of these compounds in the cooling and second heating cycle is very strange. Whereas we expect at least a crystallisation peak in the cooling run, no peak at all is seen, even no glass transition. Further investigation of their thermal properties (DSC, thermo-optical microscopy and synchrotron diffraction) gave us the opportunity to discover the large influence of the structure hereon.

6.2.1 Thermal Behaviour of the Ligands

4-alkoxybenzoic acids are well known because of their liquid crystalline behaviour. Moreover, these compounds show several mesophases (often a smectic C and a nematic phase). The most interesting is that the rigid core of the mesogens (which is a condition to form a mesophase) is built by intermolecular hydrogen bonds between the carboxylic acids functions.

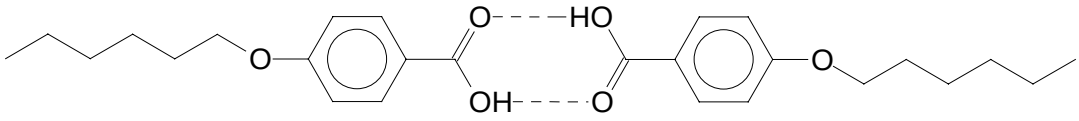

Figure 6-1 Dimer built by intermolecular hydrogen bonds in 4-hexyloxybenzoic acid

The phase behaviour of 4-alkoxybenzoic acids depends on the chain length. Whereas for the shorter ones (e.g. 4-butyloxy and 4-hexyloxybenzoic acid) only one mesophase is observed (i.e. a nematic phase), two mesophases are present for the longer homologues (i.e. a smectic C and a nematic phase). Only a smectic C phase is formed for the homologues with very long alkyl chains [9]. In Table 4.2-1, Appendix 4 the transition temperatures of the 4-alkoxybenzoic acids used for complexation are given.

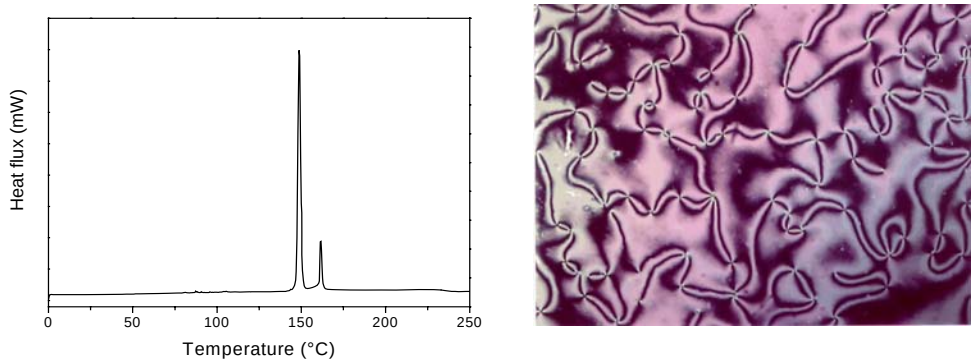

Figure 6-2 DSC thermogram of 4-alkoxybenzoic acid (left) and the Schlieren texture of its nematic phase

Because of the pronounced mesomorphic behaviour of these compounds, we tried to find out if complexation of 4-alkoxybenzoic acids with lanthanides would influence this thermal behaviour.

6.2.2 Structural Properties

For clearness several possible layered structures are given in Figure 6-3 - Figure 6-5.

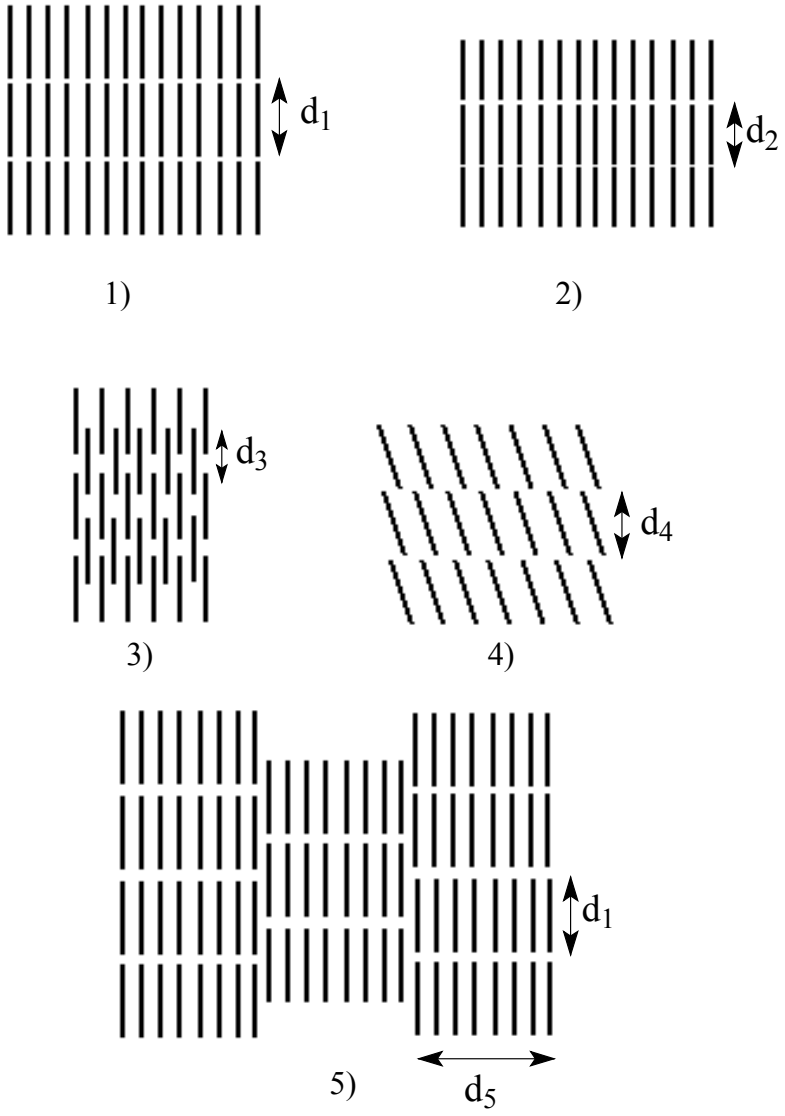

Figure 6-3 Several forms of layered structures: 1) normal layered structure, molecules are fully stretched; 2) smectic A structure, molecules are not fully stretched; 3) intercalated smectic structure; 4) smectic C structure ($d_1 > d_2$, d_3, d_4); 5) modulated SmÃ

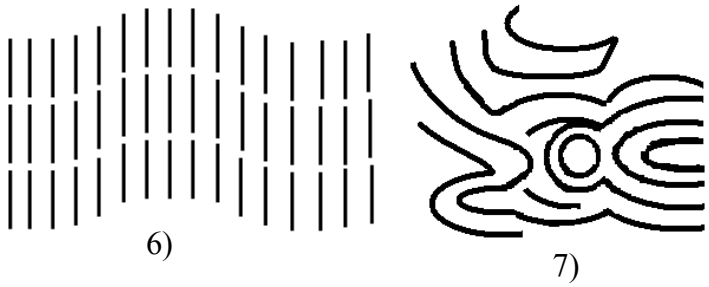

Figure 6-4 Less ordered structures: 6) undulating layered structure; 7) random domains.

Figure 6-5 Total randomisation, no structure at all.

The differences of the structures are shown in the X-ray diffraction spectra. A normal layered structure (structure 1) gives rise to higher order of peaks in the small angle region. Heating does not much affect the *d* value of the layers.

Higher orders of peaks are also possible for a smectic A and a smectic C structure and also for intercalated smectic structures (resp. structure 2, 4 and 3). However for these structures the *d* values change under influence of temperature. In a smectic A structure, the *d* value decreases as a function of the temperature, whereas the *d* value of a smectic C structure increases [10].

Modulated smectic phases are built by biaxial ribbons, which is clearly visible in its diffraction pattern. Diffraction patterns of compounds with this structure show apart from the diffraction peak of the layers a second peak at higher *d* values (see Figure 6-3, structure 5) [10]. This peak comes from the broadness of the ribbons (d_5).

This type of smectic phases has been observed with mesogens having strongly polar end groups [11 - 12]. But also steric effects can induce these structures which makes the presence of this phase in the lanthanide(III) 4-alkoxybenzoates very probable.

The main difference of these structures compared to the undulating layered structure (structure 6) and the structure with random domains (structure 7) is that for the latter higher order peaks are less probable. In the case of a structure with random domains, scattering peaks are rather broad. For the undulating layered structure a peak at higher *d* value is probable and comes because of the undulation.
When total randomisation occurs, no peak is observed.

6.2.3 Thermal Behaviour of the Complexes

The thermal behaviour of these compounds will be explained by a few examples. The behaviour of the other compounds is taken as analoguous from thermo-optical microscopy and DSC-measurements. The transition temperatures and enthalpies can be found in Appendix 4 (Table 4.2-2 - Table 4.2-6).

6.2.3.1 Influence of the Lanthanide Ion on the Thermal Properties of the Series $Ln(C_6H_{13}OC_6H_4CO_2)_3$

Compounds from the series $Ln(C_6H_{13}OC_6H_4CO_2)_3$ can be divided in four groups. The first group with Ln = La and Pr shows in the thermograms two peaks. The enthalpy of the first peak is much higher than that of the second one, indicating the existence of a mesophase. Also in the thermo-optical microscopy both transitions are visible, although the viscosity of the compounds in the region between both transitions is very high.

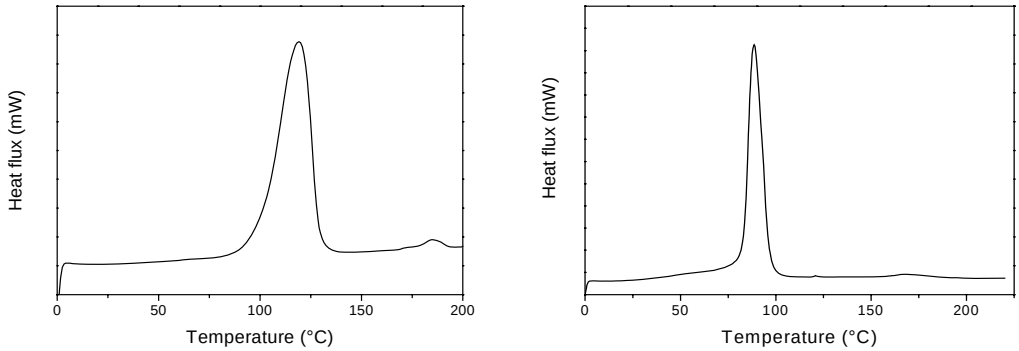

Figure 6-6 DSC-thermograms of $La(C_6H_{13}OC_6H_4CO_2)_3$ (left) and $Eu(C_6H_{13}OC_6H_4CO_2)_3$, endothermic peaks are pointing upwards

These compounds are liquid crystalline, what is confirmed by synchrotron measurements.

At room temperature the compounds show a complex type of biaxial SmA structure, i.e. a modulated SmÃ structure what is visible in the appearance of a diffraction peak of this compound at high *d* values.

The layered structure remains after the first phase transition although the *d* value decreases. Second order peaks are observed. The modulated structure disappears (see Figure 6-7) which means that infinite layers are formed.

In Figure 6-7 the change of the *d* value is given as a function of the temperature. At 110°C there is a clear decrease of the *d* value. This can be attributed to the melting of the alkyl chains and the formation of the mesophase. This temperature is lower than the peak position from DSC-measurements. However the peaks in the DSC thermograms are that broad that this temperature is still correct (up to 40°C for 1 transition).

At 185°C there is no shift in *d* value but the peak broadens and its intensity increases. Here the synchrotron measurements show still some structure in the isotropic liquid. This means that not all the structure is lost, but that some random domains remain (phase 7).

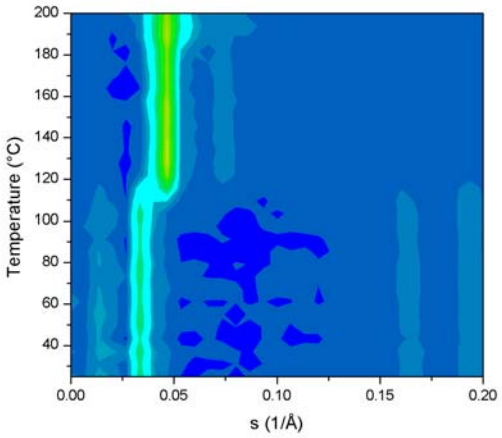

Figure 6-7 Change of the *d* value as a function of the temperature ($La(C_6H_{13}OC_6H_4CO_2)_3$)

The second group are the compounds $Ln(C_6H_{13}OC_6H_4CO_2)_3$ with Ln = Nd, Sm, Eu. For these compounds only one transition is observed with the three techniques (Figure 6-6). These compounds are not mesomorphic but melt from the solid layered phase to the phase with random domains (transition from phase 1 to phase 7).

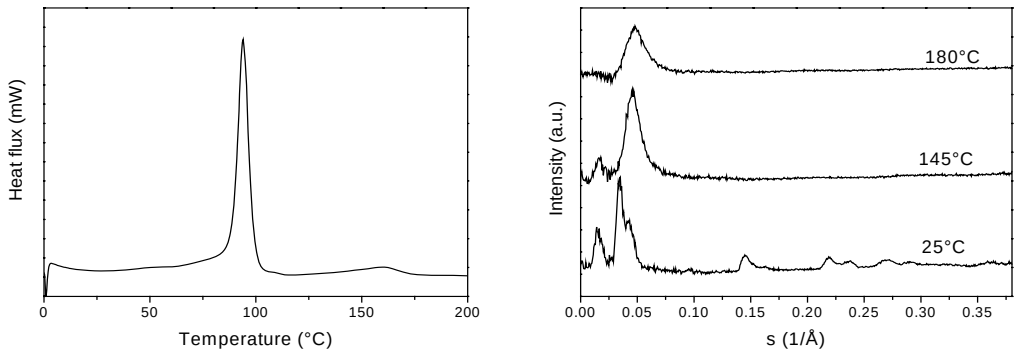

Figure 6-8 DSC-thermogram (left) and synchrotron diffractograms at different temperatures of $Tb(C_6H_{13}OC_6H_4CO_2)_3$

The third group are the compounds $Gd(C_6H_{13}OC_6H_4CO_2)_3$, $Tb(C_6H_{13}OC_6H_4CO_2)_3$ and $Ho(C_6H_{13}OC_6H_4CO_2)_3$. They show in their DSC-thermograms two transitions. The temperature of the first transition is 85-90°C, the second one ca. 165°C. There is a large difference in the transition enthalpies, which could point in the direction of a mesophase (see Table 4.2-3, Appendix 4 and Figure 6-8). However, in thermo-optical

microscopy this phase transition is visible, although the compounds do not show any fluidity. This means that this is a crystal –crystal transition, but it is also possible that at room temperature two different crystal structures are present.
In the synchrotron measurements two layered structures can be assigned to these compounds, i. e. structure 1 and structure 6. Except for the first peak assigned to the modulated SmÃ (s = 0.014 $Å^{-1}$), the second peak is in fact a double peak of two layered structures (s = 0.034 $Å^{-1}$ and 0.042 $Å^{-1}$). At the first transition the further peaks disappear whereas the intensity of the latter peak increases (s = 0.045 $Å^{-1}$). This means that the compound rearranges to structure 6, so the complete bulk is in this phase after the first transition.At the last transition most of the structure is lost and random domains are formed. (see Figure 6-8).

A last group in the series $Ln(C_6H_{13}OC_6H_4CO_2)_3$ are the compounds with Ln = Dy, Er, Yb and Lu. They also show two transitions in their DSC thermograms, but the enthalpy of both peaks is comparable and low in comparison to the enthalpy changes observed for the first three groups (see Table 4.2-3, Appendix 4). For these compounds at room temperature the undulating layered structure is mostly present. So the enthalpy of the first transition is only assigned to the small amount of molecules that are oriented in a different way. The evidence for this structure is a comparison of the synchrotron diffractogram of compounds of the third group and of this last group. The peak position of this structure in the third group is at s = 0.042 $Å^{-1}$, in the latter group s = 0.044 $Å^{-1}$. Moreover, in the latter group this peak does not shift to smaller *d* values when a transition occurs (see Figure 6-9). The peak at high *d* values (s = 0.015 $Å^{-1}$) can be assigned to the length of the undulation.
The second transition is the transition of the undulating layered structure to the structure with random domains. Because the rearrangement of the molecules is rather low, the enthalpy hereof is very low (see Figure 6-9).

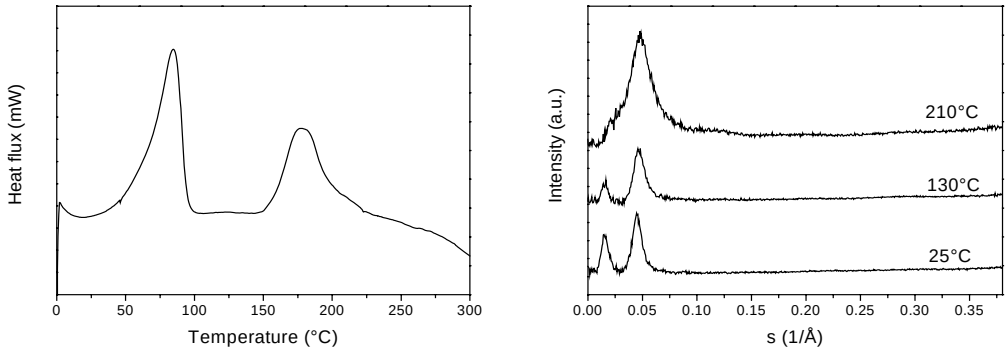

Figure 6-9 DSC thermogram (left) and synchrotron diffractograms at different temperatures of $Er(C_6H_{13}OC_6H_4CO_2)_3$

So there is a marked influence of the lanthanide ion on the thermal properties of the complexes (see Figure 6-10). Although we could not assign the difference in thermal behaviour of the normal lanthanide(III) alkanoates to a difference in structure, it was possible to do this for the lanthanide(III) 4-alkoxybenzoates. From synchrotron measurements it was clear that the different compounds crystallise in a different form. The compounds of the first and second group (Ln = La, Pr, Nd, Sm, Eu) have the same structure at room temperature. Only $La(C_6H_{13}OC_6H_4CO_2)_3$ and $Pr(C_6H_{13}OC_6H_4CO_2)_3$ are liquid crystalline. This means that the size of the lanthanide ion provides its mesomorphic behaviour. These liquid crystalline properties are comparable with the normal lanthanide(III) alkanoates. The melting of the alkyl chain and the stability of the ionic lanthanide and carboxylate layers largely determines the melting behaviour of these compounds. The ionic size of lanthanum(III) and praseodymium(III) are large enough to stabilise the ionic layer and the interactions between the phenyl groups. Melting to a mesophase is due to the melting of the alkyl chains. When Ln = Nd, Sm and Eu the lanthanide ion is too small for the necessary stabilisation. At heating unfavourable electrostatic interactions between the carboxylate groups and between the phenyl groups become that high that breakdown of the layers occur to form a less-ordered non-mesogenic structure before the alkyl chains are completely molten.

The lanthanide ions of group 3 and 4 are that small that a normal layered structure can not be formed because of the too large negative electrostatic interactions between the carboxylate groups and between the phenyl groups. Here, the formation of an undulating layered structure or of random domains is more favoured.

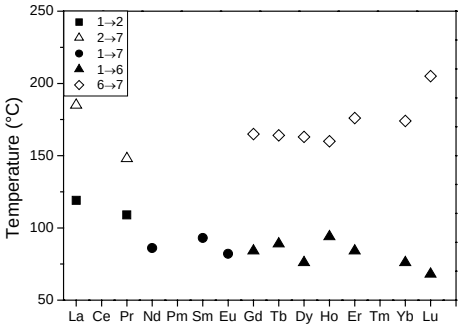

Figure 6-10 Effect of the lanthanide ion on the thermal properties of $Ln(C_6H_{13}OC_6H_4CO_2)_3$, the numbers refer to the structures described in 6.2.2

The fact that the temperature of the first transition does not change much over the lanthanide series can be assigned to the hydration of the compounds. Most of the compounds are di- or trihydrates. It is acceptable to assume that the dehydration temperature does not change that much over the lanthanide series. However the loss of the water molecules will strongly affect the structure and introduce a phase transition. This is in contrast to the normal lanthanide(III) alkanoates, where the presence of water does not influence the phase behaviour.

Whereas the normal lanthanide soaps are hemi- or monohydrates, lanthanide 4-alkoxybenzoates are di- or trihydrates. So the amount of water in these complexes is much larger than in the case of normal lanthanide(III) alkanoates. A second difference is the structure of the complexes. Whereas the lanthanide(III) alkanoates have a structure connecting the lanthanide ions to each other by the carboxylate groups to form a polymeric structure, we do not know if this is also the case for lanthanide(III) 4-alkoxybenzoates. In fact we do not know anything about the first and second coordination sphere of the lanthanide ion and the conformation of the phenyl group in regard to the alkyl chain. We only know that some kind of layered structure is formed,

but nothing is known about the order in the layers and how the lanthanide(III) ions are connected to each other.

Complexes of 4-alkoxybenzoic acids do not crystallise when cooling from the phase with random domains. At heating the layered structure is broken down into a less-ordered layered structure with random domains. Because of the strong steric hindrance due to the phenyl groups, it is very difficult to restore the layered structure and the structure will remain more or less random (i.e. the same structure as formed at the last phase transition). At cooling the motion of the molecules will diminish gradually and no enthalpy change is present in DSC, neither a change in *d* spacing in diffraction measurements. This gradually process is reversible, in the sense that in the second heating run no transition can be seen in DSC en XRD, although softening of the compounds is observed in thermo-optical microscopy.

6.2.3.2 Influence of the Chain Length on the Thermal Behaviour of the Series $Ho(C_xH_{2x+1}OC_6H_4CO_2)_3$

The chain length has an influence on the thermal properties of lanthanide(III) 4-alkoxybenzoates, although this can be assigned to the crystallinity at room temperature. Synchrotron diffractograms are recorded for x = 4, 8, 9 and 10.
$Ho(C_4H_9OC_6H_4CO_2)_3$ shows in DSC a weak transition at 69°C and a stronger one at 193°C. This compound is amorphous in the solid state (see Figure 6-11) and changes to a random domain structure at ca. 195°C. The strong increase in intensity of the synchrotron radiation measurements at 190°C can be attributed to the sinking of the product in the sample holder, because of the increased fluidity in this phase.

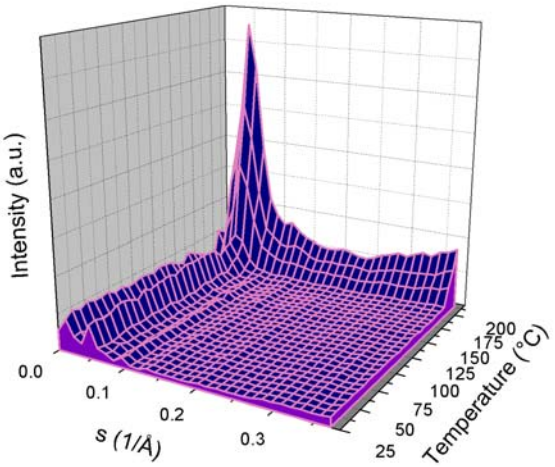

Figure 6-11 Change of the *d* value as a function of the temperature for $(Ho(C_4H_9OC_6H_4CO_2)_3$

$Ho(C_8H_{17}OC_6H_4CO_2)_3$, $Ho(C_9H_{19}OC_6H_4CO_2)_3$, $Ho(C_{10}H_{21}OC_6H_4CO_2)_3$ show the same phase behaviour as compounds from group three as explained in 6.2.3.1 . At room temperature two crystal structures are present, i.e. the normal and the undulating layered structure. At the first transition only the latter is left, which disappears after the clearing point. In Figure 6-12 synchrotron diffractograms of the different phases are given.

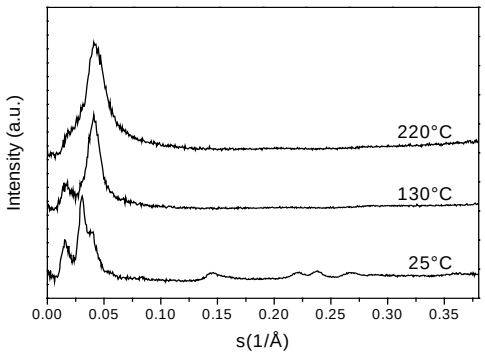

Figure 6-12 Synchrotron diffractograms of $Ho(C_8H_{17}OC_6H_4CO_2)_3$ at different temperatures

As illustrated in Figure 6-13 the influence of the chain length on the transition temperature is rather small for these compounds (see also Table 4.2-2 - Table 4.2-6, Appendix 4). The explanation for this can be found in the shape of the ligands. They

have a large rigid head group and a flexible chain. So the main part of the structure and therefore of the thermal properties is determined by this rigid head group.

However the chain length determines if a compound of a homologous series is liquid crystalline or not. This is the case for $La(C_xH_{2x+1}OC_6H_4CO_2)_3$ and $Pr(C_xH_{2x+1}OC_6H_4CO_2)_3$. For La(III) the complexes with x = 6, 8 and 9 are liquid crystalline, for Pr(III) x = 6.

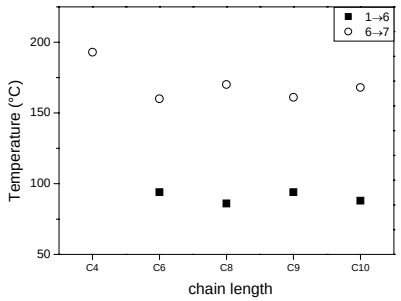

Figure 6-13 Influence of the chain length on the transition temperatures for the compounds of the series $Ho(C_xH_{2x+1}OC_6H_4CO_2)_3$, the numbers refer to the structures described in 6.2.2

6.2.4 Conclusion

It is clear that the thermal behaviour of lanthanide(III) 4-alkoxybenzoates is completely different from that of the ligands. Whereas in the ligands the rigid core is built by hydrogen bonds between the carboxylate groups, here the ligands are hold together by lanthanide ions. This gives rise to a much more rigid layered structure with totally different thermal properties.

We found that for this kind of complexes the thermal behaviour strongly depends on the structure of the solid compound. With synchrotron diffraction measurements we were able to attach different kinds of structures to different complexes. The structure depends on the size of the lanthanide ion. However, lanthanide(III) 4-alkoxybenzoates do not crystallise when cooling from the isotropic liquid, because of the strong steric hindrance of the phenyl groups.

The phase behaviour of compounds with a normal layered structure in the solid state does not depend that much on the normal lanthanide(III) alkanoates. Here also, the formation of a mesophase depends on the size of the lanthanide ion, i.e. only complexes with large lanthanide ions (e.g. lanthanum(III) and praseodymium(III)) form a mesophase.
In the case of smaller lanthanide ions, no normal layered structure is formed, but a structure with undulating layers or with random domains.

The chain length also influences the thermal behaviour of this kind of complexes. In the case of the smallest chain length (4-butyloxybenzoic acid), the compounds are rather amorphous. Increasing the chain length gives rise to a more or less layered structure, depending on the lanthanide ion. However, the chain length has a minor influence on the transition temperatures of complexes with the same structure. The major part of the thermal behaviour is set by the structure and the rigid core around the lanthanide ion, rather than the melting of the alkyl chain.

Complex formation drastically changes the thermal behaviour of the ligands. Whereas 4-alkoxybenzoic acids are well-known liquid crystals showing several mesophases and whereby the rigid core of the mesogen is formed by hydrogen bonds, the introduction of a lanthanide ion gives rise to an other kind of layered structure. The crystallinity and hence the thermal behaviour depends hereon.

References

[1] Y. G. Galyametdinov, G. I. Ivanova, I. V. Ovchinnikov *Bull. Acad. Sci. USSR, Div. Chem. Sci.* **40** (1991) 1109.

[2] M. Marcos, P. Romero, J. L. Serrano *J. Chem. Soc. Chem. Comm.* **1989** 1641.

[3] R. Van Deun, K. Binnemans *Liq. Cryst.* **28** (2001) 621.

[4] K. Binnemans, K. Lodewyckx, R. Van Deun Y. G. Galyametdinov, D. Hinz, G. Meyer *Liq. Cryst.* **28** (2011) 279.

[5] A. Kula, W. Brzyska *Polish J. Chem.* **74** (2000) 45.

[6] Z. Keli, Y. Jibing, Y. Liangjie, S. Jutang *J. Rare Earths* **17** (1999) 255.

[7] M. D. Taylor, C. P. Carter, C. I. Wynter *J. inorg. nucl. Chem.* **30** (1968) 1503.

[8] W. Ferenc, B. Bocian, D. Mazur *Croatica Chimica Acta* **72** (1999) 779

[9] J. Herbert *Trans. Faraday Soc.* **63** (1967) 555.

[10] J. M. Seddon in *Handbook of Liquid Crystals* (eds. D. Demus, J. Goodby, G. W. Gray, H.-W. Spiess) Vol.1 Chap. 3,VCH-Wiley, Weinheim New York, **1998**.

[11] B. I. Ostrovskii *Liq. Cryst.* **14** (1993) 131.

[12] T. A. Lobko, B. I. Ostrovskii, Pavluchenko A. I., Sulianov S. N. *Liq. Cryst.* **15** (1993) 361.

Chapter 7 Lanthanide(III) Dodecylsulphates

7.1 Synthesis and Characterisation

The lanthanide(III) dodecylsulphates were synthesized via a metathesis reaction [1]. To an aqueous solution of sodium dodecylsulphate the desired lanthanide ion dissolved in water was added dropwise. The lanthanide(III) alkylsulphate precipitated immediately. The product was filtered off, washed with deionised water and dried in vacuum for 24h.
The purity of the compounds was checked by elemental analysis. All the compounds of the series $Ln(C_{12}H_{25}SO_4)_3$ were found to be monohydrates. Thermogravimetric analysis points also in this direction. The analysis results are listed in Table 4.2-1, Appendix 5.

Exptl. for $La(C_{12}H_{25}SO_4)_3 \cdot H_2O$: Experimental for C: 45.83%, for H: 8.20%; Calculated for C: 45.37%, for H: 8.14%.

7.2 Structure

For $Nd(C_{12}H_{25}SO_4)_3 \cdot H_2O$ and for $Yb(C_{12}H_{25}SO_4)_3 \cdot H_2O$ room temperature X-ray diffraction analysis was performed. These compounds show several reflections in the small-angle region where the *d* values calculated with the Bragg law vary as 1:1/2:1/3:…1/n (Figure 7-1). This corresponds to the (00*l*) reflections and indicates a lamellar structure. The experimental *d* values are about twice the length of the dodecylsulphate; hence a bilayer structure can be assumed.

The diffractograms show within the layers also a diffuse reflection at ca. 4.1Å. This is caused by in-plane scattering of the alkyl chains. The peak is very diffuse, so the alkyl chains are not regularly structured.

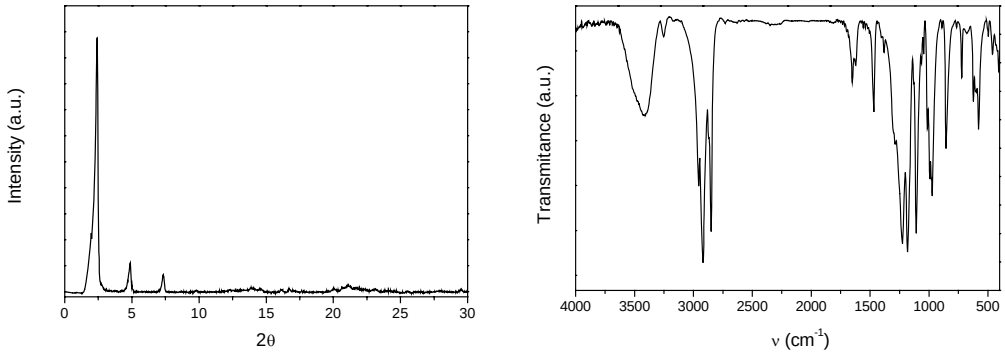

Figure 7-1 X-ray diffractogram (left) and IR spectrum of $Nd(C_{12}H_{25}SO_4)_3 \cdot H_2O$

In Figure 7-1 the infrared spectrum of $Nd(C_{12}H_{25}SO_4)_3 \cdot H_2O$ is given. If compared with the spectrum of the sodium dodecylsulphate, the stretchings and bendings of the alkyl chains (3000-2850 and 1470 cm^{-1} respectively) are the same for the complexes and for the sodium salt.

However peaks assigned to the sulphate group according to tables taken from Kato [2] showed a shift from sodium alkylsulphates to the lanthanide complexes. The assignments of the observed bands for $Na(C_{12}H_{25}SO_4)_3$, $La(C_{12}H_{25}SO_4)_3 \cdot H_2O$ and $Nd(C_{12}H_{25}SO_4)_3 \cdot H_2O$ are given in Table 7.2-1.
The peak positions do not change significantly from one lanthanide ion to the other except for a slight shift to higher wavenumber at the end of the lanthanide series for the stretching of the C-O* bond and for a continuous shift to higher energy for the S-O stretching for the oxygens coordinated to the lanthanide ion.

Table 7.2-1 IR Assignment for $Na(C_{12}H_{25}SO_4)_3$, $La(C_{12}H_{25}SO_4)_3 \cdot H_2O$ and $Nd(C_{12}H_{25}SO_4)_3 \cdot H_2O$

Assignment[a]	Intensity[b]	$Na(C_{12}H_{25}SO_4)_3$ / cm^{-1}	$La(C_{12}H_{25}SO_4)_3 \cdot H_2O$ / cm^{-1}	$Nd(C_{12}H_{25}SO_4)_3 \cdot H_2O$ / cm^{-1}
ν(O-H) / water	b	3470	3462	3411
$\nu_{as}(CH_2)$	s	2956	2956	2956
$\nu_{as}(CH_3)$	s	2918	2918	2918
$\nu_s(CH_3)$	s	2873	2872	2873
$\nu_s(CH_2)$	s	2850	2850	2850
δ(C-H)	m	1469	1469	1469
ν(S-O)	s	1220	1209	1220
ν(S-O*)	s	1085	1108	1105
ν(C-O*)	w	1065	1067	1061
ν(S-O)	m	1018	1014	1013
long chain rocking	w	721	723	721
$\delta(SO_3)$	m	636	622	625
$\delta(SO_3)$	m	591	580	577

[a] The asterisk indicates the oxygen bridging the sulphur and the alkyl chain, ν denotes stretching, δ bending.
[b] s = strong, m = medium, w = weak and b = broad.

7.3 Thermal Behaviour of Lanthanide(III) Dodecylsulphates

7.3.1 TG-DTA

Lanthanide(III) dodecylsulphates show in their DSC thermograms a first endothermic peak which can be assigned to the loss of water before the compounds decompose at moderate temperatures. Because no transition was visible in microscopy, thermogravimetric studies were done on these compounds. A typical TG curve shows a first mass loss from 85 - 95°C to 120 - 135°C, due to the leaving of water molecules. A second large mass loss occurs between 150 - 170°C and 210 - 230°C. The DTA curve (which is recorded simultaneously) shows for both mass losses an endothermic peak. Figure 7-2 shows the TG-DTA of $La(C_{12}H_{25}SO_4)_3 \cdot H_2O$.

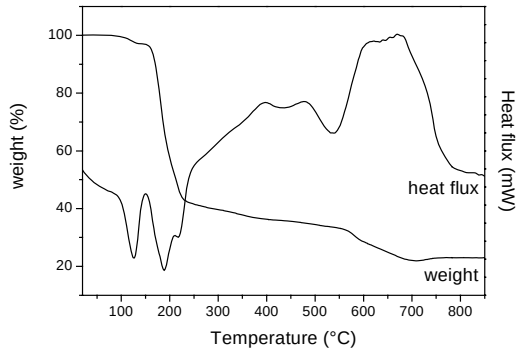

Figure 7-2 TG-DTA plot of $La(C_{12}H_{25}SO_4)_3 \cdot H_2O$, endothermic peaks are pointing downwards

All the compounds show a loss of water in the TG-DTA measurements, but the water content determined with this method was a little bit too high in comparison to the water amount obtained by elemental analysis. Lanthanide(III) dodecylsulphates are hygroscopic. Therefore they have to be stored in a dessicator.

The decomposition temperature slightly decreases over the lanthanide series. For example, lanthanum(III) dodecylsulphate decomposes at 172°C, lutetium(III) dodecylsulphate at 156°C. This small effect can be attributed to the size of the lanthanide ion. It shows that the smaller the lanthanide ion, the worse the coordination by the sulphate group, and hence a smaller thermal stability of the complex.

7.3.2 Lyotropic Mesomorphism

Just few papers are available on the lyotropic mesomorphism of rare earth containing compounds. Gin used an inverted hexagonal mesophase formed by metal complexes of 3,4,5 substituted benzoic acids as a template for nanostructured materials [3]. Yada made nanostructured rare earth oxides templated by lamellar and hexagonal mesophases formed by yttrium dodecylsulphate [4-5]. Recently Galyametdinov and Bruce, in collaboration with our group, found that the mesomorphism of lanthanide alkylsulphates depends on the composition of the solvent [6].
Here we investigated the effect of the concentration of ethylene glycol and water on the mesomorphism of five lanthanide(III) dodecylsulphates by thermo-optical microscopy.

We used the following lanthanide(III) dodecylsulphates: $La(C_{12}H_{25}SO_4)_3 \cdot H_2O$, $Pr(C_{12}H_{25}SO_4)_3 \cdot H_2O$, $Sm(C_{12}H_{25}SO_4)_3 \cdot H_2O$, $Dy(C_{12}H_{25}SO_4)_3 \cdot H_2O$ and $Yb(C_{12}H_{25}SO_4)_3 \cdot H_2O$. We made the following mixtures of ethylene glycol/water (EW, first number is the percentage of ethylene glycol, second number of the percentage of water): EW 100/0, EW 75/25, EW 50/50, EW25/75, EW 0/100. The lyotropic mesomorphism was investigated by the Lawrence penetration technique [7].

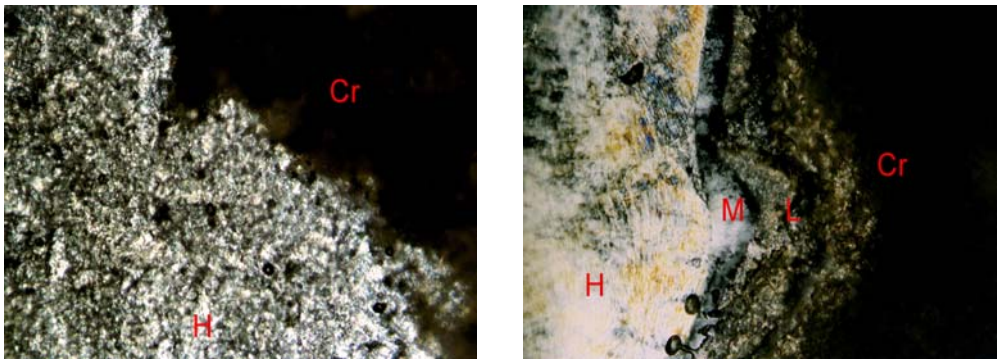

Figure 7-3 $Sm(C_{12}H_{25}SO_4)_3 \cdot H_2O$ after contact between solvent and product; only hexagonal mesophase (EW 50/50, 20°C) (left);
$Sm(C_{12}H_{25}SO_4)_3 \cdot H_2O$: hexagonal phase, mesophase M, lamellar phase and crystalline phase (EW 50/50, 33°C)

We investigated complexes with five different lanthanide ions to explore the effect of the ionic size. First conclusion is that the solubility of the compound in a certain solvent mixture decreases with decreasing ionic radius. Compounds with a small ionic radius dissolve slower at room temperature, or the dissolution temperature at heating is higher. This effect is often seen for lanthanide compounds (cfr. solubility products for lanthanide hydroxides [8]).

Secondly, the mesomorphic behaviour does not depend on the lanthanide ion. This means that all the lanthanide(III) dodecylsulphates show the same mesophases at almost the same temperatures for a given solvent composition.

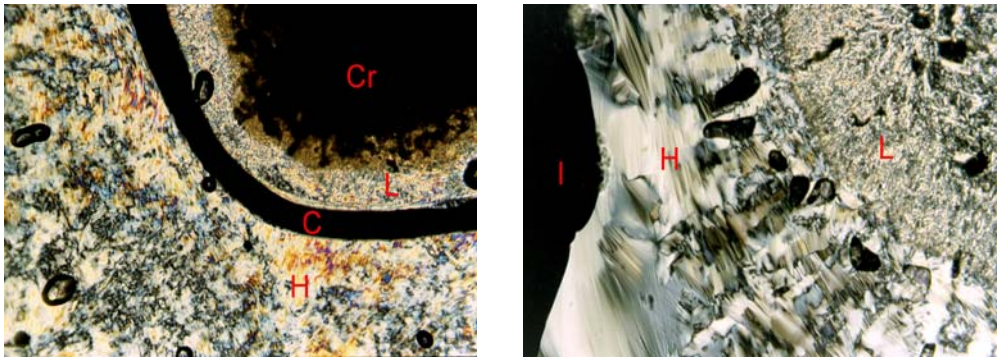

Figure 7-4 $Sm(C_{12}H_{25}SO_4)_3 \cdot H_2O$: hexagonal phase, cubic phase, lamellar phase and crystalline phase (EW 50/50, 56°C), left;
$Yb(C_{12}H_{25}SO_4)_3 \cdot H_2O$, cooling from the isotropic liquid (EW 50/50, 20°C)

In contrast to the ionic size, the composition of the solvent has an influence on the mesomorphic behaviour. For the solvent mixtures EW 100/0, EW 75/25 and EW 50/50 at room temperature a mesophase is formed immediately. At thermal equilibrium this mesophase seems to be a hexagonal phase (see Figure 7-3). Heating at 1°C min^{-1} gives rise at ca. 25°C to the formation of a small lamellar phase on the borders of the crystalline phase. By further heating a distinct grey zone (M) between L and H is formed at ca. 30°C (see Figure 7-3). This mesophase M rearranges to an isotropic cubic structure (see Figure 7-4). Further heating does not affect the presence of the phase although the compound dissolves. Complete dissolution occurs above 70°C when heating at 1°C min^{-1}.

When cooled from the isotropic liquid only the hexagonal and the lamellar phase are formed, the cubic phase not. Moreover, when the sample is left in contact with the solvent for a long time, the hexagonal phase seems to be the most stable mesophase.

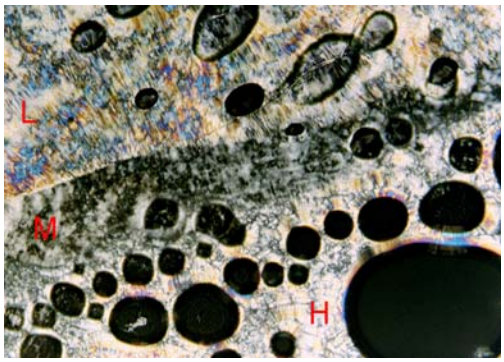

Figure 7-5 $La(C_{12}H_{25}SO_4)_3 \cdot H_2O$: lamellar phase, mesophase M and hexagonal phase (EW 0/100, 84°C)

At lower ethylene glycol concentrations (EW 25/75 and EW 0/100) the thermal behaviour of the lanthanide dodecylsulphates is quite different. Immediately after contact with the solvent a very broad hexagonal phase is formed. Almost the entire crystalline product is rearranged to this mesophase. By heating the lamellar phase is formed at about 25°C. Further heating causes the formation of an unidentified mesophase M (see Figure 7-5).

When EW 25/75 is used, this mesophase is transformed to a cubic phase at much higher temperatures as for higher concentrations of ethylene glycol (at about 60°C). Further heating does not affect the phase behaviour. When the sample is cooled down to room temperature, the entire product is transformed in a hexagonal phase at thermal equilibrium.
When EW 0/100 is used, the mesophase M does not change to a cubic phase and the dissolution of the compound is very slow.

7.3.3 Conclusion

In contrary to lanthanide(III) alkanoates lanthanide(III) dodecylsulphates are not thermotropic liquid crystals, but they form lyotropic mesophases in the presence of water and ethylene glycol and mixtures hereof.
We investigated the phase behaviour via the Lawrence penetration technique on the thermo-optical microscope. The lyotropic phase behaviour of lanthanide(III) dodecylsulphates depends on the composition of the solvent. For pure ethylene glycol and mixtures of ethylene glycol and water three different mesophases are formed (i.e. the lamellar, the cubic and the hexagonal phase), whereas when water is used as solvent no cubic phase is formed. The size of the lanthanide ion has a minor influence on the mesomorphism of lanthanide(III) dodecylsulphates. The smaller the lanthanide ion the lower the solubility, but the phase behaviour does not change through the lanthanide series.

References

[1] G. L. McIntire, D. A. Chiappardi, R. L. Casselberry, H. N. Blount *J. Chem. Phys.* **86** (1982) 2632.

[2] Y. Kato, T. Kurimoto, T. Takenaka *Spectrochimica Acta* **33A** (1977) 1033.

[3] H. Deng, D. L. Gin, R. C. Smith *J. Am. Chem. Soc.* **120** (1998) 3522.

[4] M. Yada, H. Kitumara, M. Machida, T. Kijima *Inorg. Chem.* **37** (1998) 6470.

[5] M. Yada, H. Kitumara, A. Ichinose, M. Machida, M. Kijima *Angew. Chem. Int. Ed. Engl.* **38** (1999) 3506.

[6] Y. G. Galyametdinov, H. B. Jervis, D. W. Bruce, K. Binnemans *Liq. Cryst.* **28** (2001) 1877.

[7] A. S. C. Lawrence in *Surface activity and detergency* (ed. K. Durham), chap. 7, Macmillan London **1961**.

[8] A. E. Martell, R. M. Smith *Critical Stability Constants* (Plenum Press New York and 7London) Vol. 4 **1976**.

Chapter 8 Experimental Section

8.1 Differential Scanning Calorimetry

We have a Mettler-Toledo DSC-821e instrument, which allows measurements between -70°C and 450°C. This instrument is a heat flux DSC where the temperature difference between the sample and the reference is an indication for the difference in heat flow.
The typical scan rate for a measurement was 10°C min^{-1} and was done under a helium flow of 30 mL min^{-1}.

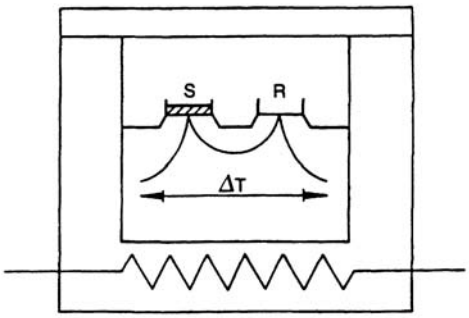

Figure 8-1 Heat flux DSC

8.2 Elemental Analysis

Elemental analyses (CHN) were performed on a CE Instruments EA-1110 elemental analyser. The accuracy of the instrument depends on the percentage of the to analyse element (e.g. accuracy for pure organic elemental analysis standards: Calc.: 1.00%, Exp.: 1.00% ± 0.02; Calc.: 50.00%, Exp.: 50.00% ± 0.3) [1].

For pure organic compounds a difference of 0.3% (absolute value) between the calculated and experimental value is accepted. For coordination compounds this value is 0.5% [2].

8.3 Infrared Spectroscopy

FT-IR spectra were recorded on a Bruker IFS-66 spectrometer. The samples were dissolved in KBr pellets.

8.4 Single Crystal Data

Intensities of the single crystals were measured with an image plate diffractometer (IPDS, Stoe) at 293K. Monochromatic Mo-Kα radiation (λ = 0.7107Å) was obtained with a graphite monochromator. The data were processed with the program systems SHELXS-97 and SHELXL-97 [3 - 4]. Scattering factors are taken according to the International Tables, Volume C [5]. Figures of crystal structures were drawn using the graphical software Diamond Version 2.

8.5 Small Angle X-ray Diffraction (Room Temperature and High Temperature)

Small-angle X-ray diffraction was measured on a STOE transmission powder diffractometer system STADI P. Monochromatic Cu-Kα radiation (λ = 1.54Å) was obtained with the aid of a curved germanium primary monochromator. Diffracted X-rays were first measured by a linear position-sensitive detector, later by an imaging plate position sensitive detector (IP-PSD).

In the case of room temperature X-ray transmission diffraction measurements the samples were placed as thin films on zero scattering foils.
In the case of high temperature X-ray measurements the instrument was equipped with a high temperature attachment version 0.65.1 (temperature range form room temperature to 1000°C). The samples were placed in a quartz capillary and spun during the measurements.

8.6 Synchrotron Measurements (ESRF-France)

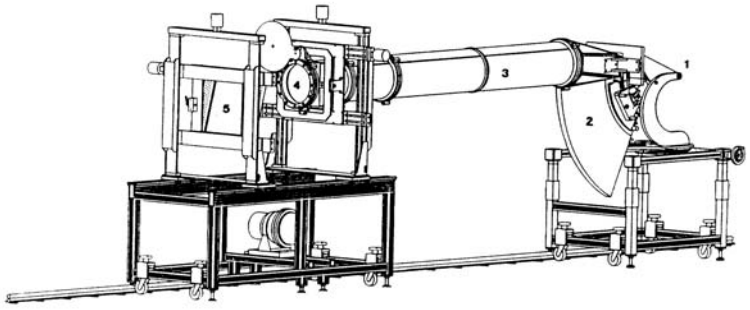

Figure 8-2 Equipment of the synchrotron measurements [**6**]

Synchrotron measurements were done in the European Synchrotron Radiation Facility (ESRF) in Grenoble (France).
In Figure 8-2 the optical bench of the SAXS/WAXS station mounted on BM26 of the ESRF is given. Number 1 refers to the sample position, 2 to the WAXS detector and electronics, 3 to the vacuum chamber between sample and detector (length variable from 0.5 to 7m), 4 to the mounting stage for beamstop, and 5 to the mounting stage for the SAXS detector.
During our measurements, the WAXS detector and the vacuum chamber between the sample and detector were removed because of the intermediate angles that were necessary for the samples. The wavelength of the diffracted beam was 0.688Å. The sample was placed in a metal mould between aluminium foils. This was placed in an oven, whereby the synchrotron beam could pass through a hole. The typical heating rate used during these measurements was 10°C min^{-1}.

8.7 Thermogravimetry

We have a Polymer Laboratories-STA 1000H thermogravimeter. With this instrument thermogravimetry, differential thermogravimetry and differential thermal analysis can be done.

8.8 Thermo-optical Microscopy

The study of optical textures of liquid crystals is investigated with an Olympus BX60 polarisation microscope, equipped with a Linkam THMS 600 hot stage and a Linkam TMS 93 programmable temperature adjustment
We used the Lawrence penetration technique to investigate lyotropic mesomorphism. Therefore the product was placed on a cover slip. Hereon a small piece of glass was placed and the product and glass piece were covered by a second cover slip. A drop of solvent was put at the end of the cover slip and preceded from one end to the other by capillary action, creating a concentration gradient across the sample [7].

8.9 UV Spectroscopy and Luminescence

Optical absorption spectra were recorded at ambient temperature on a Shimadzu UV-3100 spectrophotometer.
Luminescence spectra were recorded on an Edinburgh Instruments FS900 Steady State Spectrofluorimeter.

References

[1] Technical Specifications of EA 1110 (CE Instruments, Thermo Quest Italia S.p.A.)

[2] *Advanced Practical Organic Chemistry, 2nd Ed.* J. Leonard, B. Luggo, G. Procter, Chapman & Hall London **1995**.

[3] G. M. Sheldrick SHELXS-97 manual, University of Göttingen, Germany, 1997.

[4] G. M. Sheldrick SHELXL-97 manual, University of Göttingen, Germany, 1997.

[5] A. J. C. Wilson (Ed.) Mathematical, Physical and Chemical Tables, International Tables for Crystallography, Vol. C, Kluwer, Dordrecht, **1995**.

[6] W. Bras *J. Macromol. Sci. Phys.* **B37B** (1998) 557.

[7] A. S. C. Lawrence in *Surface activity and detergency* (ed. K. Durham), chap. 7, Macmillan London **1961**.

Summary

During this project the structure and thermal behaviour of lanthanide(III) soaps was studied. We tried to find out the determining factor for the existence of a stable lanthanide containing mesophase and what changes could be done on the composition to form such a stable mesophase

First we studied the lanthanide(III) alkanoates ($Ln(C_xH_{2x+1}CO_2)_3$). We were able to determine the crystal structure of some lanthanide(III) butyrates. These compounds form infinite layers of lanthanide ions connected by carboxylate groups. The alkyl chains are placed perpendicular to these layers and are in the *all trans* conformation. Via comparison of X-ray powder diffractograms at room temperature and of IR spectra of several compounds with these of the lanthanide(III) butyrates, we extrapolated this bilayer structure to all the lanthanide(III) alkanoates.

We found that the size of the lanthanide(III) ion has a critical effect on the existence of a mesophase. So only dodecanoates of the first four lanthanides with the largest ionic size (i.e. La, Ce, Pr and Nd) exhibit a mesophase and the mesophase stability range rapidly decreases traversing the lanthanide series. The fact that the other lanthanide(III) dodecanoates do not show mesomorphism can be attributed by their small ionic size and hence by unfavourable electrostatic interactions of the carboxylate groups. As the ionic radius of the lanthanide ion decreases, the distance between the carboxylate groups on either side of the plane containing lanthanide ions decreases. The amplitude of the thermal vibrations increases on increasing the temperature and thereby induces unfavourable electrostatic interactions (repulsions) between the carboxylate groups, not only between those of the two opposing layers, but also between adjacent carboxylate groups within the same layer. When the repulsive forces between the negative charges are stronger than the attractive forces between the negative (carboxylate groups) and positive (lanthanide ions) charges, the bilayer structure is no longer stable and breaks down. In this case, a rearrangement of the carboxylate groups and lanthanide ions to obtain a more stable solid structure (i.e. a

crystal-crystal transition) might be expected. However, melting of the compounds is observed. The alkyl chains have sufficient thermal energy for their *all trans* conformation to be lost when the layer structure breaks down.
This theory explains the decrease of the melting point within the lanthanide series. The smaller the lanthanide ion, the more unstable the layer structure becomes, and hence less thermal energy is required to break down the solid state structure.
A mesophase is formed, when, at the melting point of the alkyl chains, the electrostatic attraction between the lanthanide ions and the carboxylate groups is still sufficiently high to maintain a layer structure. This is the case for lanthanum(III), cerium(III), praseody-mium(III) and neodymium(III) compounds.
At the melting point of the non-mesogenic lanthanide(III) alkanoates and the clearing point of the mesogenic complexes, the metal soaps are converted to an isotropic less-ordered structure with a rather low viscosity.

The chain length also influences the thermal behaviour of lanthanide(III) alkanoates in the sense that the melting point increases with increasing chain length, whereas the clearing point decreases. Moreover, the short chain homologues of the mesomorphic lanthanide(III) alkanoates exhibit two mesophases. This mesophase M is formed at moderate temperatures and can be considered as a layered structure with partially molten alkyl chains. Increasing the temperatures gives rise to a rearrangement of this mesophase to a smectic A phase.

The fact that only the first three lanthanides (La, Ce and Pr) exhibit a mesophase across the complete homologous series ($4 \leq x \leq 19$), and that the neodymium series does not show mesomorphism for the longer chain lengths, can be explained by taking into account both the effect of the lanthanide ion and the chain length. Whereas for lanthanum(III), cerium(III) and praseodymium(III) alkanoates the ionic radius is sufficiently large to reduce unfavourable electrostatic interactions between the carboxylate groups (and thus the melting of the alkyl chains is the major factor determining the thermal properties of these compounds), for neodymium soaps there is a competition between the stabilisation of the ionic layers and melting of the alkyl

chains. For the shorter alkyl chains, their melting is the determining factor, whereas for the longer soaps the thermal energy required to melt the alkyl chains is so high that the ionic layer structure breaks down before the alkyl groups are completely molten.

Because the size of the lanthanide ion strongly influences the mesomorphic behaviour of lanthanide(III) alkanoates, it was interesting to find out if a mesophase could be induced by mixing a mesogenic and a non-mesogenic compound. Therefore we synthesised following complexes $[La_xLn_{1-x}(C_{11}H_{23}CO_2)_3]$ (x is the mole fraction La(III), Ln = Eu, Tb, Ho, Yb) and investigated their thermal behaviour. We observed the induction of a mesophase. This means that we were able to stabilise the ionic lanthanide layer by mixing a mesomorphic lanthanide(III) dodecanoate with a large ionic radius, and a non-mesogenic lanthanide(III) dodecanoate (the lanthanide ion has a small ionic radius).
In the case of lanthanum-europium mixtures a very small amount of lanthanum is needed to induce mesomorphism in the mixtures. The amount lanthanum necessary increases with decreasing ionic size of the lanthanide ion. These experiments are in agreement with our theory on the effect of the size of the lanthanide ion on the thermal behaviour of lanthanide(III) alkanoates.

Another possibility for the stabilisation of the ionic layer is the introduction of a neutral ligand, like 1,10-phenanthroline. We synthesised complexes with several lanthanide ions and with several chain lengths and investigated their structure and thermal behaviour. Because we were able to determine the crystal structure of three lanthanide(III) alkanoate phenanthroline complexes, we could link the thermal behaviour unambiguously to the structure. These complexes form isotropic spherical dimers without any interaction between these dimers. So it was not so surprising to find out that these complexes are not liquid crystalline. However the unfavourable ionic interactions between the carboxylate groups were stabilised, which is expressed in the high melting points.

In this project we were not only interested in normal lanthanide(III) alkanoates, but also complexes with 4-alkoxybenzoic acids were topic of investigation. These ligands are well known for their mesomorphism, so we wanted to investigate the influence of complexation with lanthanide ions hereon.
It was very clear that complexation strongly influences the mesomorphism of the ligand. To declare the strange behaviour of lanthanide(III) 4-alkoxybenzoates during DSC and thermo-optical microscopy measurements, we have done synchrotron radiation studies on these compounds. We found out that here also the size of the lanthanide ion determines the structure of the complex and hence the thermal behaviour.

A last example of not normal lanthanide(III) alkanoates are the lanthanide(III) dodecylsulphates. Instead of the carboxylate function as coordination site, here a sulphate group is used. Lanthanide(III) dodecylsulphates are not thermotropic liquid crystals, moreover they decompose at moderate temperatures. However, we found that these complexes form lyotropic liquid crystals when brought in contact with ethylene glycol or water or mixtures hereof.

It must be said that this investigation of lanthanide(III) soaps gave rise to a lot of information on the synthesis, structure and thermal behaviour of these compounds. We hope that more industrial application will be found, now their structure and thermal behaviour are understood.

Samenvatting

Tijdens dit project hebben we verschillende soorten lanthanidecomplexen gesynthetiseerd en bestudeerd. We hebben gezocht naar de factoren die bepalen of een stabiele lanthanidehoudende mesofase gevormd wordt. Daarna hebben we veranderingen aangebracht aan de samenstelling van de verbindingen opdat we een stabiele mesofase zouden bekomen.

In de eerste plaats bestudeerden we de lanthanidealkanoaten ($Ln(C_xH_{2x+1}CO_2)_3$). Het was mogelijk om de kristalstructuur van enkele lanthanidebutyraten te bepalen. Deze verbindingen bestaan uit oneindige lagen van lanthanideïonen die bij elkaar gehouden worden door carboxylaatgroepen. De alkylketens staan loodrecht op deze lagen en zijn volledig uitgestrekt (d.w.z. ze zijn in *all trans* conformatie). Aan de hand van de vergelijking van X-stralen diffractograms en van infraroodspectra van verschillende verbindingen met die van de lanthanidebutyraten, extrapoleerden we deze dubbellaagstructuur naar alle lanthanidealkanoaten.

We vonden dat de grootte van het lanthanideïon een sterke invloed heeft op het al dan niet voorkomen van een mesofase. Enkel de dodecanoaten van de eerste vier lanthanideïonen met de grootste ionstraal, vertonen een mesofase. De stabiliteit van de mesofase vermindert snel wanneer de ionstraal kleiner wordt. Het feit dat de andere lanthanidedodecanoaten niet mesomorf zijn kan verklaard worden wanneer men ongunstige elektrostatische interacties tussen de carboxylaatgroepen in acht neemt. Immers, wanneer de ionstraal van het lanthanideïon kleiner wordt, wordt de afstand tussen carboxylaatgroepen aan beide zijden van het vlak waarin de lanthanideïonen zich bevinden, kleiner. Bij stijgende temperatuur neemt de amplitude van de thermische vibraties toe zodat ongunstige elektrostatische interacties (i.e. afstoting) tussen de carboxylaatgroepen ontstaan. Deze ontstaan niet alleen tussen carboxylaatgroepen van twee tegenoverstaande lagen, maar ook tussen opeenvolgende carboxylaatgroepen binnen dezelfde laag. Wanneer de afstoting tussen de negatieve ladingen groter is dan de aantrekking tussen negatieve (carboxylaat-groepen) en

positieve ladingen (lanthanideïonen), is de dubbellaagstructuur niet langer stabiel en zal deze doorbreken. Men verwacht dan een herschikking van de carboxylaat-groepen en de lanthanideïonen zodat een stabielere vaste fase ontstaat. Er zou met andere woorden een kristal-kristal transitie plaatsvinden. Dit is echter niet het geval, want de verbindingen smelten. De alkylketens hebben immers voldoende energie zodat hun *all trans* conformatie verloren gaat wanneer de laagstructuur verloren gaat.
Deze theorie verklaart de daling van het smeltpunt doorheen de lanthanidereeks. Hoe kleiner het lanthanide ion, hoe minder stabiel de laagstructuur, dus hoe minder thermische energie nodig om de vaste stof structuur te doorbreken.
Bij het smelten van de alkylketens vormt zich een mesofase wanneer de elektrostatische aantrekking tussen de lanthanideïonen en de carboxylaatgroepen nog groot genoeg is om de laagstructuur te behouden. Dit is het geval bij lanthaan(III), cerium(III), praseodymium(III) en neodymium(III).
Bij het smeltpunt voor de niet mesomorfe lanthanidedodecanoaten en bij het klaarpunt voor de mesomorfe, zijn de metaalzepen omgezet in een isotrope weinig-geordende structuur met een relatief lage viscositeit.

Ook de ketenlengte heeft een invloed op het thermische gedrag van lanthanidealkanoaten. Het smeltpunt stijgt terwijl het klaarpunt daalt, wanneer de ketenlengte langer wordt. Boven vertonen de mesomorfe lanthanidealkanoaten een tweede mesofase wanneer de alkylketen relatief kort is. De mesofase M vormt zich bij relatief lage temperaturen en kan beschouwd worden als een gelaagde structuur met gedeeltelijk gesmolten akyl ketens. Bij stijgende temperatuur wordt deze mesofase omgezet in de smectische A fase.

Enkel complexen van de eerste drie lanthaniden (La, Ce en Pr) vertonen een mesofase doorheen de homologe reeks ($4 \leq x \leq 19$), in tegenstelling met de neodymiumalkanoaten waar slechts een mesofase aanwezig is voor de kortere ketenlengtes ($x \leq 14$). Dit kan verklaard worden door zowel het effect van de ketenlengte als de grootte van het lanthanideïon in beschouwing te nemen. Terwijl bij lanthaan-, cerium- en praseodymiumalkanoaten de ionstraal groot genoeg is om de

ongunstige elektrostatische interacties tussen de carboxylaatgroepen tot een minimum te herleiden zodat het smelten van de alkylketens de bepalende factor is van het thermische gedrag, bij neodymium-alkanoaten is er een competitie tussen de stabilisatie van de ionische lagen en het smelten van de alkylketens. Bij de korte ketenlengten is het smelten van de keten de bepalende factor voor het bestaan van een mesofase. Bij de langere zepen is de thermische energie die nodig is om de alkylketens te laten smelten zodanig hoog dat de ionische laag verbroken wordt voordat de alkylketens volledig gesmolten zijn.

Aangezien de grootte van het lanthanideïon een sterke invloed heeft op de het mesomorfe gedrag van lanthanidealkanoaten, was het interessant om na te gaan of een mesofase geïnduceerd kon worden door het mengen van een mesogene en een niet-mesogene component. Daarom synthetiseerden we de volgende reeks verbindingen: $[La_xLn_{1-x}(C_{11}H_{23}CO_2)_3]$ (Ln = Eu, Tb, Ho, Yb) en we observeerden de inductie van een mesofase vanaf een bepaalde concentratie aan lanthaan. Deze experimenten bevestigen de theorie over het effect van de grootte van het lanthanideïon op het thermische gedrag.
De aanwezigheid van een mesofase betekent dat we in staat zijn om een mesofase te induceren door het mesomorfe lanthaandodecanoaat te mengen met een niet-mesomorf lanthanidedodecanoaat met een kleine ionstraal.
In het geval van de lanthaan-europium mengsels is slechts een zeer kleine hoeveelheid lanthaan nodig om een mesofase te induceren. De hoeveelheid lanthaan nodig voor mesofase inductie neemt toe wanneer de ionstraal van het tweede lanthanideïon kleiner is.

Een andere mogelijkheid voor het stabiliseren van de ionische laag is de introductie van een neutraal ligand zoals 1,10-fenantroline. Complexen met verschillende lanthanide ionen en verschillende ketenlengtes werden gesynthetiseerd en onderzocht. Omdat we in staat waren om de kristalstructuur van drie adducten van lanthanidealkanoaten met 1,10-fenantroline te bepalen, konden we hier, nog meer als bij de normale lanthanidealkanoaten, de thermische eigenschappen linken aan de

structuur. Deze complexen vormen namelijk isotrope sferische dimeren zonder enige interactie. Daarom was het niet zo verwonderlijk dat deze complexen niet vloeibaar kristallijn bleken te zijn. In elk geval zijn we met deze complexen geslaagd om de ionische interacties tussen de carboxylaatgroepen te stabiliseren, wat zich uit in hoge smeltpunten.

Niet enkel n-alkanoaten waren een interessepunt in dit onderzoek. Ook complexen met 4-alkoxybenzoëzuren werden onderzocht. Het mesomorfisme van de liganden is goed gekend en daarom wilden we het effect van complexatie met lanthanide ionen hierop nagaan.
Het was zeer duidelijk dat complexatie een zeer sterke invloed heeft op het mesomorfisme van het ligand. Om het vreemde gedrag van de lanthanide-4-alkoxybenzoaten tijdens DSC en thermo-optische microscopie te verklaren, hebben we synchrotronstralings-metingen hierop gedaan. We vonden dat de grootte van het lanthanideïon de structuur van het complex bepaalt en zodus de thermische eigenschappen beïnvloedt.

Een laatste voorbeeld van niet gewone lanthanidealkanoaten zijn de lanthanide-dodecylsulfaten. In de plaats van een carboxylaatfunctie als chelerend agens wordt hier een sulfaatgroep gebruikt. Deze complexen zijn geen thermotrope vloeibare kristallen, ze ontbinden zelfs bij relatief lage temperaturen. Desondanks bleken lanthanide-dodecylsulfaten lyotrope vloeibare kristallen te zijn wanneer ze in contact gebracht worden met ethyleen glycol, water of mengsels hiervan.

Tot slot mogen we zeggen dat dit project geleid heeft tot een grote hoeveelheid informatie over de synthese, structuur en thermische eigenschappen van lanthanidezepen. We hopen dan ook dat er meer industriële toepassingen zullen gevonden worden voor deze verbindingen, nu de structuur en thermische eigenschappen beter gekend zijn.

List of Publications

K. Binnemans, L. Jongen, C. Görller-Walrand, W. D'Olieslager, D. Hinz, G. Meyer, *Eur. J. Inorg. Chem.* (2000) 1429 - 1436.
Lanthanide(III) dodecanoates: structure, thermal behaviour and ion-size effects on the mesomorphism

K. Binnemans, L. Jongen, C. Bromant, D. Hinz, G. Meyer, *Inorg. Chem.*, 39 (2000) 5938 - 5945.
Structure and mesomorphism of neodymium(III) alkanoates

L. Jongen, G. Meyer, K. Binnemans, *J. All. Comp.* 323-324 (2001) 142 - 146.
Crystal Structure of Lanthanum(III) Butyrate Monohydrate

L. Jongen, K. Binnemans, D. Hinz, G. Meyer, *Liq. Cryst.* 28 (2001) 819 - 825.
Mesomorphic behaviour of praseodymium(III) alkanoates

L. Jongen, K. Binnemans, D. Hinz, G. Meyer, *Mat. Sci. Eng C* 18 (2001) 199 - 204.
Mesomorphic behaviour of cerium(III) alkanoates

L. Jongen, D. Hinz, G. Meyer, K. Binnemans *Chem. Mat.* 13 (2001) 2243 - 2246.
Induced mesophases in binary mixtures of lanthanide(III) dodecanoates

L. Jongen, K. Binnemans, D. Hinz, G. Meyer, *Liq. Cryst.* 28 (2001) 1727 – 1733.
Thermal Behaviour of Lanthanum(III) Alkanoates

K. Binnemans, L. Jongen, C. Görller-Walrand *Phys. Chem. Chem. Phys.* 3 (2001) 4796 – 4799.
Optical Properties of Vitrified Rare-Earth Soaps.

Appendix 1 $Ln(C_xH_{2x+1}CO_2)_3$

1.1 CHN Results for $Ln(C_xH_{2x+1}CO_2)_3$

Table 1.1-1 CHN results for the series $Ln(C_{11}H_{23}CO_2)_3$

Compound	%C[a]	%H[a]	% Ln^{3+} [a]	# H_2O
$La(C_{11}H_{23}CO_2)_3$	57.80 (57.97)	9.29 (9.46)	18.88 (18.85)	0.5
$Ce(C_{11}H_{23}CO_2)_3$	57.29 (57.19)	9.48 (9.46)	18.48 (18.98)	1
$Pr(C_{11}H_{23}CO_2)_3$	57.66 (57.82)	9.44 (9.43)	19.16 (19.07)	0.5
$Nd(C_{11}H_{23}CO_2)_3$	57.57 (57.56)	9.35 (9.39)	19.20 (19.43)	0.5
$Sm(C_{11}H_{23}CO_2)_3$	56.62 (56.42)	9.26 (9.34)	20.10 (20.09)	1
$Eu(C_{11}H_{23}CO_2)_3$	55.04 (56.31)	9.09 (9.32)	19.85 (20.26)	1
$Gd(C_{11}H_{23}CO_2)_3$	56.45 (56.58)	9.26 (9.23)	20.30 (20.82)	0.5
$Tb(C_{11}H_{23}CO_2)_3$	56.32 (56.46)	9.30 (9.21)	21.16 (21.01)	0.5
$Dy(C_{11}H_{23}CO_2)_3$	55.74 (55.54)	9.17 (9.19)	21.30 (21.37)	1
$Ho(C_{11}H_{23}CO_2)_3$	55.86 (55.37)	9.13 (9.16)	21.93 (21.63)	1
$Er(C_{11}H_{23}CO_2)_3$	55.77 (55.21)	9.02 (9.14)	22.30 (21.63)	1
$Tm(C_{11}H_{23}CO_2)_3$	54.92 (55.09)	9.07 (9.12)	22.22 (22.03)	1
$Yb(C_{11}H_{23}CO_2)_3$	55.12 (55.44)	9.10 (9.04)	22.68 (22.44)	0.5
$Lu(C_{11}H_{23}CO_2)_3$	55.07 (55.30)	8.99 (9.02)	22.60 (22.63)	0.5

[a] The calculated values are given in brackets. For the calculations the stoechiometries $Ln(C_{11}H_{23}CO_2)_3 \cdot xH_2O$, depending on the water content

Table 1.1-2 CHN results for the series $Ln(C_{17}H_{35}CO_2)_3$

Compound	%C[a]	%H[a]
$La(C_{17}H_{35}CO_2)_3$	64.80 (64.97)	10.60 (10.70)
$Ce(C_{17}H_{35}CO_2)_3$	64.74 (64.89)	10.60 (10.69)
$Pr(C_{17}H_{35}CO_2)_3$	64.77 (64.84)	10.54 (10.68)
$Nd(C_{17}H_{35}CO_2)_3$	64.88 (64.62)	10.60 (10.64)
$Sm(C_{17}H_{35}CO_2)_3$	63.81 (64.23)	10.28 (10.58)
$Eu(C_{17}H_{35}CO_2)_3$	63.88 (64.13)	10.43 (10.56)
$Gd(C_{17}H_{35}CO_2)_3$	63.90 (63.79)	10.42 (10.51)
$Tb(C_{17}H_{35}CO_2)_3$	63.30 (63.13)	10.36 (10.49)
$Dy(C_{17}H_{35}CO_2)_3$	63.20 (63.47)	10.36 (10.46)
$Ho(C_{17}H_{35}CO_2)_3$	63.00 (63.32)	10.34 (10.43)
$Er(C_{17}H_{35}CO_2)_3$	62.71 (63.17)	10.37 (10.41)
$Tm(C_{17}H_{35}CO_2)_3$	62.57 (63.07)	10.31 (10.39)
$Yb(C_{17}H_{35}CO_2)_3$	62.73 (62.82)	10.30 (10.35)
$Lu(C_{17}H_{35}CO_2)_3$	62.58 (62.70)	10.25 (10.33)

[a] The calculated values are given in brackets. For the calculations the stoechiometries $Ln(C_{17}H_{35}CO_2)_3 \cdot ½H_2O$ were used.

Table 1.1-3 CHN results for the series $La(C_xH_{2x+1}CO_2)_3$

compound	%C[a]	%H[a]
$La(C_3H_7CO_2)_3$	34.96 (34.46)	5.60 (5.54)
$La(C_4H_9CO_2)_3$	40.45 (39.92)	6.32 (6.25)
$La(C_5H_{11}CO_2)_3$	43.79 (43.82)	6.85 (6.95)
$La(C_6H_{13}CO_2)_3$	47.42 (47.10)	7.44 (7.53)
$La(C_7H_{15}CO_2)_3$	50.09 (49.91)	7. 90(8.02)
$La(C_8H_{17}CO_2)_3$	52.06 (52.34)	8 .36(8.46)
$La(C_9H_{19}CO_2)_3$	54.30 (54.46)	8.74 (8.84)
$La(C_{10}H_{21}CO_2)_3$	55.80 (56.32)	9.14 (9.17)
$La(C_{11}H_{23}CO_2)_3$	57.80 (57.97)	9.29 (9.46)
$La(C_{12}H_{25}CO_2)_3$	59.22 (59.45)	9.56 (9.72)
$La(C_{13}H_{27}CO_2)_3$	60.80 (60.78)	9.84 (9.96)
$La(C_{14}H_{29}CO_2)_3$	63.18 (61.98)	10.42 (10.17)
$La(C_{15}H_{31}CO_2)_3$	63.22 (63.06)	10.28 (10.36)
$La(C_{16}H_{33}CO_2)_3$	64.68 (64.06)	10.56 (10.54)
$La(C_{17}H_{35}CO_2)_3$	64.88 (64.97)	10.60 (10.70)
$La(C_{18}H_{37}CO_2)_3$	65.94 (65.80)	10.78 (10.85)
$La(C_{19}H_{39}CO_2)_3$	66.69 (66.57)	10.92 (10.99)

[a] The calculated values are given in brackets. For the calculations the stoechiometries $La(C_xH_{2x+1}CO_2)_3 \cdot 0.5H_2O$ were used except for $La(C_3H_7CO_2)_3 \cdot H_2O$ which is a monohydrate.

Table 1.1-4 CHN results for the series $Ce(C_xH_{2x+1}CO_2)_3$

Compound	% C [a]	% H [a]	# H_2O
$Ce(C_5H_{11}CO_2)_3$	43.00 (42.93)	6.62 (7.00)	1
$Ce(C_6H_{13}CO_2)_3$	46.82 (46.22)	7.52 (7.57)	1
$Ce(C_7H_{15}CO_2)_3$	49.37 (49.04)	8.04 (8.06)	1
$Ce(C_8H_{17}CO_2)_3$	51.76 (51.49)	8.39 (8.49)	1
$Ce(C_9H_{19}CO_2)_3$	53.90 (53.63)	8.84 (8.85)	1
$Ce(C_{10}H_{21}CO_2)_3$	55.14 (55.51)	9.03 (9.18)	1
$Ce(C_{11}H_{23}CO_2)_3$	57.62 (57.88)	9.37 (9.44)	0.5
$Ce(C_{12}H_{25}CO_2)_3$	59.73 (59.36)	9.61 (9.71)	0.5
$Ce(C_{13}H_{27}CO_2)_3$	60.81 (60.69)	9.93 (9.94)	0.5
$Ce(C_{14}H_{29}CO_2)_3$	61.86 (61.89)	10.05 (10.16)	0.5
$Ce(C_{15}H_{31}CO_2)_3$	62.96 (62.98)	9.82 (10.35)	0.5
$Ce(C_{16}H_{33}CO_2)_3$	64.20 (64.58)	10.55 (10.52)	0
$Ce(C_{17}H_{35}CO_2)_3$	64.74 (64.48)	10.60 (10.68)	0

[a] The calculated values are given in brackets. For the calculations the stoechiometries $Ce(C_xH_{2x+1}CO_2)_3 \cdot xH_2O$, depending on the water content

Table 1.1-5 CHN results for the series $Pr(C_xH_{2x+1}CO_2)_3$

Compound	% C[a]	% H[a]	# H_2O
$Pr(C_5H_{11}CO_2)_3$	42.71 (42.86)	6.82 (6.99)	1
$Pr(C_6H_{13}CO_2)_3$	46.54 (46.16)	7.58 (7.56)	1
$Pr(C_7H_{15}CO_2)_3$	49.14 (48.98)	8.12 (8.05)	1
$Pr(C_8H_{17}CO_2)_3$	51.06 (51.42)	8.35 (8.47)	1
$Pr(C_9H_{19}CO_2)_3$	53.41 (53.36)	9.13 (8.84)	1
$Pr(C_{10}H_{21}CO_2)_3$	55.45 (55.45)	9.06 (9.17)	1
$Pr(C_{11}H_{23}CO_2)_3$	57.03 (57.13)	9.40 (9.46)	1
$Pr(C_{12}H_{25}CO_2)_3$	58.40 (58.63)	9.71 (9.71)	1
$Pr(C_{13}H_{27}CO_2)_3$	60.17 (59.98)	9.84 (9.95)	1
$Pr(C_{14}H_{29}CO_2)_3$	61.93 (61.83)	10.04 (10.18)	0.5
$Pr(C_{15}H_{31}CO_2)_3$	62.86 (62.93)	10.20 (10.37)	0.5
$Pr(C_{16}H_{33}CO_2)_3$	64.54 (64.53)	10.47 (10.51)	0
$Pr(C_{17}H_{35}CO_2)_3$	64.77 (65.43)	10.54 (10.68)	0
$Pr(C_{18}H_{37}CO_2)_3$	65.91 (66.25)	10.88 (10.83)	0
$Pr(C_{19}H_{39}CO_2)_3$	66.64 (66.74)	11.02 (10.96)	0

[a] The calculated values are given in brackets. For the calculations the stoechiometries $Pr(C_xH_{2x+1}CO_2)_3 \cdot xH_2O$, depending on the water content

Table 1.1-6 CHN results for the series $Nd(C_xH_{2x+1}CO_2)_3$

Compound	% C[a]	% H[a]	% Ln[a]	# H_2O
$Nd(C_3H_7CO_2)_3$	33.84 (34.03)	5.27 (5.47)	n.d.[b]	1
$Nd(C_4H_9CO_2)_3$	38.80 (38.69)	6.26 (6.28)	n.d.	1
$Nd(C_5H_{11}CO_2)_3$	43.57 (43.45)	7.05 (6.87)	n.d.	0.5
$Nd(C_6H_{13}CO_2)_3$	46.06 (45.88)	7.31 (7.52)	n.d.	1
$Nd(C_7H_{15}CO_2)_3$	48.62 (48.70)	7.82 (8.00)	25.03 (24.37)	1
$Nd(C_8H_{17}CO_2)_3$	51.33 (51.15)	8.35 (8.43)	23.54 (22.75)	1
$Nd(C_9H_{19}CO_2)_3$	53.71 (54.02)	8.72 (8.76)	21.57 (21.62)	0.5
$Nd(C_{10}H_{21}CO_2)_3$	55.38 (55.19)	9.10 (9.12)	20.48 (20.09)	1
$Nd(C_{11}H_{23}CO_2)_3$	57.57 (57.56)	9.35 (9.39)	19.20 (19.20)	0.5
$Nd(C_{12}H_{25}CO_2)_3$	58.74 (59.05)	9.48 (9.66)	17.98 (18.18)	0.5
$Nd(C_{13}H_{27}CO_2)_3$	59.80 (59.74)	9.88 (9.91)	17.49 (17.08)	1
$Nd(C_{14}H_{29}CO_2)_3$	61.70 (61.60)	10.06 (10.11)	15.76 (16.44)	0.5
$Nd(C_{15}H_{31}CO_2)_3$	63.06 (62.70)	10.36 (10.30)	15.37 (15.67)	0.5
$Nd(C_{16}H_{33}CO_2)_3$	63.74 (63.70)	10.41 (10.48)	n.d.	0.5
$Nd(C_{17}H_{35}CO_2)_3$	64.88 (64.62)	10.60 (10.64)	14.04 (14.37)	0.5
$Nd(C_{18}H_{37}CO_2)_3$	65.53 (65.47)	10.74 (10.80)	13.44 (13.79)	0.5
$Nd(C_{19}H_{39}CO_2)_3$	66.51 (66.25)	10.90 (10.93)	13.24 (13.26)	0.5

[a] The calculated values are given in brackets. For the calculations the stoechiometries $Nd(C_xH_{2x+1}CO_2)_3 \cdot xH_2O$ were used, depending on the water content.

Table 1.1-7 CHN results for the series $Sm(C_xH_{2x+1}CO_2)_3$

Compound	% C[a]	% H[a]	# H_2O
$Sm(C_6H_{13}CO_2)_3$	46.37 (46.42)	7.37 (7.3)	0.5
$Sm(C_7H_{15}CO_2)_3$	48.55 (48.20)	7.75 (7.92)	1
$Sm(C_8H_{17}CO_2)_3$	50.96 (50.66)	8.29 (8.35)	1
$Sm(C_9H_{19}CO_2)_3$	53.18 (52.82)	8.75 (8.72)	1
$Sm(C_{10}H_{21}CO_2)_3$	54.73 (54.73)	9.07 (9.05)	1
$Sm(C_{11}H_{23}CO_2)_3$	55.38 (55.13)	9.21 (9.38)	2
$Sm(C_{12}H_{25}CO_2)_3$	57.24 (56.68)	9.33 (9.63)	2
$Sm(C_{13}H_{27}CO_2)_3$	58.08 (58.08)	9.56 (9.86)	2
$Sm(C_{14}H_{29}CO_2)_3$	60.40 (60.56)	9.49 (10.05)	1
$Sm(C_{15}H_{31}CO_2)_3$	61.67 (61.84)	10.18 (10.24)	1
$Sm(C_{16}H_{33}CO_2)_3$	62.89 (62.72)	10.36 (10.42)	1
$Sm(C_{17}H_{35}CO_2)_3$	63.15 (63.66)	10.54 (10.59)	1
$Sm(C_{18}H_{37}CO_2)_3$	64.43 (64.53)	10.78 (10.74)	1
$Sm(C_{19}H_{39}CO_2)_3$	64.98 (65.34)	10.81 (10.87)	1

[a] The calculated values are given in brackets. For the calculations the stoechiometries $Sm(C_xH_{2x+1}CO_2)_3 \cdot xH_2O$ were used, depending on the water content.

Table 1.1-8 CHN results for the series $Eu(C_xH_{2x+1}CO_2)_3$

Compound	% C[a]	% H[a]
$Eu(C_7H_{15}CO_2)_3$	46.79 (48.08)	7.55 (7.90)
$Eu(C_8H_{17}CO_2)_3$	50.47 (50.54)	8.21 (8.32)
$Eu(C_9H_{19}CO_2)_3$	52.14 (52.70)	8.43 (8.70)
$Eu(C_{10}H_{21}CO_2)_3$	54.78 (54.61)	8.92 (9.03)
$Eu(C_{11}H_{23}CO_2)_3$	55.04 (56.31)	9.09 (9.32)
$Eu(C_{12}H_{25}CO_2)_3$	57.68 (57.83)	9.46 (9.58)
$Eu(C_{13}H_{27}CO_2)_3$	59.35 (59.20)	9.68 (9.81)
$Eu(C_{14}H_{29}CO_2)_3$	60.21 (60.45)	9.97 (10.03)
$Eu(C_{15}H_{31}CO_2)_3$	61.44 (61.58)	10.10 (10.23)
$Eu(C_{16}H_{33}CO_2)_3$	62.94 (62.61)	10.47 (10.40)
$Eu(C_{17}H_{35}CO_2)_3$	63.88 (63.56)	10.43 (10.57)
$Eu(C_{18}H_{37}CO_2)_3$	64.44 (62.44)	10.71 (10.72)
$Eu(C_{19}H_{39}CO_2)_3$	65.03 (65.24)	10.78 (10.88)

[a] The calculated values are given in brackets. For the calculations the stoechiometries $Eu(C_xH_{2x+1}CO_2)_3 \cdot H_2O$ were used.

1.2 X-ray Powder Diffraction

Table 1.2-1 Calculated and experimental *d* spacing for the series $Ln(C_{11}H_{23}CO_2)_3$

Compound	d_{max} (calc) /Å	d_{max} (exp) /Å
$La(C_{11}H_{23}O_2)_3$	34.74	34.67
$Ce(C_{11}H_{23}O_2)_3$	34.67	33.87
$Pr(C_{11}H_{23}O_2)_3$	34.65	34.34
$Nd(C_{11}H_{23}O_2)_3$	34.62	34.34
$Sm(C_{11}H_{23}O_2)_3$	34.57	34.44
$Eu(C_{11}H_{23}O_2)_3$	34.55	34.74
$Gd(C_{11}H_{23}O_2)_3$	34.52	34.83
$Tb(C_{11}H_{23}O_2)_3$	34.50	34.32
$Dy(C_{11}H_{23}O_2)_3$	34.48	34.28
$Ho(C_{11}H_{23}O_2)_3$	34.45	34.56
$Tm(C_{11}H_{23}O_2)_3$	34.41	34.24
$Yb(C_{11}H_{23}O_2)_3$	34.39	34.24
$Lu(C_{11}H_{23}O_2)_3$	34.37	33.98

Table 1.2-2 Calculated and experimental *d* spacing for the series $La(C_xH_{2x+1}CO_2)_3$

Compound	d_{max} (calc) /Å	d_{max} (exp) /Å
$La(C_6H_{13}CO_2)_3$	21.70	22.13
$La(C_7H_{15}CO_2)_3$	23.96	24.65
$La(C_8H_{17}CO_2)_3$	26.65	27.17
$La(C_9H_{19}CO_2)_3$	29.48	29.70
$La(C_{10}H_{21}CO_2)_3$	31.95	32.22
$La(C_{11}H_{23}CO_2)_3$	34.67	34.74
$La(C_{12}H_{25}CO_2)_3$	37.46	37.26
$La(C_{13}H_{27}CO_2)_3$	40.39	39.79
$La(C_{14}H_{29}CO_2)_3$	41.62	42.31
$La(C_{15}H_{31}CO_2)_3$	45.65	44.83
$La(C_{16}H_{33}CO_2)_3$	48.10	47.36
$La(C_{17}H_{35}CO_2)_3$	50.67	49.88
$La(C_{18}H_{37}CO_2)_3$	53.29	52.40
$La(C_{19}H_{39}CO_2)_3$	56.05	54.93

Table 1.2-3 Calculated and experimental *d* spacing for the series $Nd(C_xH_{2x+1}CO_2)_3$

Compound	d_{max} (calc) /Å	d_{max} (exp) /Å
$Nd(C_3H_7CO_2)_3$	14.09	14.61
$Nd(C_4H_9CO_2)_3$	16.18	17.14
$Nd(C_5H_{11}CO_2)_3$	19.28	19.66
$Nd(C_6H_{13}CO_2)_3$	21.57	22.18
$Nd(C_7H_{15}CO_2)_3$	24.61	24.71
$Nd(C_8H_{17}CO_2)_3$	26.91	27.21
$Nd(C_9H_{19}CO_2)_3$	29.54	29.75
$Nd(C_{10}H_{21}CO_2)_3$	32.36	32.28
$Nd(C_{11}H_{23}CO_2)_3$	34.67	34.80
$Nd(C_{12}H_{25}CO_2)_3$	37.23	37.32
$Nd(C_{13}H_{27}CO_2)_3$	39.94	39.84
$Nd(C_{14}H_{29}CO_2)_3$	42.4	42.37
$Nd(C_{15}H_{31}CO_2)_3$	45.18	44.89
$Nd(C_{16}H_{33}CO_2)_3$	47.52	47.41
$Nd(C_{17}H_{35}CO_2)_3$	50.11	49.94
$Nd(C_{18}H_{37}CO_2)_3$	53.00	52.46
$Nd(C_{19}H_{39}CO_2)_3$	55.12	54.98

1.3 Crystal Structure Data

Table 1.3-1 Selected bond lengths (Å) and angles (deg) for lanthanum(III) butyrate monolydrate

Tridentate bridging carboxylates			
La(1)-O(1b)	2.611(14)	O(1b)-C(11)	1.26(2)
La(1)-O(2a)	2.606(15)	O(2a)-C(21)	1.22(2)
La(1)-O(2b)	2.477(16)	O(2b)-C(21)	1.30(3)
La(1)-O(2b)	2.615(15)	O(3a)-C(31)	1.31(2)
La(1)-O(3a)	2.533(16)	O(3b)-C(31)	1.30(3)
La(2)-O(1a)	2.556(13)	O(4a)-C(41)	1.29(2)
La(2)-O(3a)	2.629(15)	O(4b)-C(41)	1.25(2)
La(2)-O(3b)	2.610(18)	O(5a)-C(51)	1.22(3)
La(2)-O(4a)	2.577(14)	O(5b)-C(51)	1.31(2)
La(2)-O(4b)	2.520(14)		
La(2)-O(4b)	2.708(14)		
La(2)-O(5a)	2.626(11)		
La(2)-O(5b)	2.547(15)		
O(1a)-C(11)-O(1b)	122.8(19)		
O(2a)-C(21)-O(2b)	122.3(18)		
O(3a)-C(31)-O(3b)	116.9(19)		
O(4a)-C(41)-O(4b)	122.3(19)		
O(5a)-C(51)-O(5b)	122(2)		
Bidentate bridging carboxylates			
La(1)-O(6a)	2.512(14)	O(6a)-C(61)	1.25(2)
La(2)-O(6b)	2.502(15)	O(6b)-C(61)	1.35(2)
O(6a)-C(61)-O(6b)	117.0(19)		
Coordinated water			
La(1)-O(7)	2.643(13)		
La(1)-O(8)	2.566(13)		

Table 1.3-2 Selected bond lengths (Å) and angles (deg) for neodymium(III) butyrate monolydrate

Tridentate bridging carboxylates			
Nd(1)-O(1a)	2.659(10)	O(1a)-C(11)	1.263(15)
Nd(1)-O(1b)	2.514(9)	O(1b)-C(11)	1.226(17)
Nd(1)-O(2a)	2.505(10)	O(2a)-C(21)	1.274(16)
Nd(1)-O(2b)	2.444(10)	O(2b)-C(21)	1.284(15)
Nd(1)-O(2b)	2.546(9)	O(3a)-C(31)	1.307(15)
Nd(1)-O(3a)	2.447(10)	O(3b)-C(31)	1.243(16)
Nd(2)-O(1a)	2.460(9)	O(4a)-C(41)	1.266(15)
Nd(2)-O(3a)	2.577(10)	O(4b)-C(41)	1.296(14)
Nd(2)-O(3b)	2.519(9)	O(5a)-C(51)	1.248(18)
Nd(2)-O(4a)	2.482(9)	O(5b)-C(51)	1.281(17)
Nd(2)-O(4b)	2.452(9)		
Nd(2)-O(4b)	2.658(9)		
Nd(2)-O(5a)	2.582(8)		
Nd(2)-O(5b)	2.490(10)		
O(1a)-C(11)-O(1b)	120.7(12)		
O(2b)-C(21)-O(2a)	117.2(11)		
O(3b)-C(31)-O(3a)	118.5(11)		
O(4a)-C(41)-O(4b)	117.9(11)		
O(5a)-C(51)-O(5b)	116.2(13)		
Bidentate bridging carboxylates			
Nd(1)-O(6a)	2.421(9)	O(6a)-C(61)	1.243(16)
Nd(2)-O(6b)	2.470(9)	O(6b)-C(61)	1.273(15)
O(6a)-C(61)-O(6b)	123.3(12)		
Coordinated water			
Nd(1)-O(7)	2.556(9)		
Nd(1)-O(8)	2.502(9)		

1.4 Transition Temperatures

Table 1.4-1 Transition temperatures for the series $Ln(C_{11}H_{23}CO_2)_3$

Compound	Transition	T /°C	$\Delta H/kJmol^{-1}$
$La(C_{11}H_{23}CO_2)_3$	Cr → SmA	110	63.72
	SmA → I	161	1.31
$Ce(C_{11}H_{23}CO_2)_3$	Cr → SmA	106	113.58
	SmA → I	138	0.91
$Pr(C_{11}H_{23}CO_2)_3$	Cr → SmA	98	89.63
	SmA → I	128	1.33
$Nd(C_{11}H_{23}CO_2)_3$	Cr → SmA	91	57.14
	SmA→ I	117	1.30
$Sm(C_{11}H_{23}CO_2)_3$	Cr → I	91	103.27
$Eu(C_{11}H_{23}CO_2)_3$	Cr → I	90	84.81
$Gd(C_{11}H_{23}CO_2)_3$	Cr → I	93	89.29
$Tb(C_{11}H_{23}CO_2)_3$	Cr → I	90	95.90
$Dy(C_{11}H_{23}CO_2)_3$	Cr → I	87	109.83
$Ho(C_{11}H_{23}CO_2)_3$	Cr → I	85	108.35
$Er(C_{11}H_{23}CO_2)_3$	Cr → I	84	116.65
$Tm(C_{11}H_{23}CO_2)_3$	Cr → I	83	117.97
$Yb(C_{11}H_{23}CO_2)_3$	Cr → I	81	117.56
$Lu(C_{11}H_{23}CO_2)_3$[I]	Cr → I	78	104.93

Table 1.4-2 Transition temperatures for the series $Ln(C_{17}H_{35}CO_2)_3$

Compound	Transition	T /°C	$\Delta H/kJmol^{-1}$
$La(C_{17}H_{35}CO_2)_3$	Cr → SmA	126	46.91
	SmA → I	148	1.24
$Ce(C_{17}H_{35}CO_2)_3$	Cr → SmA	120	80.16
	SmA → I	129	1.24
$Pr(C_{17}H_{35}CO_2)_3$	Cr → SmA	115	n.d.[a]
	SmA → I	119	n.d.
$Nd(C_{17}H_{35}CO_2)_3$	Cr → I	112	90.45
$Sm(C_{17}H_{35}CO_2)_3$	Cr → I	106	132.50
$Eu(C_{17}H_{35}CO_2)_3$	Cr → I	108	110.93
$Gd(C_{17}H_{35}CO_2)_3$	Cr → I	97	90.63
$Tb(C_{17}H_{35}CO_2)_3$	Cr → I	96	97.07
$Dy(C_{17}H_{35}CO_2)_3$	Cr → I	93	124.60
$Ho(C_{17}H_{35}CO_2)_3$	Cr → I	96	134.14
$Er(C_{17}H_{35}CO_2)_3$	Cr → I	98	139.29
$Tm(C_{17}H_{35}CO_2)_3$	Cr → I	98	75.78
$Yb(C_{17}H_{35}CO_2)_3$	Cr → I	93	68.49
$Lu(C_{17}H_{35}CO_2)_3$	Cr → I	100	79.08

[a] n.d. = not determined

Table 1.4-3 Transition temperatures for the series $La(C_xH_{2x+1}CO_2)_3$

Compound	Transition	T /°C	ΔH/kJmol^{-1}
$La(C_3H_{11}CO_2)_3$	Cr → I	188	13.36
$La(C_4H_{11}CO_2)_3$	Cr → M	93	n.d. [a]
	M → SmA	139	n.d.
	SmA →I	190	n.d.
$La(C_5H_{11}CO_2)_3$	Cr → M	94	22.34
	M → SmA	137	2.73
	SmA →I	189	2.23
$La(C_6H_{13}CO_2)_3$	Cr → M	97	72.66
	M → SmA	133	7.32
	SmA →I	189	1.98
$La(C_7H_{15}CO_2)_3$	Cr → M	94	n.d.
	M → SmA	122	n.d.
	SmA →I	175	1.14
$La(C_8H_{17}CO_2)_3$	Cr → M	98	65.09
	M → SmA	121	5.24
	SmA →I	179	0.79
$La(C_9H_{19}CO_2)_3$	Cr → M	95	41.6
	M → SmA	122	8.62
	SmA →I	172	0.74
$La(C_{10}H_{21}CO_2)_3$	Cr → SmA	106	91.45
	SmA →I	165	0.94
$La(C_{11}H_{23}CO_2)_3$	Cr → SmA	110	63.7
	SmA →I	160	1.30
$La(C_{12}H_{25}CO_2)_3$	Cr → SmA	116	26.1
	SmA →I	154	1.27
$La(C_{13}H_{27}CO_2)_3$	Cr → SmA	120	35.48
	SmA →I	157	1.50
$La(C_{14}H_{29}CO_2)_3$	Cr → SmA	121	29.60
	SmA →I	157	1.60
$La(C_{15}H_{31}CO_2)_3$	Cr → SmA	123	57.02
	SmA →I	148	1.69
$La(C_{16}H_{33}CO_2)_3$	Cr → SmA	123	46.10
	SmA →I	149	1.90
$La(C_{17}H_{35}CO_2)_3$	Cr → SmA	125	46.91
	SmA →I	148	1.24

$La(C_{18}H_{37}CO_2)_3$	Cr → SmA	126	78.77
	SmA →I	140	1.27
$La(C_{19}H_{39}CO_2)_3$	Cr → SmA	128	89.10
	SmA →I	143	1.23

[a] n.d. = not determined

Table 1.4-4 Transition temperatures for the series $Ce(C_xH_{2x+1}CO_2)_3$

Compound	Transition	T/°C	ΔH/kJmol^{-1}
$Ce(C_5H_{11}CO_2)_3$	Cr → M	74	n.d.[a]
	M → SmA	110	n.d.
	SmA → I	159	1.66
$Ce(C_6H_{13}CO_2)_3$	Cr → M	73	n.d.
	M → SmA	106	n.d.
	SmA → I	161	2.05
$Ce(C_7H_{15}CO_2)_3$	Cr → M	75	n.d.
	M → SmA	102	n.d.
	SmA → I	152	1.17
$Ce(C_8H_{17}CO_2)_3$	Cr → M	81	55.58
	M → SmA	96	n.d.
	SmA → I	148	0.67
$Ce(C_9H_{19}CO_2)_3$	Cr → M	86	107.60
	M → SmA	93	n.d.
	SmA → I	148	1.13
$Ce(C_{10}H_{21}CO_2)_3$	Cr → SmA	101	106.88
	SmA → I	142	0.50
$Ce(C_{11}H_{23}CO_2)_3$	Cr → SmA	106	47.45
	SmA → I	142	0.85
$Ce(C_{12}H_{25}CO_2)_3$	Cr → SmA	107	39.82
	SmA → I	133	1.09
$Ce(C_{13}H_{27}CO_2)_3$	Cr → SmA	111	47.57
	SmA → I	131	1.29
$Ce(C_{14}H_{29}CO_2)_3$	Cr → SmA	115	59.89
	SmA → I	130	1.43
$Ce(C_{15}H_{31}CO_2)_3$	Cr → SmA	116	60.26
	SmA → I	129	1.47
$Ce(C_{16}H_{33}CO_2)_3$	Cr → SmA	119	70.06
	SmA → I	127	1.00
$Ce(C_{17}H_{35}CO_2)_3$	Cr → SmA	120	80.16
	SmA → I	129	1.24

[a] n. d. = not determined

Table 1.4-5 Transition temperatures for the series $Pr(C_xH_{2x+1}CO_2)_3$

Compound	Transition	T/°C	ΔH/kJmol^{-1}
$Pr(C_5H_{11}CO_2)_3$	Cr → M	86	n.d.[a]
	M → SmA	109	n.d.
	SmA → I	142	4.08
$Pr(C_6H_{13}CO_2)_3$	Cr → M	90	n.d.
	M → SmA	111	n.d.
	SmA → I	144	2.11
$Pr(C_7H_{15}CO_2)_3$	Cr → M	90	6.78
	M → SmA	112	0.14
	SmA → I	144	1.89
$Pr(C_8H_{17}CO_2)_3$	Cr → M	86	65.8
	M → SmA	95	n.d.
	SmA → I	135	0.72
$Pr(C_9H_{19}CO_2)_3$	Cr → SmA	90	86.6
	SmA → I	136	1.03
$Pr(C_{10}H_{21}CO_2)_3$	Cr → SmA	99	116.8
	SmA → I	133	1.17
$Pr(C_{11}H_{23}CO_2)_3$	Cr → SmA	102	123
	SmA → I	129	0.96
$Pr(C_{12}H_{25}CO_2)_3$	Cr → SmA	105	134
	SmA → I	124	1.02
$Pr(C_{13}H_{27}CO_2)_3$	Cr → SmA	106	88.3
	SmA → I	122	0.96
$Pr(C_{14}H_{29}CO_2)_3$	Cr → SmA	110	62.0
	SmA → I	120	1.51
$Pr(C_{15}H_{31}CO_2)_3$	Cr → SmA	112	61.5
	SmA → I	120	0.94
$Pr(C_{16}H_{33}CO_2)_3$	Cr → SmA	113	n.d.
	SmA → I	118	n.d.
$Pr(C_{17}H_{35}CO_2)_3$	Cr → SmA	115	n.d.
	SmA → I	119	n.d.
$Pr(C_{18}H_{37}CO_2)_3$	Cr → SmA	116	n.d.
	SmA → I	120	n.d.
$Pr(C_{19}H_{39}CO_2)_3$	Cr → SmA	117	n.d.
	SmA → I	122	n.d.

[a] n.d. = not determined

Table 1.4-6 Transition temperatures for the series $Nd(C_xH_{2x+1}CO_2)_3$

Compound	Transition	T /°C	ΔH/kJmol^{-1}
$Nd(C_3H_7CO_2)_3$	Cr → I	166	9.90
$Nd(C_4H_9CO_2)_3$	Cr → M	77	3.50
	M → SmA	95	n.d.[a]
	SmA → I	113	6.32
$Nd(C_5H_{11}CO_2)_3$	Cr → M	81	6.31
	M → SmA	94	n.d.
	SmA → I	128	1.80
$Nd(C_6H_{13}CO_2)_3$	Cr → SmA	86	59.91
	Cr → M	101	n.d.
	M → I	133	2.31
$Nd(C_7H_{15}CO_2)_3$	Cr → M	83	64.51
	M → SmA	92	n.d.
	SmA → I	126	1.20
$Nd(C_8H_{17}CO_2)_3$	Cr → M	82	68.86
	M → SmA	90	n.d.
	SmA → I	127	1.03
$Nd(C_9H_{19}CO_2)_3$	Cr → M	85	88.08
	M → SmA	94	n.d.
	SmA → I	125	1.10
$Nd(C_{10}H_{21}CO_2)_3$	Cr → M	90	94.08
	M → SmA	97	n.d.
	SmA → I	120	1.19
$Nd(C_{11}H_{23}CO_2)_3$	Cr → SmA	91	26.74
	SmA → SmI	117	1.14
$Nd(C_{12}H_{25}CO_2)_3$	Cr → SmA	101	36.23
	SmA → I	116	1.94
$Nd(C_{13}H_{27}CO_2)_3$	Cr → SmA	98	101.36
	SmA → I	111	1.18
$Nd(C_{14}H_{29}CO_2)_3$	Cr → SmA	108	54.20
	SmA → I	114	1.21
$Nd(C_{15}H_{31}CO_2)_3$	Cr → I	107	101.97
$Nd(C_{16}H_{33}CO_2)_3$	Cr → I	111	71.46
$Nd(C_{17}H_{35}CO_2)_3$	Cr → I	112	90.45
$Nd(C_{18}H_{37}CO_2)_3$	Cr → I	116	101.60
$Nd(C_{19}H_{39}CO_2)_3$	Cr → I	115	109.91

[a] n.d. = not determined

Table 1.4-7 Transition temperatures for the series $Sm(C_xH_{2x+1}CO_2)_3$

Compound	Transition	T /°C	ΔH/kJ mol^{-1}
$Sm(C_6H_{13}CO_2)_3$	Cr → I	93	n.d.[a]
$Sm(C_7H_{15}CO_2)_3$	Cr → I	89	n.d.
$Sm(C_8H_{17}CO_2)_3$	Cr → I	86	n.d.
$Sm(C_9H_{19}CO_2)_3$	Cr → I	87	n.d.
$Sm(C_{10}H_{21}CO_2)_3$	Cr → I	86	n.d.
$Sm(C_{11}H_{23}CO_2)_3$	Cr → I	91	103.20
$Sm(C_{12}H_{25}CO_2)_3$	Cr → I	87	70.95
$Sm(C_{13}H_{27}CO_2)_3$	Cr → I	94	81.19
$Sm(C_{14}H_{29}CO_2)_3$	Cr → I	97	81.99
$Sm(C_{15}H_{31}CO_2)_3$	Cr → I	99	70.44
$Sm(C_{16}H_{33}CO_2)_3$	Cr → I	103	78.15
$Sm(C_{17}H_{35}CO_2)_3$	Cr → I	106	132.50
$Sm(C_{18}H_{37}CO_2)_3$	Cr → I	112	132.40
$Sm(C_{19}H_{39}CO_2)_3$	Cr → I	113	93.20

[a] n.d. = not determined

Table 1.4-8 Transition temperatures for the series $Eu(C_xH_{2x+1}CO_2)_3$

Compound	Transition	T /°C	ΔH/kJ mol^{-1}
$Eu(C_7H_{15}CO_2)_3$	Cr → I	80	38.96
$Eu(C_8H_{17}CO_2)_3$	Cr → I	82	65.92
$Eu(C_9H_{19}CO_2)_3$	Cr → I	85	118.87
$Eu(C_{10}H_{21}CO_2)_3$	Cr → I	86	101.82
$Eu(C_{11}H_{23}CO_2)_3$	Cr → I	90	84.81
$Eu(C_{12}H_{25}CO_2)_3$	Cr → I	92	95.16
$Eu(C_{13}H_{27}CO_2)_3$	Cr → I	96	104.40
$Eu(C_{14}H_{29}CO_2)_3$	Cr → I	98	102.43
$Eu(C_{15}H_{31}CO_2)_3$	Cr → I	101	112.64
$Eu(C_{16}H_{33}CO_2)_3$	Cr → I	107	112.18
$Eu(C_{17}H_{35}CO_2)_3$	Cr → I	107	110.48
$Eu(C_{18}H_{37}CO_2)_3$	Cr → I	108	150.96
$Eu(C_{19}H_{39}CO_2)_3$	Cr → I	115	158.30

[a] n.d. = not determined

1.5 Spectroscopic Data

Table 1.5-1 Measured and calculated dipole strengths for the transitions in the absorption spectrum of holmium(III) octadecanoate. All transitions start from the $^5I_8$ ground state.

Transition $\leftarrow {}^5I_8$	ν /cm^{-1}	D_{exp} /10^{-6} Debye^2	D_{calc} /10^{-6} Debye^2	$D_{exp} - D_{calc}$ /10^{-6} Debye^2	D_{calc} / D_{exp}
$^5F_5$	15525	444	458	-15	0.97
$^5S_2$,$^5F_4$	18570	543	501	+42	1.08
$^5F_3$	20550	144	137	+7	1.05
$^5F_2$, $^3K_8$	21070	99	181	-82	0.55
$^5F_1$,$^5G_6$	22240	2272	2270	+2	1.00
$^5G_5$	23880	291	293	-2	0.99
$^3K_7$,$^5G_4$	25825	63	91	-28	0.69

The Judd-Ofelt parameters used for the intensity calculation are: $\Omega_2 = (6.44\pm0.30)\cdot10^{-20}$ cm^2, $\Omega_4 = (3.07\pm0.45)\cdot10^{-20}$ cm^2 and $\Omega_6 = (2.21\pm0.27)\cdot10^{-20}$ cm^2.
The R.M.S. value is $49\cdot10^{-6}$ Debye^2.

Table 1.5-2Measured and calculated dipole strengths for the transitions in the absorption spectrum of vitrified neodymium(III) octadecanoate. All transitions start form the $^4I_{9/2}$ ground state.

Transition $\leftarrow {}^4I_{9/2}$	ν /cm^{-1}	D_{exp} /10^{-6} Debye^2	D_{calc} /10^{-6} Debye^2	$D_{exp} - D_{calc}$ /10^{-6} Debye^2	D_{calc} / D_{exp}
$^4F_{3/2}$	11470	347	422	-75	0.82
$^4F_{5/2}$,$^4H_{9/2}$	12490	1238	1247	-9	0.99
$^4F_{7/2}$,$^4S_{3/2}$	13415	1198	1206	-8	0.99
$^4F_{9/2}$	14700	82	86	-5	0.95
$^4G_{5/2}$,$^2G_{7/2}$	17115	2030	2038	-8	1.00
$^2K_{13/2}$,$^4G_{7/2}$, $^4G_{9/2}$	19050	718	604	113	1.19
$^2K_{15/2}$,$^2G_{9/2}$,$^2D_{3/2}$ $^2P_{3/2}$,$^4G_{11/2}$	21030	146	127	19	1.15
$^2P_{1/2}$	23290	26	56	-30	0.46

The Judd-Ofelt parameters used for the intensity calculation are: $\Omega_2 = (3.63 \pm 0.46)\cdot10^{-20}$ cm^2, $\Omega_4 = (4.69 \pm 0.67)\cdot10^{-20}$ cm^2 and $\Omega_6 = (5.69 \pm 0.30)\cdot10^{-20}$ cm^2.
The R.M.S. value is $63\cdot10^{-6}$ Debye^2.

Appendix 2 [$La_xLn_{1-x}(C_{11}H_{23}CO_2)_3$]

2.1 CHN Results

Table 2.1-1 Analysis results for the series [$La_xEu_{1-x}(C_{11}H_{23}CO_2)_3$]

Compound	% C[a]	% H[a]
[$La_{0.01}Eu_{0.99}(C_{11}H_{23}CO_2)_3$]	56.69 (56.32)	9.18 (9.32)
[$La_{0.02}Eu_{0.98}(C_{11}H_{23}CO_2)_3$]	56.51 (56.33)	9.19 (9.32)
[$La_{0.03}Eu_{0.97}(C_{11}H_{23}CO_2)_3$]	56.37 (56.34)	9.25 (9.32)
[$La_{0.04}Eu_{0.96}(C_{11}H_{23}CO_2)_3$]	56.44 (56.34)	9.03 (9.32)
[$La_{0.05}Eu_{0.95}(C_{11}H_{23}CO_2)_3$]	56.39 (56.35)	9.23 (9.33)
[$La_{0.06}Eu_{0.94}(C_{11}H_{23}CO_2)_3$]	56.30 (56.32)	9.19 (9.33)
[$La_{0.07}Eu_{0.93}(C_{11}H_{23}CO_2)_3$]	56.60 (56.37)	9.20 (9.33)
[$La_{0.08}Eu_{0.92}(C_{11}H_{23}CO_2)_3$]	56.84 (56.38)	9.24(9.33)
[$La_{0.09}Eu_{0.91}(C_{11}H_{23}CO_2)_3$]	56.44 (56.39)	9.18 (9.33)
[$La_{0.10}Eu_{0.90}(C_{11}H_{23}CO_2)_3$]	56.80 (56.40)	9.27 (9.34)
[$La_{0.15}Eu_{0.85}(C_{11}H_{23}CO_2)_3$]	56.99 (56.45)	9.29 (9.34)
[$La_{0.20}Eu_{0.80}(C_{11}H_{23}CO_2)_3$]	56.74 (56.50)	9.59 (9.35)
[$La_{0.25}Eu_{0.75}(C_{11}H_{23}CO_2)_3$]	56.33 (56.55)	9.30 (9.36)
[$La_{0.30}Eu_{0.70}(C_{11}H_{23}CO_2)_3$]	56.20 (56.60)	9.16 (9.37)
[$La_{0.35}Eu_{0.65}(C_{11}H_{23}CO_2)_3$]	56.86 (56.64)	9.08 (9.38)
[$La_{0.40}Eu_{0.60}(C_{11}H_{23}CO_2)_3$]	57.60 (56.69)	9.34 (9.38)
[$La_{0.45}Eu_{0.55}(C_{11}H_{23}CO_2)_3$]	57.39 (56.74)	9.38 (9.39)
[$La_{0.50}Eu_{0.50}(C_{11}H_{23}CO_2)_3$]	56.80 (56.79)	9.25 (9.40)
[$La_{0.55}Eu_{0.45}(C_{11}H_{23}CO_2)_3$]	57.12 (56.84)	9.32 (9.41)
[$La_{0.60}Eu_{0.40}(C_{11}H_{23}CO_2)_3$]	57.01 (56.89)	9.27 (9.42)
[$La_{0.65}Eu_{0.35}(C_{11}H_{23}CO_2)_3$]	57.14 (56.94)	9.69 (9.42)
[$La_{0.70}Eu_{0.30}(C_{11}H_{23}CO_2)_3$]	56.98 (56.98)	9.63 (9.43)
[$La_{0.725}Eu_{0.275}(C_{11}H_{23}CO_2)_3$]	57.09 (57.01)	9.70 (9.44)
[$La_{0.75}Eu_{0.25}(C_{11}H_{23}CO_2)_3$]	57.30 (57.13)	9.20 (9.48)
[$La_{0.775}Eu_{0.225}(C_{11}H_{23}CO_2)_3$]	57.06 (57.06)	9.34 (9.44)
[$La_{0.80}Eu_{0.20}(C_{11}H_{23}CO_2)_3$]	56.97 (57.08)	9.51 (9.45)
[$La_{0.825}Eu_{0.175}(C_{11}H_{23}CO_2)_3$]	57.13 (57.11)	9.16 (9.45)
[$La_{0.85}Eu_{0.15}(C_{11}H_{23}CO_2)_3$]	56.45 (57.03)	9.35 (9.45)
[$La_{0.875}Eu_{0.125}(C_{11}H_{23}CO_2)_3$]	56.92 (57.16)	9.32 (9.46)
[$La_{0.90}Eu_{0.10}(C_{11}H_{23}CO_2)_3$]	56.82 (57.18)	9.23 (9.46)
[$La_{0.925}Eu_{0.085}(C_{11}H_{23}CO_2)_3$]	57.58 (57.20)	9.41 (9.47)

$[La_{0.95}Eu_{0.05}(C_{11}H_{23}CO_2)_3]$	56.90 (57.23)	9.35 (9.47)
$[La_{0.975}Eu_{0.025}(C_{11}H_{23}CO_2)_3]$	57.48 (57.26)	9.38 (9.48)

[a] The calculated values are given in brackets. For the calculations the stoechiometries $La_xEu_{1-x}(C_{11}H_{23}CO_2)_3 \cdot H_2O$ were used.

Table 2.1-2 Analysis results for the series $[La_xNd_{1-x}(C_{11}H_{23}CO_2)_3]$

Compound	% C[a]	% H[a]
$[La_{0.05}Nd_{0.95}(C_{11}H_{23}CO_2)_3]$	55.62 (56.90)	9.13 (9.42)
$[La_{0.10}Nd_{0.90}(C_{11}H_{23}CO_2)_3]$	57.10 (56.92)	9.35 (9.42)
$[La_{0.15}Nd_{0.85}(C_{11}H_{23}CO_2)_3]$	56.88 (56.94)	9.34 (9.42)
$[La_{0.25}Nd_{0.75}(C_{11}H_{23}CO_2)_3]$	55.82 (56.98)	9.15 (9.43)
$[La_{0.50}Nd_{0.50}(C_{11}H_{23}CO_2)_3]$	56.98 (57.08)	9.33 (9.45)
$[La_{0.75}Nd_{0.25}(C_{11}H_{23}CO_2)_3]$	57.37 (57.18)	9.42 (9.46)
$[La_{0.90}Nd_{0.10}(C_{11}H_{23}CO_2)_3]$	56.76 (57.24)	9.30 (9.47)

[a] The calculated values are given in brackets. For the calculations the stoechiometries $[La_xEu_{1-x}(C_{11}H_{23}CO_2)_3 \cdot H_2O]$ were used.

Table 2.1-3 Analysis results for the series $[La_xTb_{1-x}(C_{11}H_{23}CO_2)_3]$

Compound	% C[a]	% H[a]
$[La_{0.05}Tb_{0.95}(C_{11}H_{23}CO_2)_3]$	56.40 (55.87)	9.24 (9.25)
$[La_{0.10}Tb_{0.90}(C_{11}H_{23}CO_2)_3]$	56.52 (55.94)	9.25 (9.26)
$[La_{0.15}Tb_{0.85}(C_{11}H_{23}CO_2)_3]$	56.01 (56.02)	9.17 (9.27)
$[La_{0.25}Tb_{0.75}(C_{11}H_{23}CO_2)_3]$	56.38 (56.16)	9.22 (9.30)
$[La_{0.50}Tb_{0.50}(C_{11}H_{23}CO_2)_3]$	56.56 (56.53)	9.27 (9.36)
$[La_{0.75}Tb_{0.25}(C_{11}H_{23}CO_2)_3]$	56.84 (56.90)	9.38 (9.42)
$[La_{0.90}Tb_{0.10}(C_{11}H_{23}CO_2)_3]$	57.06 (57.13)	9.18 (9.45)

[a] The calculated values are given in brackets. For the calculations the stoechiometries $[La_xEu_{1-x}(C_{11}H_{23}CO_2)_3 \cdot H_2O]$ were used.

Table 2.1-4 Analysis results for the series $[La_xHo_{1-x}(C_{11}H_{23}CO_2)_3]$

Compound	% C[a]	% H[a]
$[La_{0.05}Ho_{0.95}(C_{11}H_{23}CO_2)_3]$	55.21 (55.46)	8.94 (9.18)
$[La_{0.15}Ho_{0.85}(C_{11}H_{23}CO_2)_3]$	55.87 (55.65	9.05 (9.21)
$[La_{0.25}Ho_{0.75}(C_{11}H_{23}CO_2)_3]$	55.90 (55.84)	9.08 (9.24)
$[La_{0.50}Ho_{0.50}(C_{11}H_{23}CO_2)_3]$	56.19 (56.31)	9.17 (9.32)
$[La_{0.60}Ho_{0.40}(C_{11}H_{23}CO_2)_3]$	56.44 (56.50)	9.25 (9.35)
$[La_{0.70}Ho_{0.30}(C_{11}H_{23}CO_2)_3]$	56.12 (56.69)	9.22 (9.38)
$[La_{0.75}Ho_{0.25}(C_{11}H_{23}CO_2)_3]$	57.27 (56.79)	9.35 (9.40)
$[La_{0.80}Ho_{0.20}(C_{11}H_{23}CO_2)_3]$	56.66 (56.89)	9.32 (9.41)
$[La_{0.85}Ho_{0.15}(C_{11}H_{23}CO_2)_3]$	56.56 (56.99)	9.32 (9.43)
$[La_{0.90}Ho_{0.10}(C_{11}H_{23}CO_2)_3]$	57.04 (57.08)	9.39 (9.45)
$[La_{0.95}Ho_{0.05}(C_{11}H_{23}CO_2)_3]$	57.13 (57.18)	9.40 (9.46)

[a] The calculated values are given in brackets. For the calculations the stoechiometries $[La_xEu_{1-x}(C_{11}H_{23}CO_2)_3 \cdot H_2O]$ were used.

Table 2.1-5 Analysis results for the series $[La_xYb_{1-x}(C_{11}H_{23}CO_2)_3]$

Compound	% C[a]	% H[a]
$[La_{0.05}Yb_{0.95}(C_{11}H_{23}CO_2)_3]$	55.03 (54.92)	9.06 (9.09)
$[La_{0.10}Yb_{0.90}(C_{11}H_{23}CO_2)_3]$	55.06 (55.04)	9.06 (9.11)
$[La_{0.15}Yb_{0.85}(C_{11}H_{23}CO_2)_3]$	54.36 (55.16)	8.97 (9.13)
$[La_{0.25}Yb_{0.75}(C_{11}H_{23}CO_2)_3]$	55.46 (55.40)	9.11 (9.17)
$[La_{0.50}Yb_{0.50}(C_{11}H_{23}CO_2)_3]$	55.66 (56.01)	9.13 (9.27)
$[La_{0.60}Yb_{0.40}(C_{11}H_{23}CO_2)_3]$	56.15 (56.26)	9.27 (9.31)
$[La_{0.70}Yb_{0.30}(C_{11}H_{23}CO_2)_3]$	56.65 (56.51)	9.34 (9.35)
$[La_{0.75}Yb_{0.25}(C_{11}H_{23}CO_2)_3]$	56.53 (58.01)	9.28 (9.37)
$[La_{0.80}Yb_{0.20}(C_{11}H_{23}CO_2)_3]$	56.82 (56.77)	9.35 (9.40)
$[La_{0.85}Yb_{0.15}(C_{11}H_{23}CO_2)_3]$	56.97 (56.90)	9.42 (9.42)
$[La_{0.90}Yb_{0.10}(C_{11}H_{23}CO_2)_3]$	56.68 (57.02)	9.33 (9.44)
$[La_{0.95}Yb_{0.05}(C_{11}H_{23}CO_2)_3]$	56.52 (57.15)	9.33 (9.46)

[a] The calculated values are given in brackets. For the calculations the stoechiometries $[La_xEu_{1-x}(C_{11}H_{23}CO_2)_3 \cdot H_2O]$ were used.

2.2 Transition Temperatures

Table 2.2-1 Transition temperatures for the series $[La_xEu_{1-x}(C_{11}H_{23}CO_2)_3]$

Compound	Transition	T /°C	ΔH /kJ mol^{-1}
$[La_{0.01}Eu_{0.99}(C_{11}H_{23}CO_2)_3]$	Cr → I	82	76.34
$[La_{0.02}Eu_{0.98}(C_{11}H_{23}CO_2)_3]$	Cr → I	81	77.82
$[La_{0.03}Eu_{0.97}(C_{11}H_{23}CO_2)_3]$	Cr → I	83	n.d.[(c)]
$[La_{0.04}Eu_{0.96}(C_{11}H_{23}CO_2)_3]$	Cr → SmA	82	73.13
	SmA → I	84	n.d.
$[La_{0.05}Eu_{0.95}(C_{11}H_{23}CO_2)_3]$	Cr → SmA	81	123.4
	SmA → I	83	n.d.
$[La_{0.06}Eu_{0.94}(C_{11}H_{23}CO_2)_3]$	Cr → SmA	82	103.44
	SmA → I	84	n.d.
$[La_{0.07}Eu_{0.93}(C_{11}H_{23}CO_2)_3]$	Cr → SmA	82	87.9
	SmA → I	84	n.d.
$[La_{0.08}Eu_{0.92}(C_{11}H_{23}CO_2)_3]$	Cr → SmA	83	124.08
	SmA → I	86	n.d.
$[La_{0.09}Eu_{0.91}(C_{11}H_{23}CO_2)_3]$	Cr → SmA	83	n.d.
	SmA → I	87	n.d.
$[La_{0.10}Eu_{0.90}(C_{11}H_{23}CO_2)_3]$	Cr → SmA	83	123.52
	SmA → I	88	n.d.
$[La_{0.15}Eu_{0.85}(C_{11}H_{23}CO_2)_3]$	Cr → SmA	82	106.78
	SmA → I	89	n.d.
$[La_{0.20}Eu_{0.80}(C_{11}H_{23}CO_2)_3]$	Cr → SmA	84	107.48
	SmA → I	92	n.d.
$[La_{0.25}Eu_{0.75}(C_{11}H_{23}CO_2)_3]$	Cr → SmA	88	83.8
	SmA → I	96	n.d.
$[La_{0.30}Eu_{0.70}(C_{11}H_{23}CO_2)_3]$	Cr → SmA	88	80.9
	SmA → I	97	n.d.
$[La_{0.35}Eu_{0.65}(C_{11}H_{23}CO_2)_3]$	Cr → SmA	88	88.82
	SmA → I	101	n.d.
$[La_{0.40}Eu_{0.60}(C_{11}H_{23}CO_2)_3]$	Cr → SmA	89	117.04
	SmA → I	107	0.22
$[La_{0.45}Eu_{0.55}(C_{11}H_{23}CO_2)_3]$	Cr → SmA	90	117.69
	SmA → I	113	0.45
$[La_{0.50}Eu_{0.50}(C_{11}H_{23}CO_2)_3]$	Cr → SmA	91	111
	SmA → I	114	1.06

$[La_{0.55}Eu_{0.45}(C_{11}H_{23}CO_2)_3]$	Cr → SmA	95	112.64
	SmA → I	122	1.28
$[La_{0.60}Eu_{0.40}(C_{11}H_{23}CO_{23}]$	Cr → SmA	98	100.37
	SmA → I	126	0.36
$[La_{0.65}Eu_{0.35}(C_{11}H_{23}CO_2)_3]$	Cr → SmA	100	103.3
	SmA → I	130	1.07
$[La_{0.70}Eu_{0.30}(C_{11}H_{23}CO_2)_3]$	Cr → SmA	101	113.67
	SmA → I	135	1.36
$[La_{0.725}Eu_{0.275}(C_{11}H_{23}CO_2)_3]$	Cr → SmA	102	110.23
	SmA → I	137	1.24
$[La_{0.75}Eu_{0.25}(C_{11}H_{23}CO_2)_3]$	Cr → SmA	105	93.08
	SmA → I	138	0.27
$[La_{0.775}Eu_{0.225}(C_{11}H_{23}CO_2)_3]$	Cr → SmA	102	118.15
	SmA → I	141	1.12
$[La_{0.80}Eu_{0.20}(C_{11}H_{23}CO_2)_3]$	Cr → SmA	104	106.88
	SmA → I	143	0.70
$[La_{0.825}Eu_{0.175}(C_{11}H_{23}CO_2)_3]$	Cr → SmA	105	115.06
	SmA → I	141	0.72
$[La_{0.85}Eu_{0.15}(C_{11}H_{23}CO_2)_3]$	Cr → SmA	105	102.88
	SmA → I	144	0.77
$[La_{0.875}Eu_{0.125}(C_{11}H_{23}CO_2)_3]$	Cr → SmA	106	99.00
	SmA → I	146	0.69
$[La_{0.90}Eu_{0.10}(C_{11}H_{23}CO_2)_3]$	Cr → SmA	107	88.03
	SmA → I	148	0.35
$[La_{0.925}Eu_{0.085}(C_{11}H_{23}CO_2)_3]$	Cr → SmA	108	115.51
	SmA → I	154	1.22
$[La_{0.95}Eu_{0.05}(C_{11}H_{23}CO_2)_3]$	Cr → SmA	107	109.77
	SmA → I	153	0.75
$[La_{0.975}Eu_{0.025}(C_{11}H_{23}CO_2)_3]$	Cr → SmA	108	109.31
	SmA → I	154	1.00

Linear regression for the melting point: $T_m = 80.21 + 29.59x$ (R = 0.991)
Linear regression for the clearing point: $T_c = 78.44 + 79.18x$ (R = 0.997)

Table 2.2-2 Transition temperatures for the series $[La_xNd_{1-x}(C_{11}H_{23}CO_2)_3]$

Compound	Transition	T /°C	ΔH /kJ mol^{-1}
$[La_{0.05}Nd_{0.95}(C_{11}H_{23}CO_2)_3]$	Cr → SmA	96	103.71
	SmA → I	113	0.47
$[La_{0.10}Nd_{0.90}(C_{11}H_{23}CO_2)_3]$	Cr → SmA	97	123.93
	SmA → I	121	1.06
$[La_{0.15}Nd_{0.85}(C_{11}H_{23}CO_2)_3]$	Cr → SmA	97	125.93
	SmA → I	123	1.35
$[La_{0.25}Nd_{0.75}(C_{11}H_{23}CO_2)_3]$	Cr → SmA	98	110.96
	SmA → I	124	0.82
$[La_{0.50}Nd_{0.50}(C_{11}H_{23}CO_2)_3]$	Cr → SmA	101	118.75
	SmA → I	139	1.18
$[La_{0.75}Nd_{0.25}(C_{11}H_{23}CO_2)_3]$	Cr → SmA	107	125.12
	SmA → I	149	1.27
$[La_{0.90}Nd_{0.10}(C_{11}H_{23}CO_2)_3]$	Cr → SmA	108	115.63
	SmA → I	146	1.07

Linear regression for the melting point: $T_m = 95.37 + 14.95x$ (R = 0.987)
Linear regression for the clearing point: $T_c = 116.14 + 43.66x$ (R = 0.994)

Table 2.2-3 Transition temperatures for the series $[La_xTb_{1-x}(C_{11}H_{23}CO_2)_3]$

Compound	Transition	T /°C	ΔH /kJ mol^{-1}
$[La_{0.05}Tb_{0.95}(C_{11}H_{23}CO_2)_3]$	Cr → I	87	115.49
$[La_{0.10}Tb_{0.90}(C_{11}H_{23}CO_2)_3]$	Cr → I	87	108.72
$[La_{0.15}Tb_{0.85}(C_{11}H_{23}CO_2)_3]$	Cr → I	91	92.15
$[La_{0.25}Tb_{0.75}(C_{11}H_{23}CO_2)_3]$	Cr → I	89	102.49
$[La_{0.50}Tb_{0.50}(C_{11}H_{23}CO_2)_3]$	Cr → SmA	93	125.94
	SmA → I	102	1.16
$[La_{0.75}Tb_{0.25}(C_{11}H_{23}CO_2)_3]$	Cr → SmA	100	106.65
	SmA → I	135	1.16
$[La_{0.90}Tb_{0.10}(C_{11}H_{23}CO_2)_3]$	Cr → SmA	107	112.17
	SmA → I	149	1.13

Linear regression for the melting point: $T_m = 85.79 + 21.20x$ (R = 0.960)
Linear regression for the clearing point: $T_c = 44.24 + 118.50x$ (R = 0.995)

Table 2.2-4 Transition temperatures for the series $[La_xHo_{1-x}(C_{11}H_{23}CO_2)_3]$

Compound	Transition	T /°C	ΔH /kJ mol$_-^{-1}$
$[La_{0.05}Ho_{0.95}(C_{11}H_{23}CO_2)_3]$	Cr → I	81	100.72
$[La_{0.15}Ho_{0.85}(C_{11}H_{23}CO_2)_3]$	Cr → I	86	105.51
$[La_{0.25}Ho_{0.75}(C_{11}H_{23}CO_2)_3]$	Cr → I	88	101.7
$[La_{0.50}Ho_{0.50}(C_{11}H_{23}CO_2)_3]$	Cr → I	91	98.36
$[La_{0.60}Ho_{0.40}(C_{11}H_{23}CO_2)_3]$	Cr → SmA	91	110.4
	SmA → I	107	0.22
$[La_{0.70}Ho_{0.30}(C_{11}H_{23}CO_2)_3]$	Cr → SmA	93	97.43
	SmA → I	121	0.68
$[La_{0.75}Ho_{0.25}(C_{11}H_{23}CO_2)_3]$	Cr → SmA	96	108.9
	SmA → I	129	1.29
$[La_{0.80}Ho_{0.20}(C_{11}H_{23}CO_2)_3]$	Cr → SmA	102	105.4
	SmA → I	135	1.22
$[La_{0.85}Ho_{0.15}(C_{11}H_{23}CO_2)_3]$	Cr → SmA	101	108.85
	SmA → I	140	1.12
$[La_{0.90}Ho_{0.10}(C_{11}H_{23}CO_2)_3]$	Cr → SmA	103	101.1
	SmA → I	148	1.25
$[La_{0.95}Ho_{0.05}(C_{11}H_{23}CO_2)_3]$	Cr → SmA	105	111.36
	SmA → I	154	1.34

Linear regression for the melting point: $T_m = 81.02 + 23.36x$ (R = 0.949)
Linear regression for the clearing point: $T_c = 28.46 + 132.98x$ (R = 0.999)

Table 2.2-5 Transition temperatures for the series $[La_xYb_{1-x}(C_{11}H_{23}CO_2)_3]$

Compound	Transition	T /°C	ΔH /kJ mol^{-1}
$[La_{0.05}Yb_{0.95}(C_{11}H_{23}CO_2)_3]$	Cr → I	83	135.74
$[La_{0.10}Yb_{0.90}(C_{11}H_{23}CO_2)_3]$	Cr → I	78	116.64
$[La_{0.15}Yb_{0.85}(C_{11}H_{23}CO_2)_3]$	Cr → I	82	107.8
$[La_{0.25}Yb_{0.75}(C_{11}H_{23}CO_2)_3]$	Cr → I	82	113.19
$[La_{0.50}Yb_{0.50}(C_{11}H_{23}CO_2)_3]$	Cr → I	85	87.44
$[La_{0.60}Yb_{0.40}(C_{11}H_{23}CO_2)_3]$	Cr → I	88	107.56
$[La_{0.70}Yb_{0.30}(C_{11}H_{23}CO_2)_3]$	Cr → SmA	91	84.51
	SmA → I	117	0.25
$[La_{0.75}Yb_{0.25}(C_{11}H_{23}CO_2)_3]$	Cr → SmA	94	74.65
	SmA → I	124	0.47
$[La_{0.80}Yb_{0.20}(C_{11}H_{23}CO_2)_3]$	Cr → SmA	94	95.21
	SmA → I	130	1.32
$[La_{0.85}Yb_{0.15}(C_{11}H_{23}CO_2)_3]$	Cr → SmA	95	91.05
	SmA → I	138	1.45
$[La_{0.90}Yb_{0.10}(C_{11}H_{23}CO_2)_3]$	Cr → SmA	102	106.39
	SmA → I	145	1.35
$[La_{0.95}Yb_{0.05}(C_{11}H_{23}CO_2)_3]$	Cr → SmA	104	96.49
	SmA → I	150	1.31

Linear regression for the melting point: $T_m = 77.54 + 23.18x$ ($R = 0.932$)
Linear regression for the clearing point: $T_c = 24.30 + 133.63x$ ($R = 0.998$)

Appendix 3 [$Ln(C_xH_{2x+1}CO_2)_3$·1,10-phenanthroline]

3.1 CHN Results

Table 3.1-1 CHN results for the series [$Ln(C_5H_{11}CO_2)_3$·1,10- phenanthroline]

Compound[a]	% C [b]	% H[b]	% N[b]
[$Pr(C_5H_{11}CO_2)_3$·phen]	51.56 (52.63)	5.84 (6.33)	4.80 (4.09)
[$Nd(C_5H_{11}CO_2)_3$·phen]	53.08 (52.39)	5.80 (6.30)	4.29 (4.07)
[$Sm(C_5H_{11}CO_2)_3$·phen]	51.81 (51.92)	5.83 (6.24)	4.48 (4.04)
[$Eu(C_5H_{11}CO_2)_3$·phen]	52.99 (51.80)	6.04 (6.23)	4.06 (4.03)
[$Gd(C_5H_{11}CO_2)_3$·phen]	52.06 (51.41)	5.92 (6.18)	4.22 (4.00)
[$Tb(C_5H_{11}CO_2)_3$·phen]	51.88 (51.28)	5.89 (6.17)	4.21 (3.99)
[$Dy(C_5H_{11}CO_2)_3$·phen]	51.18 (51.02)	5.79 (6.14)	4.32 (3.97)
[$Ho(C_5H_{11}CO_2)_3$·phen]	50.46 (50.85)	5.65 (6.12)	4.51 (3.95)
[$Er(C_5H_{11}CO_2)_3$·phen]	51.04 (50.68)	5.84 (6.10)	4.32 (3.94)
[$Tm(C_5H_{11}CO_2)_3$·phen]	49.76 (50.56)	5.59 (6.08)	4.64 (3.93)
[$Yb(C_5H_{11}CO_2)_3$·phen]	49.76 (50.27)	5.34 (6.05)	4.80 (3.91)
[$Lu(C_5H_{11}CO_2)_3$·phen]	50.90 (50.14)	5.62 (6.03)	3.85 (3.90)

[a] phen is the abbreviation of 1,10-phenanthroline.

[b] The calculated values are given in brackets. For the calculations the stoechiometry [$Ln(C_5H_{11}CO_2)_3$·1,10- phenanthroline]·H_2O is used.

Table 3.1-2 CHN results for the series [Ln($C_{11}H_{23}CO_2$)$_3$·1,10- phenanthroline]

Compound[a]	% C[b]	% H[b]	% N[b]
[Sm($C_{11}H_{23}CO_2$)$_3$·phen]	56.78 (60.91)	8.31 (8.41)	2.38 (2.96)
[Eu($C_{11}H_{23}CO_2$)$_3$·phen]	61.30 (60.81)	8.34 (8.40)	3.04 (2.95)
[Gd($C_{11}H_{23}CO_2$)$_3$·phen]	59.90 (60.47)	8.33 (8.35)	2.43 (2.94)
[Tb($C_{11}H_{23}CO_2$)$_3$·phen]	59.62 (60.36)	8.19 (8.34)	2.52 (2.93)
[Dy($C_{11}H_{23}CO_2$)$_3$·phen]	58.97 (60.14)	8.28 (8.31)	2.36 (2.92)
[Ho($C_{11}H_{23}CO_2$)$_3$·phen]	59.40 (59.98)	7.88 (8.28)	3.12 (2.91)
[Er($C_{11}H_{23}CO_2$)$_3$·phen]	58.34 (59.84)	8.15 (8.26)	2.54 (2.91)
[Tm($C_{11}H_{23}CO_2$)$_3$·phen]	58.70 (59.74)	7.88 (8.25)	3.29 (2.90)

[a] phen is the abbreviation of 1,10-phenanthroline.
[b] The calculated values are given in brackets. For the calculations the stoechiometry [Ln($C_{11}H_{23}CO_2$)$_3$·1,10- phenanthroline]·H_2O is used.

Table 3.1-3 CHN results for the series [Eu($C_xH_{2x+1}CO_2$)$_3$·1,10- phenanthroline]

Compound[a]	% C[b]	% H[b]	% N[b]
[Eu($C_5H_{11}CO_2$)$_3$·phen]	52.99 (51.80)	6.04 (6.23)	4.06 (4.03)
[Eu($C_6H_{13}CO_2$)$_3$·phen]	53.68 (53.73)	6.34 (6.69)	4.16 (3.80)
[Eu($C_7H_{15}CO_2$)$_3$·phen]	55.91 (55.45)	6.85 (7.11)	3.76 (3.59)
[Eu($C_8H_{17}CO_2$)$_3$·phen]	57.16 (56.99)	7.22 (7.48)	3.52 (3.41)
[Eu($C_9H_{19}CO_2$)$_3$·phen]	57.31 (58.39)	7.80 (7.82)	2.50 (3.24)
[Eu($C_{10}H_{21}CO_2$)$_3$·phen]	58.96 (59.65)	7.90 (8.12)	3.02 (3.09)
[Eu($C_{11}H_{23}CO_2$)$_3$·phen]	61.30 (60.81)	8.34 (8.40)	3.04 (2.95)

[a] phen is the abbreviation of 1,10-phenanthroline.

[b] The calculated values are given in brackets. For the calculations the stoechiometry [Eu($C_xH_{2x+1}CO_2$)$_3$·1,10- phenanthroline]·H_2O is used.

3.2 Crystal Structure Data

Table 3.2-1 Selected bond lengths (Å) and angles (deg) for [$Tb(C_5H_{11}CO_2)_3$·1,10-phenanthroline]

Tridentate chelating carboxylate			
Tb(1)-O(1)	2.326(5)	O(1)-C(13)	1.262(9)
Tb(1)-O(2)	2.467(5)	O(2)-C(13)	1.249(9)
Tb(1)-O(1)	2.602(5)		
O(2)-C(13)-O(1)		120.4(7)	
Bidentate chelating carboxylate			
Tb(1)-O(3)	2.398(5)	O(3)-C(19)	1.249(8)
Tb(1)-O(4)	2.505(5)	O(4)-C(19)	1.232(8)
O(4)-C(19)-O(3)		121.2(7)	
Bidentate bridging carboxylate			
Tb(1)-O(5)	2.335(4)	O(5)-C(25)	1.261(8)
Tb(1)-O(6)	2.386(4)	O(6)-C(25)	1.252(8)
O(6)-C(25)-O(5)		126.5(6)	
Phenanthroline			
Tb(1)-N(2)	2.577(5)		
Tb(1)-N(1)	2.604(5)		
C(10)-N(2)-C(11)		117.6(6)	
C(1)-N(1)-C(12)		117.6(6)	

3.3 Transition Temperatures

Table 3.3-1 Transition temperatures for the series [Ln($C_5H_{11}CO_2$)$_3$·1,10- phenanthroline]

Compound	Transition	T /°C	ΔH /kJ mol^{-1}
[Pr($C_5H_{11}CO_2$)$_3$·phen]	Cr → I	220	40.48
[Nd($C_5H_{11}CO_2$)$_3$·phen]	Cr → I	234	43.41
[Sm($C_5H_{11}CO_2$)$_3$·phen]	Cr → I	238	44.29
[Eu($C_5H_{11}CO_2$)$_3$·phen]	Cr → I	246	42.20
[Gd($C_5H_{11}CO_2$)$_3$·phen]	Cr → I	241	47.66
[Tb($C_5H_{11}CO_2$)$_3$·phen]	Cr → I	236	43.74
[Dy($C_5H_{11}CO_2$)$_3$·phen]	Cr → I	230	43.77
[Ho($C_5H_{11}CO_2$)$_3$·phen]	Cr → I	225	48.16
[Er($C_5H_{11}CO_2$)$_3$·phen]	Cr → I	216	37.54
[Tm($C_5H_{11}CO_2$)$_3$·phen]	Cr → I	207	41.03
[Yb($C_5H_{11}CO_2$)$_3$·phen]	Cr → I	194	43.55
[Lu($C_5H_{11}CO_2$)$_3$·phen]	Cr → I	185	45.15

Table 3.3-2 Transition Temperatures for the series [Ln($C_{11}H_{23}CO_2$)$_3$·1,10-phenanthroline]

Compound	Transition	T /°C	ΔH /kJ mol^{-1}
[Sm($C_{11}H_{23}CO_2$)$_3$·phen]	Cr → Cr1	62	5.49
	Cr1 → Cr2	96	11.70
	Cr2 → I	207	13.18
[Eu($C_{11}H_{23}CO_2$)$_3$·phen]	Cr → Cr2	63	37.02
	Cr2 → I	215	42.11
[Gd($C_{11}H_{23}CO_2$)$_3$·phen]	Cr → Cr1	65	12.63
	Cr1 → Cr2	93	6.95
	Cr2 → I	212	23.81
[Tb($C_{11}H_{23}CO_2$)$_3$·phen]	Cr → Cr1	64	19.14
	Cr1 → Cr2	86	6.12
	Cr2 → I	210	29.96
[Dy($C_{11}H_{23}CO_2$)$_3$·phen]	Cr → Cr1	64	20.00
	Cr1 → Cr2	88	13.13
	Cr2 → I	201	28.68
[Ho($C_{11}H_{23}CO_2$)$_3$·phen]	Cr → Cr1	61	14.22
	Cr1 → Cr2	97	34.20
	Cr2 → I	197	45.52
[Er($C_{11}H_{23}CO_2$)$_3$·phen]	Cr → Cr1	62	14.74
	Cr1 → Cr2	82	n.d.
	Cr2 → I	195	26.58
[Tm($C_{11}H_{23}CO_2$)$_3$·phen]	Cr → Cr1	71	14.77
	Cr1 → Cr2	84	0.57
	Cr2 → I	188	39.55

Table 3.3-3 Transition temperatures for the series [Eu($C_xH_{2x+1}CO_2$)$_3$·1,10- phenanthroline]

Compound	Transition	T /°C	ΔH /kJ mol^{-1}
[Eu($C_5H_{11}CO_2$)$_3$·phen]	Cr → I	246	n.d.[a]
[Eu($C_6H_{13}CO_2$)$_3$·phen]	Cr → I	232	39.01
[Eu($C_7H_{15}CO_2$)$_3$·phen]	Cr1 → Cr2	56	n.d.
	Cr2 → I	231	40.62
[Eu($C_8H_{17}CO_2$)$_3$·phen]	Cr1 → Cr2	62	n.d.
	Cr2 → I	226	35.25
[Eu($C_9H_{19}CO_2$)$_3$·phen]	Cr1 → Cr2	75	41.38
	Cr2 → I	220	23.48
[Eu($C_{10}H_{21}CO_2$)$_3$·phen]	Cr1 → Cr2	82	4.16
	Cr2 → I	218	29.54
[Eu($C_{11}H_{23}CO_2$)$_3$·phen]	Cr1 → Cr2	63	37.03
	Cr2 → I	215	42.11

[a] n.d. = not determined

Appendix 4 $Ln(C_xH_{2x+1}OC_6H_4CO_2)_3$

4.1 CHN Results

Table 4.1-1 CHN-results for the series $C_xH_{2x+1}OC_6H_4CO_2H$

Compound	%C[a]	%H[a]
$C_4H_9OC_6H_4CO_2H$	68.30 (68.02)	7.40 (7.26)
$C_6H_{13}OC_6H_4CO_2H$	70.32 (70.24)	8.50 (8.16)
$C_8H_{17}OC_6H_4CO_2H$	71.67 (71.97)	8.84 (8.86)
$C_9H_{19}OC_6H_4CO_2H$	72.11 (72.69)	9.24 (9.15)
$C_{10}H_{21}OC_6H_4CO_2H$	72.95 (73.34)	9.38 (9.41)

[a] The calculated values are given in brackets.

Table 4.1-2 CHN-results for the series $Ln(C_4H_9OC_6H_4CO_2)_3$

Compound	% C[a]	% H[a]	# H_2O
$La(C_4H_9OC_6H_4CO_2)_3$	52.56 (52.32)	5.92 (6.12)	2
$Pr(C_4H_9OC_6H_4CO_2)_3$	52.30 (52.18)	5.87 (6.10)	2
$Nd(C_4H_9OC_6H_4CO_2)_3$	51.84 (51.95)	5.81 (6.08)	2
$Sm(C_4H_9OC_6H_4CO_2)_3$	50.29 (50.55)	5.48 (5.78)	3
$Eu(C_4H_9OC_6H_4CO_2)_3$	51.26 (51.63)	5.14 (5.64)	2
$Gd(C_4H_9OC_6H_4CO_2)_3$	49.97 (50.11)	4.95 (5.73)	3
$Tb(C_4H_9OC_6H_4CO_2)_3$	51.55 (51.17)	5.15 (5.59)	2
$Dy(C_4H_9OC_6H_4CO_2)_3$	52.41 (52.14)	4.65 (5.44)	1
$Ho(C_4H_9OC_6H_4CO_2)_3$	49.60 (49.63)	5.00 (5.68)	3
$Er(C_4H_9OC_6H_4CO_2)_3$	49.18 (50.11)	5.06 (5.73)	3
$Yb(C_4H_9OC_6H_4CO_2)_3$	49.27 (49.13)	5.02 (5.62)	3

[a] The calculated values are given in brackets. For the calculations the stoechiometries $Ln(C_4H_9OC_6H_4CO_2)_3 \cdot x\ H_2O$ were used, with x depending on the water content

Table 4.1-3 CHN-results for the series $Ln(C_6H_{13}OC_6H_4CO_2)_3$

Compound	% C [a]	% H [a]	# H_2O
$La(C_6H_{13}OC_6H_4CO_2)_3$	55.45 (55.65)	6.72 (6.94)	2
$Pr(C_6H_{13}OC_6H_4CO_2)_3$	55.02 (55.51)	6.38 (6.93)	2
$Nd(C_6H_{13}OC_6H_4CO_2)_3$	55.08 (54.33)	6.60 (6.66)	3
$Sm(C_6H_{13}OC_6H_4CO_2)_3$	53.37 (53.95)	6.12 (6.22)	3
$Eu(C_6H_{13}OC_6H_4CO_2)_3$	54.29 (53.85)	6.42 (6.60)	3
$Gd(C_6H_{13}OC_6H_4CO_2)_3$	53.66 (53.53)	6.40 (6.56)	3
$Tb(C_6H_{13}OC_6H_4CO_2)_3$	52.86 (53.42)	6.37 (6.55)	3
$Dy(C_6H_{13}OC_6H_4CO_2)_3$	52.31 (53.21)	6.99 (6.53)	3
$Ho(C_6H_{13}OC_6H_4CO_2)_3$	53.19 (53.06)	6.36 (6.51)	3
$Er(C_6H_{13}OC_6H_4CO_2)_3$	54.32 (52.92)	6.17 (6.49)	3
$Yb(C_6H_{13}OC_6H_4CO_2)_3$	53.84 (53.48)	6.25 (6.67)	2
$Lu(C_6H_{13}OC_6H_4CO_2)_3$	52.30 (52.46)	6.03 (6.43)	3

[a] The calculated values are given in brackets. For the calculations the stoechiometries $Ln(C_4H_9OC_6H_4CO_2)_3$. x H_2O were used, with x depending on the water content

Table 4.1-4 CHN-results for the series $Ln(C_8H_{17}OC_6H_4CO_2)_3$

Compound	% C[a]	% H[a]	# H_2O
$La(C_8H_{17}OC_6H_4CO_2)_3$	58.19 (57.44)	7.31 (7.39)	3
$Pr(C_8H_{17}OC_6H_4CO_2)_3$	58.20 (57.32)	7.27 (7.38)	3
$Nd(C_8H_{17}OC_6H_4CO_2)_3$	57.97 (57.12)	7.30 (7.35)	3
$Sm(C_8H_{17}OC_6H_4CO_2)_3$	56.07 (56.75)	7.00 (7.30)	3
$Eu(C_8H_{17}OC_6H_4CO_2)_3$	56.42 (56.66)	6.94 (7.29)	3
$Gd(C_8H_{17}OC_6H_4CO_2)_3$	56.23 (56.34)	7.13 (7.25)	3
$Tb(C_8H_{17}OC_6H_4CO_2)_3$	56.54 (56.24)	7.20 (7.24)	3
$Dy(C_8H_{17}OC_6H_4CO_2)_3$	56.01 (56.04)	7.40 (7.21)	3
$Ho(C_8H_{17}OC_6H_4CO_2)_3$	54.88 (55.90)	6.61 (7.19)	3
$Er(C_8H_{17}OC_6H_4CO_2)_3$	57.49 (57.91)	6.98 (7.02)	1
$Tm(C_8H_{17}OC_6H_4CO_2)_3$	55.60 (55.66)	6.98 (7.16)	3

[a] The calculated values are given in brackets. For the calculations the stoechiometries $Ln(C_4H_9OC_6H_4CO_2)_3 \cdot x\ H_2O$ were used, with x depending on the water content

Table 4.1-5 CHN-results for the series $Ln(C_9H_{19}OC_6H_4CO_2)_3$

Compound	% C[a]	% H[a]	# H_2O
$La(C_9H_{19}OC_6H_4CO_2)_3$	59.02 (58.65)	7.57 (7.69)	3
$Pr(C_9H_{19}OC_6H_4CO_2)_3$	59.17 (58.53)	7.26 (7.67)	3
$Nd(C_9H_{19}OC_6H_4CO_2)_3$	58.55 (58.33)	7.70 (7.64)	3
$Sm(C_9H_{19}OC_6H_4CO_2)_3$	58.88 (57.97)	7.77 (7.60)	3
$Eu(C_9H_{19}OC_6H_4CO_2)_3$	59.51 (58.94)	7.35 (7.52)	2
$Gd(C_9H_{19}OC_6H_4CO_2)_3$	57.17 (57.57)	7.33 (7.55)	3
$Tb(C_9H_{19}OC_6H_4CO_2)_3$	56.67 (57.48)	7.24 (7.54)	3
$Dy(C_9H_{19}OC_6H_4CO_2)_3$	57.74 (57.27)	7.27 (7.51)	3
$Ho(C_9H_{19}OC_6H_4CO_2)_3$	56.73 (57.14)	7.19 (7.49)	3
$Er(C_9H_{19}OC_6H_4CO_2)_3$	56.65 (57.00)	7.16 (7.47)	3
$Tm(C_9H_{19}OC_6H_4CO_2)_3$	58.50 (56.91)	7.29 (7.46)	3
$Yb(C_9H_{19}OC_6H_4CO_2)_3$	57.42 (56.68)	7.04 (7.43)	3
$Lu(C_9H_{19}OC_6H_4CO_2)_3$	55.60 (56.57)	6.97 (7.42)	3

[a] The calculated values are given in brackets. For the calculations the stoechiometries $Ln(C_4H_9OC_6H_4CO_2)_3 \cdot x\ H_2O$ were used, with x depending on the water content

Table 4.1-6 CHN-results for the series $Ln(C_{10}H_{21}OC_6H_4CO_2)_3$

Compound	% C[a]	% H[a]	# H_2O
$La(C_{10}H_{21}OC_6H_4CO_2)_3$	60.52 (60.82)	8.00 (7.91)	2
$Pr(C_{10}H_{21}OC_6H_4CO_2)_3$	60.00 (59.64)	7.98 (7.95)	3
$Nd(C_{10}H_{21}OC_6H_4CO_2)_3$	59.35 (59.45)	7.90 (7.92)	3
$Sm(C_{10}H_{21}OC_6H_4CO_2)_3$	60.01 (60.14)	7.93 (7.82)	2
$Eu(C_{10}H_{21}OC_6H_4CO_2)_3$	58.90 (59.00)	7.87 (7.80)	3
$Gd(C_{10}H_{21}OC_6H_4CO_2)_3$	59.88 (59.74)	7.85 (7.76)	2
$Tb(C_{10}H_{21}OC_6H_4CO_2)_3$	59.66 (59.64)	7.87 (7.75)	2
$Dy(C_{10}H_{21}OC_6H_4CO_2)_3$	59.38 (56.43)	7.56 (7.73)	2
$Ho(C_{10}H_{21}OC_6H_4CO_2)_3$	58.97 (56.29)	7.67 (7.71)	2
$Er(C_{10}H_{21}OC_6H_4CO_2)_3$	60.29 (59.16)	7.78 (7.69)	2
$Tm(C_{10}H_{21}OC_6H_4CO_2)_3$	59.35 (59.87)	7.66 (7.58)	1
$Yb(C_{10}H_{21}OC_6H_4CO_2)_3$	58.68 (59.06)	7.66 (7.68)	2
$Lu(C_{10}H_{21}OC_6H_4CO_2)_3$	58.89 (58.72)	7.29 (7.63)	2

[a] The calculated values are given in brackets. For the calculations the stoechiometries $Ln(C_4H_9OC_6H_4CO_2)_3 \cdot x\ H_2O$ were used, with x depending on the water content

4.2 Transition Temperatures

Table 4.2-1 Transition temperatures for the series $C_xH_{2x+1}OC_6H_4CO_2H$

Compound	Transition	T/°C	ΔH/kJmol^{-1}
$C_4H_9OC_6H_4CO_2H$	Cr → N	147	17.89
	N → I	161	2.93
$C_6H_{13}OC_6H_4CO_2H$	Cr → N	106	12.65
	N → I	153	2.99
$C_8H_{17}OC_6H_4CO_2H$	Cr → SmC	101	10.27
	SmC → N	107	0.90
	N → I	148	3.40
$C_9H_9OC_6H_4CO_2H$	Cr → SmC	95	32.38
	SmC → N	118	1.58
	N → I	144	2.71
$C_{10}H_{21}OC_6H_4CO_2H$	Cr → SmC	97	10.61
	SmC → N	124	1.61
	N → I	143	3.18

Table 4.2-2 Transition Temperatures for the series $Ln(C_4H_9OC_6H_4CO_2)_3$

Compound	Transition[a][b]	T/°C	ΔH/kJ mol^{-1}
$La(C_4H_9OC_6H_4CO_2)_3$	$1 \rightarrow 6$	117	119.03
	$6 \rightarrow 7$	266	24.71
$Pr(C_4H_9OC_6H_4CO_2)_3$	$1 \rightarrow 6$	106	94.14
	$6 \rightarrow 7$	242	23.94
$Nd(C_4H_9OC_6H_4CO_2)_3$	$1 \rightarrow 6$	104	87.80
	$6 \rightarrow 7$	230	23.11
$Sm(C_4H_9OC_6H_4CO_2)_3$	$1 \rightarrow 6$	97	87.28
	$6 \rightarrow 7$	233	16.36
$Eu(C_4H_9OC_6H_4CO_2)_3$	$1 \rightarrow 6$	66	5.04
	$6 \rightarrow 7$	232	12.46
$Gd(C_4H_9OC_6H_4CO_2)_3$	$1 \rightarrow 6$	64	6.52
	$6 \rightarrow 7$	227	0.53
$Tb(C_4H_9OC_6H_4CO_2)_3$	$1 \rightarrow 6$	64	4.91
	$6 \rightarrow 7$	214	17.58
$Dy(C_4H_9OC_6H_4CO_2)_3$	$1 \rightarrow 6$	59	0.78
	$6 \rightarrow 7$	206	20.61
$Ho(C_4H_9OC_6H_4CO_2)_3$	$1 \rightarrow 6$	69	3.01
	$6 \rightarrow 7$	193	22.09
$Er(C_4H_9OC_6H_4CO_2)_3$	$1 \rightarrow 6$	63	7.45
	$6 \rightarrow 7$	173	15.07
$Yb(C_4H_9OC_6H_4CO_2)_3$	$1 \rightarrow 6$	99	1.43
	$6 \rightarrow 7$	236	37.35

[a] The numbers refer to the structures shown in 6.2.2 .

[b] Although here for all the compounds transition $1 \rightarrow 6$ and $6 \rightarrow 7$ are written, some remark must be given, namely most of the compounds of this series are very less crystalline at room temperature, so just a small amount of the molecules shows this transition.

Table 4.2-3 Transition Temperatures for the series $Ln(C_6H_{13}OC_6H_4CO_2)_3$

Compound	Transition[a]	T /°C	ΔH /kJ mol^{-1}
$La(C_6H_{13}OC_6H_4CO_2)_3$	$1 \rightarrow 2$	119	118.77
	$2 \rightarrow 7$	185	2.80
$Pr(C_6H_{13}OC_6H_4CO_2)_3$	$1 \rightarrow 2$	109	89.37
	$2 \rightarrow 7$	148	0.61
$Nd(C_6H_{13}OC_6H_4CO_2)_3$	$1 \rightarrow 7$	86	103.88
$Sm(C_6H_{13}OC_6H_4CO_2)_3$	$1 \rightarrow 7$	85	97.02
$Eu(C_6H_{13}OC_6H_4CO_2)_3$	$1 \rightarrow 7$	82	83.17
$Gd(C_6H_{13}OC_6H_4CO_2)_3$	$1 \rightarrow 6$	84	94.12
	$6 \rightarrow 7$	165	4.94
$Tb(C_6H_{13}OC_6H_4CO_2)_3$	$1 \rightarrow 6$	89	104.50
	$6 \rightarrow 7$	164	5.44
$Dy(C_6H_{13}OC_6H_4CO_2)_3$	$1 \rightarrow 6$	76	10.22
	$6 \rightarrow 7$	163	5.81
$Ho(C_6H_{13}OC_6H_4CO_2)_3$	$1 \rightarrow 6$	94	70.74
	$6 \rightarrow 7$	160	7.62
$Er(C_6H_{13}OC_6H_4CO_2)_3$	$1 \rightarrow 6$	84	16.41
	$6 \rightarrow 7$	176	4.81
$Yb(C_6H_{13}OC_6H_4CO_2)_3$	$1 \rightarrow 6$	76	38.54
	$6 \rightarrow 7$	184	4.35
$Lu(C_6H_{13}OC_6H_4CO_2)_3$	$1 \rightarrow 6$	68	14.75
	$6 \rightarrow 7$	205	15.78

[a] The numbers refer to the structures shown in 6.2.2 .

Table 4.2-4 Transition Temperatures for the series $Ln(C_8H_{17}OC_6H_4CO_2)_3$

Compound	Transition[a]	T/°C	ΔH /kJ mol^{-1}
$La(C_8H_{17}OC_6H_4CO_2)_3$	$1 \rightarrow 2$	117	162.40
	$2 \rightarrow 7$	171	1.21
$Pr(C_8H_{17}OC_6H_4CO_2)_3$	$1 \rightarrow 7$	105	153.11
$Nd(C_8H_{17}OC_6H_4CO_2)_3$	$1 \rightarrow 7$	93	153.94
$Sm(C_8H_{17}OC_6H_4CO_2)_3$	$1 \rightarrow 7$	93	118.72
$Eu(C_8H_{17}OC_6H_4CO_2)_3$	$1 + 6 \rightarrow 6$	95	115
	$6 \rightarrow 7$	179	1.02
$Gd(C_8H_{17}OC_6H_4CO_2)_3$	$1 + 6 \rightarrow 6$	94	130.47
	$6 \rightarrow 7$	167	1.18
$Tb(C_8H_{17}OC_6H_4CO_2)_3$	$1 + 6 \rightarrow 6$	91	138.23
	$6 \rightarrow 7$	168	2.98
$Dy(C_8H_{17}OC_6H_4CO_2)_3$	$1 + 6 \rightarrow 6$	87	125.51
	$6 \rightarrow 7$	197	5.12
$Ho(C_8H_{17}OC_6H_4CO_2)_3$	$1 + 6 \rightarrow 6$	86	109.03
	$6 \rightarrow 7$	170	8.12
$Er(C_8H_{17}OC_6H_4CO_2)_3$	$1 + 6 \rightarrow 6$	80	84.66
	$6 \rightarrow 7$	166	1.06
$Tm(C_8H_{17}OC_6H_4CO_2)_3$	$1 + 6 \rightarrow 6$	83	122.69
	$6 \rightarrow 7$	179	2.66

[a] The numbers refer to the structures shown in 6.2.2 .

Table 4.2-5 Transition Temperatures for the series $Ln(C_9H_{19}C_6H_4CO_2)_3$

Compound	Transition[a]	T /°C	ΔH /kJ mol^{-1}
$La(C_9H_{19}OC_6H_4CO_2)_3$	$1 \rightarrow 2$	117	195.68
	$2 \rightarrow 7$	167	1.28
$Pr(C_9H_{19}OC_6H_4CO_2)_3$	$1 \rightarrow 2$	90	n.d.[b]
	$2 \rightarrow 7$	161	n.d.
$Nd(C_9H_{19}OC_6H_4CO_2)_3$	$1 \rightarrow 7$	99	178.55
$Sm(C_9H_{19}OC_6H_4CO_2)_3$	$1 \rightarrow 7$	93	188.38
$Eu(C_9H_{19}OC_6H_4CO_2)_3$	$1 \rightarrow 7$	88	23.94
$Gd(C_9H_{19}OC_6H_4CO_2)_3$	$1 \rightarrow 7$	97	154.23
$Tb(C_9H_{19}OC_6H_4CO_2)_3$	$1 \rightarrow 6$	89	100.42
	$6 \rightarrow 7$	156	9.71
$Dy(C_9H_{19}OC_6H_4CO_2)_3$	$1 \rightarrow 6$	98	100.40
	$6 \rightarrow 7$	164	n.d.
$Ho(C_9H_{19}OC_6H_4CO_2)_3$	$1 \rightarrow 6$	94	65.99
	$6 \rightarrow 7$	161	7.01
$Er(C_9H_{19}OC_6H_4CO_2)_3$	$1 \rightarrow 6$	95	69.63
	$6 \rightarrow 7$	161	10.15
$Tm(C_9H_{19}OC_6H_4CO_2)_3$	$1 \rightarrow 7$	96	81.49
$Yb(C_9H_{19}OC_6H_4CO_2)_3$	$1 \rightarrow 7$	105	49.26
$Lu(C_9H_{19}OC_6H_4CO_2)_3$	$1 \rightarrow 6$	99	65.81
	$6 \rightarrow 7$	185	7.58

[a] The numbers refer to the structures shown in 6.2.2 .
[b] n.d. = not determined

Table 4.2-6 Transition Temperatures for the series $Ln(C_{10}H_{21}OC_6H_4CO_2)_3$

Compound	Transition[a]	T /°C	ΔH /kJ mol^{-1}
$La(C_{10}H_{21}OC_6H_4CO_2)_3$	$1 \rightarrow 7$	120	171.86
$Pr(C_{10}H_{21}OC_6H_4CO_2)_3$	$1 \rightarrow 7$	111	152.17
$Nd(C_{10}H_{21}OC_6H_4CO_2)_3$	$1 \rightarrow 6$	107	136.26
	$6 \rightarrow 7$	174	3.12
$Sm(C_{10}H_{21}OC_6H_4CO_2)_3$	$1 \rightarrow 6$	96	157.79
	$6 \rightarrow 7$	176	1.22
$Eu(C_{10}H_{21}OC_6H_4CO_2)_3$	$1 \rightarrow 6$	97	145.59
	$6 \rightarrow 7$	161	1.10
$Gd(C_{10}H_{21}OC_6H_4CO_2)_3$	$1 \rightarrow 7$	94	162.22
$Tb(C_{10}H_{21}OC_6H_4CO_2)_3$	$1 \rightarrow 6$	92	152.12
	$6 \rightarrow 7$	167	0.87
$Dy(C_{10}H_{21}OC_6H_4CO_2)_3$	$1 \rightarrow 6$	91	144.88
	$6 \rightarrow 7$	177	3.34
$Ho(C_{10}H_{21}OC_6H_4CO_2)_3$	$1 \rightarrow 6$	88	118.20
	$6 \rightarrow 7$	168	3.08
$Er(C_{10}H_{21}OC_6H_4CO_2)_3$	$1 \rightarrow 6$	90	109.37
	$6 \rightarrow 7$	167	0.77
$Tm(C_{10}H_{21}OC_6H_4CO_2)_3$	$1 \rightarrow 7$	89	140.38
$Yb(C_{10}H_{21}OC_6H_4CO_2)_3$	$1 \rightarrow 6$	88	155.06
	$6 \rightarrow 7$	190	9.92
$Lu(C_{10}H_{21}OC_6H_4CO_2)_3$	$1 \rightarrow 6$	93	111.96
	$6 \rightarrow 7$	208	8.88

[a] The numbers refer to the structures shown in 6.2.2 .

Appendix 5 $Ln(C_{12}H_{25}SO_4)_3$

Table 4.2-1 CHN results for the series $Ln(C_{12}H_{25}SO_4)_3 \cdot H_2O$

Compound	%C[a]	%H[a]
$La(C_{12}H_{25}SO_4)_3$	45.83 (45.37)	8.20 (8.14)
$Ce(C_{12}H_{25}SO_4)_3$	45.68 (45.31)	8.14 (8.13)
$Pr(C_{12}H_{25}SO_4)_3$	45.84 (45.27)	8.06 (8.13)
$Nd(C_{12}H_{25}SO_4)_3$	45.72 (45.11)	8.26 (8.10)
$Sm(C_{12}H_{25}SO_4)_3$	45.33 (44.83)	8.05 (8.05)
$Eu(C_{12}H_{25}SO_4)_3$	45.16 (44.75)	8.15 (8.03)
$Gd(C_{12}H_{25}SO_4)_3$	44.81 (44.51)	8.14 (7.99)
$Tb(C_{12}H_{25}SO_4)_3$	44.60 (44.43)	8.28 (7.98)
$Dy(C_{12}H_{25}SO_4)_3$	44.12 (44.27)	7.98 (7.95)
$Ho(C_{12}H_{25}SO_4)_3$	43.93 (44.16)	8.06 (7.93)
$Er(C_{12}H_{25}SO_4)_3$	43.96 (44.06)	8.06 (7.91)
$Tm(C_{12}H_{25}SO_4)_3$	43.86 (43.98)	8.10 (7.89)
$Yb(C_{12}H_{25}SO_4)_3$	43.36 (43.80)	8.08 (7.86)
$Lu(C_{12}H_{25}SO_4)_3$	43.70 (43.71)	8.18 (7.85)

[a] The calculated values are given in brackets. For the calculations the stoechiometry $Ln(C_{12}H_{25}SO_4)_3 \cdot H_2O$ is used.

Hagar de Verschrikkelijke door Dik Browne